

# Feasibility Study for Disposal Control Rod Assemblies Using UNF- ST&DARDS As-Loaded Zion Dual Purpose Cask Models



Bret Brickner  
Richard Reed  
Alex Lang

**June 2023**

## DOCUMENT AVAILABILITY

Reports produced after January 1, 1996, are generally available free via OSTI.GOV.

**Website** [www.osti.gov](http://www.osti.gov)

Reports produced before January 1, 1996, may be purchased by members of the public from the following source:

National Technical Information Service  
5285 Port Royal Road  
Springfield, VA 22161  
**Telephone** 703-605-6000 (1-800-553-6847)  
**TDD** 703-487-4639  
**Fax** 703-605-6900  
**E-mail** [info@ntis.gov](mailto:info@ntis.gov)  
**Website** <http://classic.ntis.gov/>

Reports are available to US Department of Energy (DOE) employees, DOE contractors, Energy Technology Data Exchange representatives, and International Nuclear Information System representatives from the following source:

Office of Scientific and Technical Information  
PO Box 62  
Oak Ridge, TN 37831  
**Telephone** 865-576-8401  
**Fax** 865-576-5728  
**E-mail** [reports@osti.gov](mailto:reports@osti.gov)  
**Website** <https://www.osti.gov/>

This report was prepared as an account of work sponsored by an agency of the United States Government. Neither the United States Government nor any agency thereof, nor any of their employees, makes any warranty, express or implied, or assumes any legal liability or responsibility for the accuracy, completeness, or usefulness of any information, apparatus, product, or process disclosed, or represents that its use would not infringe privately owned rights. Reference herein to any specific commercial product, process, or service by trade name, trademark, manufacturer, or otherwise, does not necessarily constitute or imply its endorsement, recommendation, or favoring by the United States Government or any agency thereof. The views and opinions of authors expressed herein do not necessarily state or reflect those of the United States Government or any agency thereof.

Nuclear Energy and Fuel Cycle Division

**FEASIBILITY STUDY FOR DISPOSAL CONTROL ROD ASSEMBLIES USING  
UNF-ST&DARDS AS-LOADED ZION DUAL PURPOSE CASK MODELS**

Bret Brickner  
Richard Reed  
Alex Lang

June 2023

Prepared by  
OAK RIDGE NATIONAL LABORATORY  
Oak Ridge, TN 37831  
managed by  
UT-BATTELLE LLC  
for the  
US DEPARTMENT OF ENERGY  
under contract DE-AC05-00OR22725





## CONTENTS

LIST OF FIGURES .....	iv
LIST OF TABLES.....	vi
ABBREVIATIONS .....	vii
EXECUTIVE SUMMARY .....	viii
1. INTRODUCTION .....	1
2. DATA AND METHODOLOGY DESCRIPTION.....	3
2.1 UNF-ST&DARDS DATA.....	3
2.2 DCRA DESIGN.....	12
2.2.1 DCRA Characteristics.....	12
2.2.2 DCRA Effectiveness Considerations .....	14
2.3 FEASIBILITY STUDY METHODOLOGY .....	14
2.3.1 Basket Zones and Fuel Bundle Subzones .....	14
2.3.2 Analysis Dataset Sequence .....	19
2.3.3 Characteristics of the Initial Utility Program.....	20
3. RESULTS.....	21
3.1 REACTIVITY TRENDS .....	21
3.1.1 Trends Related to Insert Rod Material, Rod Size, and Subzones .....	21
3.1.2 Results for all NA datasets.....	39
3.1.3 Results for the DB Dataset.....	63
4. ASSUMPTIONS.....	79
5. CONCLUSIONS .....	80
6. REFERENCES .....	81

## LIST OF FIGURES

Figure 1. Cost estimates for the as-loaded DB data set for the four most reactive casks. ....	x
Figure 2. Cost estimates for the as-loaded DB data set.....	xi
Figure 3. Summary of as-loaded NA data set and results of the Walker calculations [2]. ....	4
Figure 4. Summary of the as-loaded DB data set and results of the Walker calculations [2].....	5
Figure 5. Cross-sectional view of the DPC basket (left), and a 3D cut-away view of the DPC (right). ....	6
Figure 6. Arbitrarily numbered basket locations in the Zion DPCs.....	6
Figure 7. Cross-sectional diagram of a $15 \times 15$ PWR bundle.....	7
Figure 8. Isometric view of a single $15 \times 15$ PWR showing guide tube locations (left), and 3D model of a single PWR fuel bundle with 18 axial nodal sections for as-loaded spent fuel isotopic compositions.....	7
Figure 9. Total DPC fissile mass in the DPCs in the NA dataset compared to un-rodded results from Walker [2]. ....	8
Figure 10. Total DPC fissile mass in the DPCs in the DB dataset compared to un-rodded results from Walker [2]. ....	9
Figure 11. Radial distribution of total fuel bundle fissile mass in the DPCs in the DB dataset. Darker colors indicate low fissile mass bundles, and lighter colors represent higher fissile mass bundles. ....	10
Figure 12. Example of the axial distribution of total radial fuel bundle fissile mass in in the DPC. Darker colors indicate low fissile mass bundles, and lighter colors represent higher fissile mass bundles. Node 1 is at the bottom of the bundle.....	11
Figure 13. Comparison of cross sections of neutron-absorbing isotopes in DCRA materials.....	14
Figure 14. Location of basket zones. ....	15
Figure 15. Layout of the various subzones. ....	16
Figure 16. Total fissile isotope distribution per basket location for NA model TSCDF-37-TSCDF- 25. ....	22
Figure 17. Axial distribution of the fissile isotope distribution per bundle for NA model TSCDF- 37-TSCDF-25. ....	23
Figure 18. Results of NA model TSCDF-37-TSCDF-25 with DCRA material AIC and as-loaded spent fuel isotopic compositions. ....	25
Figure 19. Results of NA model TSCDF-37-TSCDF-25 with DCRA material AIC and fresh fuel isotopic compositions.....	26
Figure 20. Delta-k of fresh vs. spent fuel isotopic compositions for NA model TSCDF-37- TSCDF-25 with DCRA material AIC.....	27
Figure 21. Results of NA model TSCDF-37-TSCDF-25 with DCRA material $B_4C$ and as-loaded spent fuel isotopic compositions. ....	28
Figure 22. Results of NA model TSCDF-37-TSCDF-25 with DCRA material $B_4C$ and fresh fuel isotopic compositions.....	29
Figure 23. Delta-k of fresh vs. spent fuel isotopic compositions for the NA model TSCDF-37- TSCDF-25 with DCRA material $B_4C$ .....	30
Figure 24. Results of NA model TSCDF-37-TSCDF-25 with DCRA material $WB_2$ and as-loaded spent fuel isotopic compositions. ....	31
Figure 25. Results of NA model TSCDF-37-TSCDF-25 with DCRA material $WB_2$ and fresh fuel isotopic compositions.....	32
Figure 26. Delta-k of fresh vs. spent fuel isotopic compositions for the NA model TSCDF-37- TSCDF-25 with DCRA material $WB_2$ .....	33
Figure 27. Results of NA model TSCDF-37-TSCDF-25 with DCRA material $TiB_2$ and as-loaded spent fuel isotopic compositions. ....	34

Figure 28. Results of NA model TSCDF-37-TSCDF-25 with DCRA material $TiB_2$ and fresh fuel isotopic compositions.....	35
Figure 29. Delta-k of fresh vs. spent fuel isotopic compositions for the NA model TSCDF-37-TSCDF-25 with DCRA material $TiB_2$ .....	36
Figure 30. Delta-k of AIC to $B_4C$ , $TiB_2$ and $WB_2$ DCRA materials, respectively, for spent fuel isotopic compositions for the NA model TSCDF-37-TSCDF-25 for subzone, all rods (21).....	37
Figure 31. Comparison of the delta-k results for NA case TSCDF-37-TSCDF-25 with subzone, all rods (21) of fresh-to-spent fuel isotopic compositions for the DCRA materials in all zones. ....	38
Figure 32. Results of all NA models with DCRA material $WB_2$ and as-loaded fuel isotopic compositions; subzone 2 with small diameter rods. ....	43
Figure 33. Results of all NA models with DCRA material $WB_2$ and as-loaded fuel isotopic compositions; subzone 2 with large diameter rods. ....	44
Figure 34. Delta-k of large-to-small diameter rods for all NA models with DCRA material $WB_2$ and as-loaded fuel isotopic compositions for subzone 2.....	45
Figure 35. Results of all NA models with DCRA material $WB_2$ and as-loaded fuel isotopic compositions; subzone 2 corners with small diameter rods.....	46
Figure 36. Results of all NA models with DCRA material $WB_2$ and as-loaded fuel isotopic compositions; subzone 2 corners with large diameter rods. ....	47
Figure 37. Delta-k of large-to-small diameter rods for all NA models with DCRA material $WB_2$ and as-loaded fuel isotopic compositions; subzone 2 corners. ....	48
Figure 38. Delta-k of subzone 2 to subzone 2 corners for large diameter rods for all NA models with DCRA material $WB_2$ and as-loaded fuel isotopic compositions. ....	49
Figure 39. Delta-k of subzone 2 with small diameter rods to subzone 2 corners with large diameter rods (equal absorber mass) for all NA models with DCRA material $WB_2$ and as-loaded fuel isotopic compositions. ....	50
Figure 40. Results of all NA models with DCRA material $WB_2$ and as-loaded fuel isotopic compositions; subzone inner 12 with small diameter rods. ....	51
Figure 41. Results of all NA models with DCRA material $WB_2$ and as-loaded fuel isotopic compositions; subzone inner 12 with large diameter rods. ....	52
Figure 42. Delta-k of large-to-small diameter rods for all NA models with DCRA material $WB_2$ and as-loaded fuel isotopic compositions for inner 12. ....	53
Figure 43. Delta-k of large-to-small diameter rods for all NA models with DCRA material $WB_2$ and fresh fuel isotopic compositions for subzone inner 12.....	54
Figure 44. Delta-k of fresh-to-as-loaded spent fuel isotopic compositions for small diameter rods to small diameter rods for all NA models with DCRA material $WB_2$ for subzone inner 12. ....	55
Figure 45. Delta-k of fresh-to-as-loaded spent fuel isotopic compositions for large diameter rods to large diameter rods for all NA models with DCRA material $WB_2$ for subzone inner 12. ....	56
Figure 46. Results of all NA models with DCRA material $WB_2$ and as-loaded fuel isotopic compositions; subzone all rods (21) with small diameter rods. ....	57
Figure 47. Results of all NA models with DCRA material $WB_2$ and as-loaded fuel isotopic compositions; subzone all rods (21) with large diameter rods.....	58
Figure 48. Delta-k of large-to-small diameter rods for all NA models with DCRA material $WB_2$ and as-loaded fuel isotopic compositions for subzone all rods (21). ....	59
Figure 49. Delta-k of large-to-small diameter rods for all NA models with DCRA material $WB_2$ and fresh fuel isotopic compositions for subzone all rods (21). ....	60
Figure 50. Delta-k of fresh-to-as-loaded spent fuel isotopic compositions for small diameter rods for all NA models with DCRA material $WB_2$ for subzone all rods (21). ....	61

Figure 51. Delta-k of fresh-to-as-loaded spent fuel isotopic compositions for large diameter rods for all NA models with DCRA material WB <sub>2</sub> for subzone all rods (21). .....	62
Figure 52. Results of all DB models for various bounding combinations of fresh fuel, as-loaded spent fuel isotopic compositions, all DCRA with material large WB <sub>2</sub> rods in every location and with no rods compared to the Walker [2] DB results. ....	66
Figure 53. Results of all DB models with DCRA material WB <sub>2</sub> and as-loaded fuel isotopic compositions; subzone 2 with small diameter rods. ....	67
Figure 54. Results of all DB models with DCRA material WB <sub>2</sub> and as-loaded fuel isotopic compositions; subzone 2 with large diameter rods. ....	68
Figure 55. Delta-k of large-to-small diameter rods for all DB models with DCRA material WB <sub>2</sub> and as-loaded fuel isotopic compositions for subzone 2.....	69
Figure 56. Results of all DB models with DCRA material WB <sub>2</sub> and as-loaded fuel isotopic compositions; subzone 2 corners with small diameter rods.....	70
Figure 57. Results of all DB models with DCRA material WB <sub>2</sub> and as-loaded fuel isotopic compositions; subzone 2 corners with large diameter rods. ....	71
Figure 58. Delta-k of large-to-small diameter rods for all DB models with DCRA material WB <sub>2</sub> and as-loaded fuel isotopic compositions for subzone 2 corners.....	72
Figure 59. Results of all DB models with DCRA material WB <sub>2</sub> and as-loaded fuel isotopic compositions; subzone inner 12 with small diameter rods. ....	73
Figure 60. Results of all DB models with DCRA material WB <sub>2</sub> and as-loaded fuel isotopic compositions; subzone inner 12 with large diameter rods. ....	74
Figure 61. Delta-k of large-to-small diameter rods for all DB models with DCRA material WB <sub>2</sub> and as-loaded fuel isotopic compositions for subzone inner 12. ....	75
Figure 62. Results of all DB models with DCRA material WB <sub>2</sub> and as-loaded fuel isotopic compositions; subzone all rods (21) with small diameter rods. ....	76
Figure 63. Results of all DB models with DCRA material WB <sub>2</sub> and as-loaded fuel isotopic compositions; subzone all rods (21) with large diameter rods.....	77
Figure 64. Delta-k of large-to-small diameter rods for all DB models with DCRA material WB <sub>2</sub> and as-loaded fuel isotopic compositions for subzone all rods (21). ....	78

## LIST OF TABLES

Table 1. Summary of the zone and subzone results for the degraded basket datasets with large diameter rod DCRA with WB <sub>2</sub> .....	ix
Table 2. Characterization of the DCRA ..... ..	13
Table 3. Distribution of the number of insert rods by zone and subzone .....	16
Table 4. Total mass of B <sub>4</sub> C DCRA per zone and subzone combination and rod radius .....	17
Table 5. Total mass of WB <sub>2</sub> DCRA per zone and subzone combination and rod radius.....	17
Table 6. Total mass of TiB <sub>2</sub> DCRA per zone and subzone combination and rod radius.....	18
Table 7. Characterization of the calculation sets generated by the analysis .....	19
Table 8. Summary of the zone and subzone results for the NA datasets with large diameter rod DCRA with WB <sub>2</sub> .....	41
Table 9. Summary of the zone and subzone results for the NA datasets with small diameter rod DCRA with WB <sub>2</sub> .....	42
Table 10. Summary of zone and subzone results for DB datasets with large diameter rod DCRA with WB <sub>2</sub> .....	64
Table 11. Summary of zone and subzone results for DB datasets with small diameter rod DCRA with WB <sub>2</sub> .....	65

## **ABBREVIATIONS**

BWR	boiling water reactor
DB	degraded basket
DCRA	disposal control rod assembly
DPC	dual purpose canister
NA	neutron absorber
PWR	pressurized water reactor
RCCA	rod cluster control assembly
SNF	spent nuclear fuel
UNF-ST&DARDS	Used Nuclear Fuel-Storage, Transportation & Disposal Analysis Resource and Data System

## EXECUTIVE SUMMARY

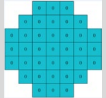
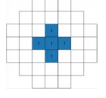
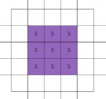
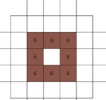
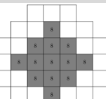
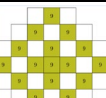
This report documents an initial evaluation to support future use of disposal control rod assemblies (DCRAs) [1] for post-closure criticality control in dual purpose canisters (DPCs). The work described herein is an extension of previous efforts performed by Walker [2] using inputs generated by the Used Nuclear Fuel-Storage, Transportation & Disposal Analysis Resource and Data System (UNF-ST&DARDS) for the Zion site DPCs with as-loaded isotopic compositions. The results of this analysis demonstrate that there are multiple pathways to using DCRA for post-closure criticality control. Various configurations of DCRA material, diameter, number of rods per DCRA, and number and location of DCRAs within a DPC were shown to be effective in varying degrees for the set of DPCs analyzed by Walker [2]. Because of the variations in DPC as-loaded isotopic compositions considered in an array of DCRA parametric sweeps (see Table 1), it can be concluded that a DPC-specific methodology is feasible (i.e., a one-size-fits-all approach may not be needed). Instead, the utility program created for this work can be expanded to develop capabilities to provide DPC-specific DCRA arrangements to limit cost and weight and to allow for operational considerations. Future work should consider the following focus areas:

- Expansion of capabilities to include all pressurized water reactor (PWR) DPCs in UNF-ST&DARDS
- Additional zone and subzone combinations
- Expansion to boiling water reactor (BWR) DPC and fuel designs
- Investigation of integration with UNF-ST&DARDS
- Development of a DCRA component system with the capability to utilize partial DCRA loading within assemblies in DPCs.
- In depth material evaluations.
- Development of a machine learning algorithm to optimize DCRA loading

The results presented in this report indicate that machine learning algorithms implemented within UNF-ST&DARDS during DPC loading could efficiently optimize the loading to the minimum number of DCRAs needed. The implementation and development of these algorithms can be independent of similar generic parametric evaluations such as those presented in this report, but the algorithm could also be improved by incorporating parametric studies as training data. The design, development, and licensing of a usable DCRA is precisely applicable to the type of generic parametric evaluations presented in this report, and this work should continue and broaden in scope. For example, one ideal situation would be for DOE to design, manufacture, and provide the DCRAs to utilities as needed to implement a DPC reactivity suppression program for post-closure criticality control. The utility would simply act as the end user of the DCRAs. Because the results summarized in Figure 1 and Figure 2 show that a generic implementation scheme can effectively control reactivity with minimal DCRA utilization for the most reactive DPCs (Figure 1) the overall cost can be expected to be very competitive with other DOE post-closure concepts. Additional, as the results for all DPCs show (Figure 2), the generic implementation may not be as effective for less reactive DPCs. Thus, evaluations should continue to develop optimization schemes for design and implementation of DCRA (material, parametric design, rodlet number etc.) using the full set of DPCs in the UDB to more fully grasp the potential of using this concept as a cost-effective approach.



**Table 1. Summary of the zone and subzone results for the degraded basket datasets with large diameter rod DCRA's with WB<sub>2</sub>**

Zone	Subcritical limit	Subzone 2 (8 rods)	Subzone 2 corners (4 rods)	Subzone 3 (12 rods)	Inner 12 (12 rods)	All rods (21 rods)	Zone layout
Zone 0 (37 assemblies)	0.95	41/61 (67.2%)	4/61 (6.6%)	61/61 (100.0%)	61/61 (100.0%)	61/61 (100.0%)	
Zone 0 (37 assemblies)	1	56/61 (91.8%)	37/61 (60.7%)	61/61 (100.0%)	61/61 (100.0%)	61/61 (100.0%)	
Zone 0 (37 assemblies)	1.03	61/61 (100.0%)	43/61 (70.5%)	61/61 (100.0%)	61/61 (100.0%)	61/61 (100.0%)	
Zone 1 (5 assemblies)	0.95	0/61 (0.0%)	0/61 (0.0%)	0/61 (0.0%)	0/61 (0.0%)	0/61 (0.0%)	
Zone 1 (5 assemblies)	1	1/61 (1.6%)	0/61 (0.0%)	2/61 (3.3%)	2/61 (3.3%)	2/61 (3.3%)	
Zone 1 (5 assemblies)	1.03	17/61 (27.9%)	4/61 (6.6%)	27/61 (44.3%)	27/61 (44.3%)	31/61 (50.8%)	
Zone 2 (8 assemblies)	0.95	0/61 (0.0%)	0/61 (0.0%)	2/61 (3.3%)	2/61 (3.3%)	2/61 (3.3%)	
Zone 2 (8 assemblies)	1	4/61 (6.6%)	2/61 (3.3%)	33/61 (54.1%)	33/61 (54.1%)	35/61 (57.4%)	
Zone 2 (8 assemblies)	1.03	37/61 (60.7%)	19/61 (31.1%)	37/61 (60.7%)	37/61 (60.7%)	44/61 (72.1%)	
Zone 5 (9 assemblies)	0.95	0/61 (0.0%)	0/61 (0.0%)	0/61 (0.0%)	0/61 (0.0%)	1/61 (1.6%)	
Zone 5 (9 assemblies)	1	3/61 (4.9%)	2/61 (3.3%)	21/61 (34.4%)	16/61 (26.2%)	33/61 (54.1%)	
Zone 5 (9 assemblies)	1.03	44/61 (72.1%)	25/61 (41.0%)	61/61 (100.0%)	61/61 (100.0%)	61/61 (100.0%)	
Zone 6 (8 assemblies)	0.95	0/61 (0.0%)	0/61 (0.0%)	0/61 (0.0%)	0/61 (0.0%)	1/61 (1.6%)	
Zone 6 (8 assemblies)	1	2/61 (3.3%)	2/61 (3.3%)	20/61 (32.8%)	16/61 (26.2%)	32/61 (52.5%)	
Zone 6 (8 assemblies)	1.03	40/61 (65.6%)	21/61 (34.4%)	58/61 (95.1%)	57/61 (93.4%)	61/61 (100.0%)	
Zone 7 (17 assemblies)	0.95	2/61 (3.3%)	0/61 (0.0%)	36/61 (59.0%)	35/61 (57.4%)	39/61 (63.9%)	
Zone 7 (17 assemblies)	1	37/61 (60.7%)	11/61 (18.0%)	48/61 (78.7%)	44/61 (72.1%)	59/61 (96.7%)	
Zone 7 (17 assemblies)	1.03	45/61 (73.8%)	38/61 (62.3%)	61/61 (100.0%)	57/61 (93.4%)	61/61 (100.0%)	
Zone 8 (13 assemblies)	0.95	0/61 (0.0%)	0/61 (0.0%)	5/61 (8.2%)	4/61 (6.6%)	19/61 (31.1%)	
Zone 8 (13 assemblies)	1	29/61 (47.5%)	3/61 (4.9%)	48/61 (78.7%)	48/61 (78.7%)	50/61 (82.0%)	
Zone 8 (13 assemblies)	1.03	56/61 (91.8%)	39/61 (63.9%)	61/61 (100.0%)	61/61 (100.0%)	61/61 (100.0%)	
Zone 9 (17 assemblies)	0.95	1/61 (1.6%)	0/61 (0.0%)	25/61 (41.0%)	19/61 (31.1%)	39/61 (63.9%)	
Zone 9 (17 assemblies)	1	35/61 (57.4%)	5/61 (8.2%)	46/61 (75.4%)	43/61 (70.5%)	59/61 (96.7%)	
Zone 9 (17 assemblies)	1.03	41/61 (67.2%)	36/61 (59.0%)	57/61 (93.4%)	56/61 (91.8%)	61/61 (100.0%)	

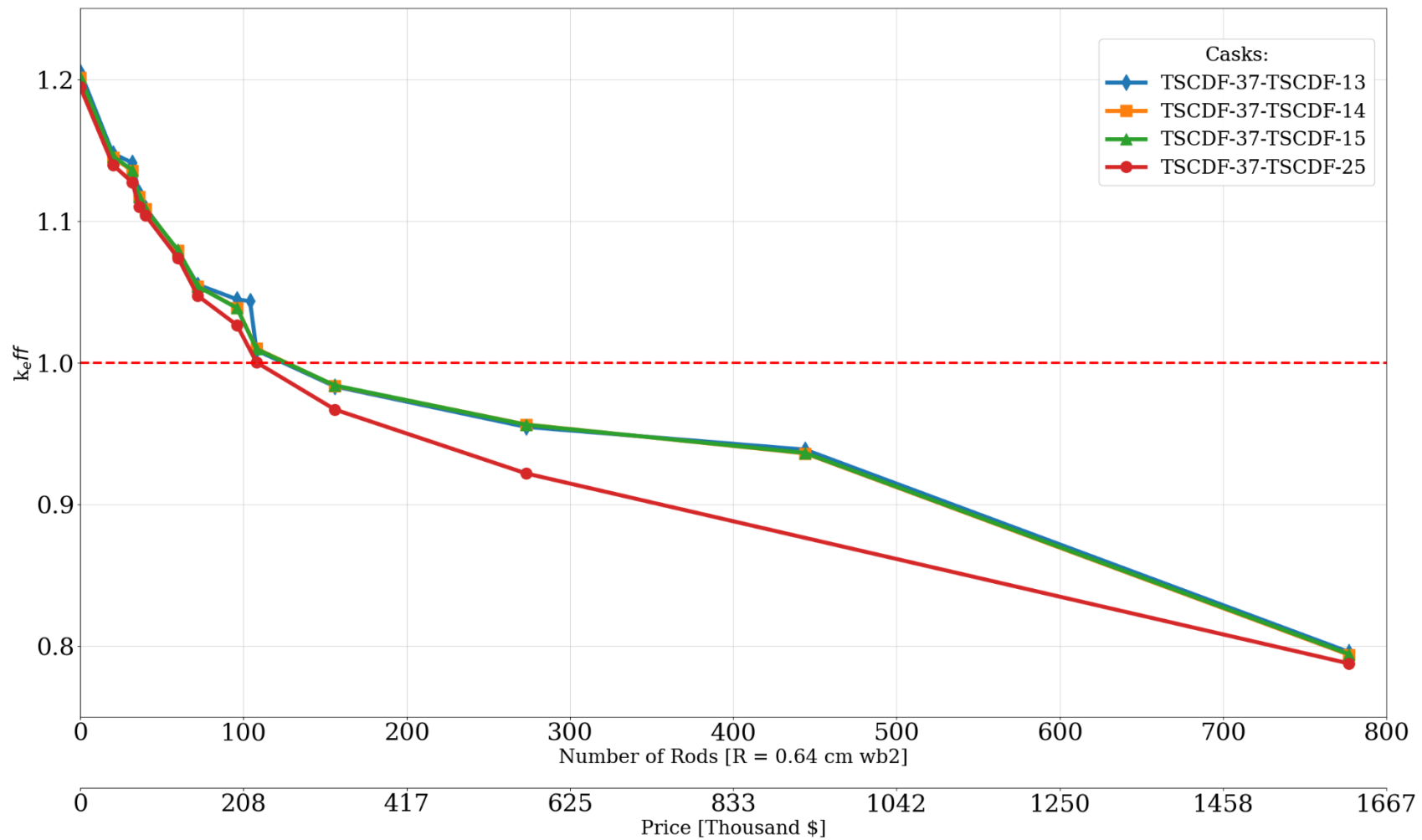


**Figure 1. Cost estimates for the as-loaded DB data set for the four most reactive casks.**

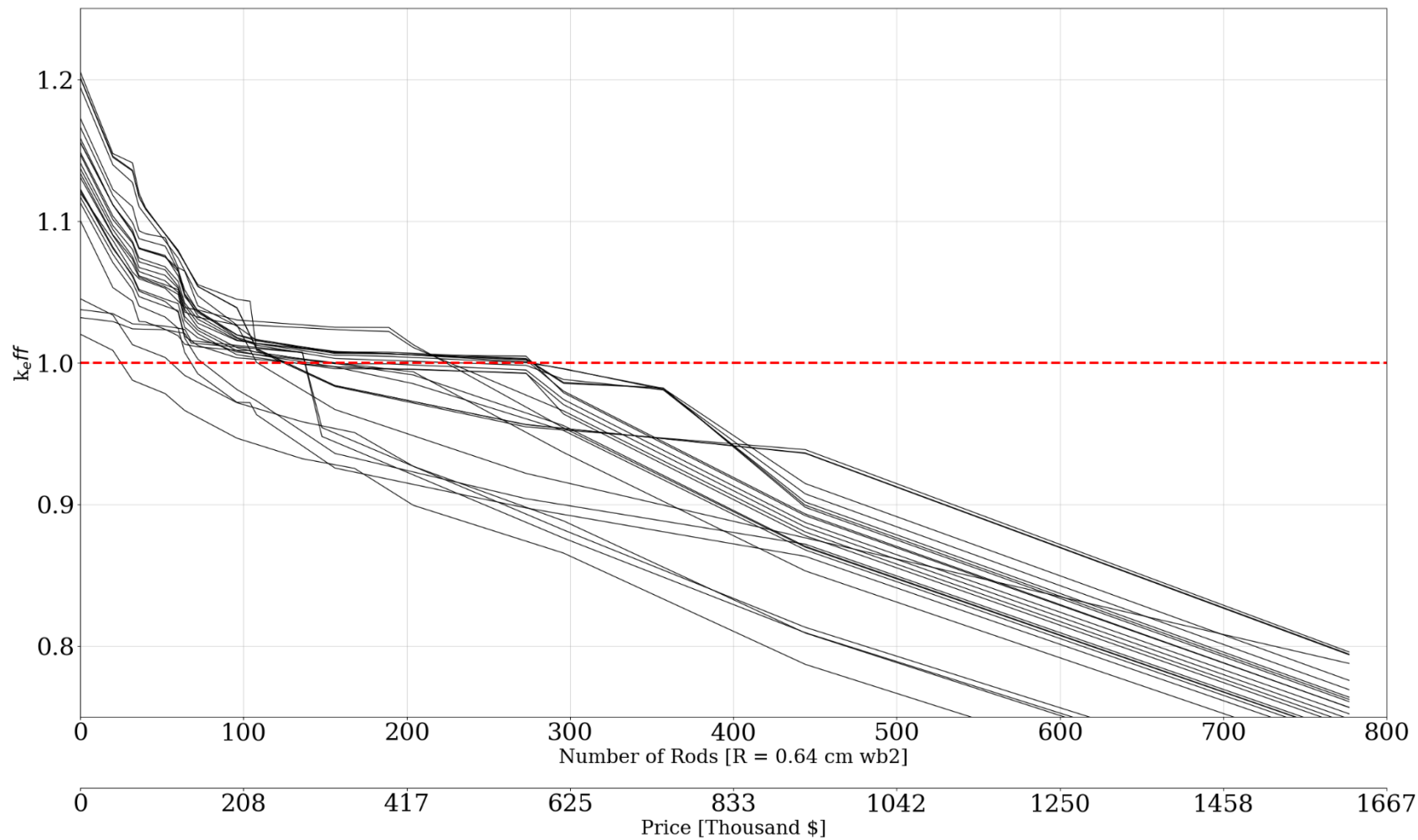


**Figure 2. Cost estimates for the as-loaded DB data set.**

## 1. INTRODUCTION

The emplacement of dual-purpose canisters (DPCs) into a national repository has been a focus of research for many years. Currently, spent nuclear fuel (SNF) bundles are placed into DPCs and stored in dry cask storage at operating nuclear power plants as part of an interim solution prior to final disposal in a repository. Repository post-closure criticality evaluations provide deterministic data to inform the probabilistic and consequence-based regulatory approach. To that end, the Used Nuclear Fuel-Storage, Transportation & Disposal Analysis Resource and Data System (UNF-ST&DARDS) [3] can generate as-loaded criticality analysis of DPCs under various assumed repository conditions to support evaluation of desired scenarios. UNF-ST&DARDS is being developed for the US Department of Energy Office of Nuclear Energy Spent Fuel and Waste Disposition program. UNF-ST&DARDS is an integrated framework that uses advanced modeling and simulation to predict the behavior of SNF to be placed in long-term storage in a disposal site. Recent work performed by Walker [2] used UNF-ST&DARDS to evaluate absorber rod worth for as-loaded DPCs at Zion. Results from this analysis show a significant reactivity effect for as-loaded DPCs in which the rod cluster control assembly (RCCA) is placed in random locations (as-loaded) within the DPC. The analysis presented in this report draws from the work described in Walker [2] and extends the study to parametric evaluation of neutron absorber materials in criticality control disposal rods (DCRAs) to evaluate potential near-term actions for future DPC loading operations. This work can be used to anticipate disposal criticality control and to develop a tool to complement or integrate with UNF-ST&DARDS.

In this report, *DCRA* refers to a rod with a design similar to that of an RCCA rod but without a fixed number of rodlets or design composition. In principle, a DCRA could be any inserted rod which meets the final design criteria and performs the function of maintaining subcriticality during post-closure conditions. Therefore, this work addresses initial evaluations to demonstrate how such rods might perform from a criticality perspective so that future work can focus on refining the design parameters and defining the performance criteria to support their use in real time.

This report provides the results from a series of scoping calculations; these results may form the basis for future analysis to establish a methodology and a utility program for UNF-ST&DARDS to implement a generic criterion for the number of various hypothetical DCRAs and to determine their ideal locations to preclude criticality under the assumed post-closure conditions for as-loaded DPCs.<sup>1</sup> The scoping studies presented in this report start with the same as-loaded Zion DPCs created by Walker [2] under the-loss-of-DPC-basket neutron absorber (NA) cases (e.g., the *NA models*) and the complete loss of basket models (e.g., the “degraded basket [*DB*<sup>2</sup>] *models*”). The objective is to establish a program to modify these existing models and implement the insertion of various DCRAs designs in specific loading patterns in a parametric fashion to determine how the permutations impact system reactivity. Additional calculations can then be used to build on the initial studies to further refine the approach until next steps can be delineated for the proposal of future work.

The basic premise behind this study is an expectation that in the future, compensatory actions could be implemented, such as using DCRAs prior to sealing DPCs for onsite dry cask storage. This approach is part of a larger effort to unify methodologies for direct disposal of DPCs at a much lower cost compared to other currently proposed repackaging solutions. Shaw et al. [4] shows that most DPCs require some sort of compensatory actions to preclude post-closure criticality. Therefore, to reduce or eliminate the growth in the number of DPCs already loaded without consideration of disposal, therefore requiring

---

<sup>1</sup> These studies are applicable to the pressurized water reactor (PWR) DPCs evaluated by Walker [2] only.

<sup>2</sup> Note that ‘NA’ and ‘DB’ are UNF-ST&DARDS terminology.

alternative, far more expensive compensatory actions, analysis such as that presented herein can serve as a basis for making decisions to meet that expectation.

While it is well known that inserting absorber rods into a fuel assembly will have a dramatic impact on reactivity, this approach has not yet been fully evaluated with respect to disposal of as-loaded DPCs under various post-closure scenarios considered proposed by programs such as UNF-ST&DARDS. Some of these scenarios include flooding with loss of NA and loss of DB. This initial study expands on the reactivity worth calculations performed by Walker [2] using UNF-ST&DARDS as-loaded data by evaluating the reactivity worth of hypothetical DCRA, exploring variations on DCRA loading configurations and the impact of the number of DCRA, their location within the bundle, and their design parameters. A key objective is to provide an initial set of data that can be used to scope out parameters for use in machine learning algorithms to develop a DCRA optimization engine for as-loaded configurations.

This study provides the basis for future work to develop (1) a utility to create DCRA loading configurations for as-loaded casks to ensure sufficient subcritical margin to preclude post-closure criticality, (2) additional compensatory actions, and (3) advanced design concepts for DCRA.

## 2. DATA AND METHODOLOGY DESCRIPTION

### 2.1 UNF-ST&DARDS DATA

Two sets of input files generated by UNF-ST&DARDS were provided by Walker [2] for use in this analysis. As part of the current UNF-ST&DARDS post-closure evaluations, two types of scenarios are considered: the loss of neutron absorber cases, or *NA cases*, which include the scenario of water ingress into the DPC, resulting in total loss of neutron absorber from the basket structure, and the loss of the basket or DB cases which involves both the total loss of neutron absorber and the loss of the basket structure itself. Both cases are evaluated in this report. These input files were created by UNF-ST&DARDS and were then modified by Walker [2] to include the as-loaded insert configurations for each cask. The results of these scenarios are listed in Figure 3 and Figure 4 for the NA and DB cases, respectively. For clarity, the filename base structure is maintained for the calculations in this report.



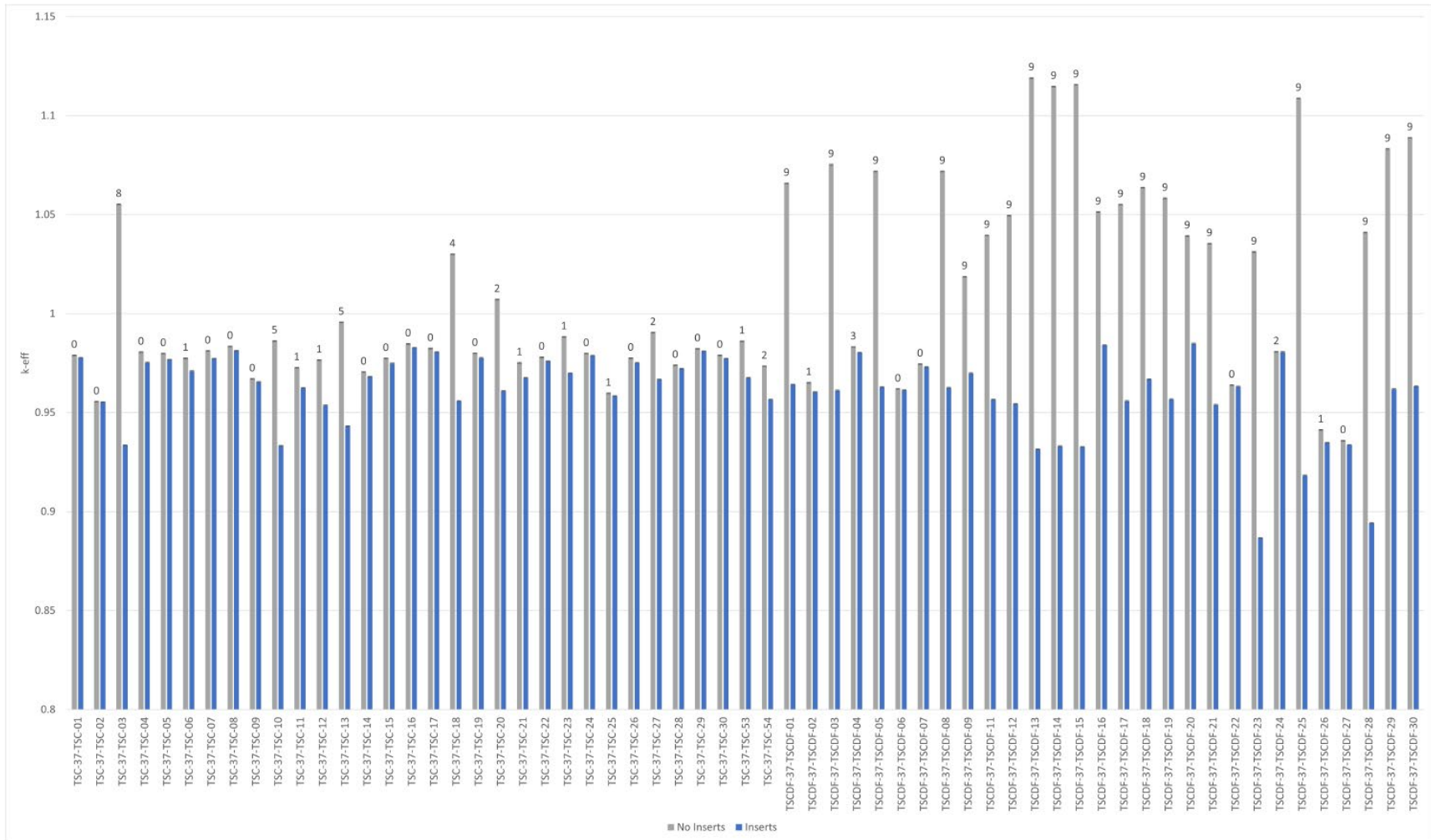


**Figure 3. Summary of as-loaded NA data set and results of the Walker calculations [2].** Gray bars show as-loaded results with no as-loaded inserts, and blue bars show as-loaded results with as-loaded inserts.

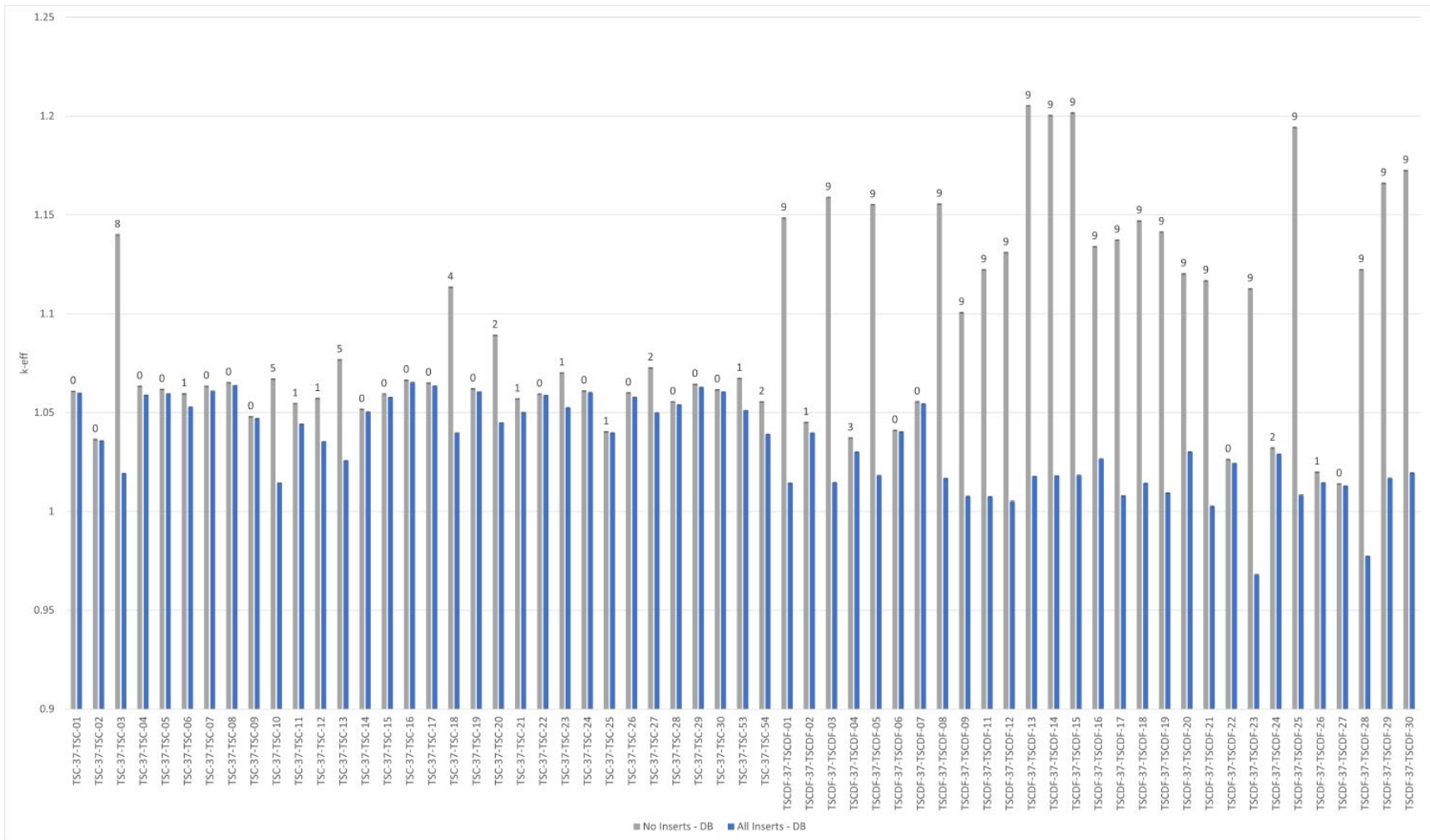


**Figure 4. Summary of the as-loaded DB data set and results of the Walker calculations [2].** Gray bars show as-loaded results with no as-loaded inserts, and blue bars show as-loaded results with as-loaded inserts.

The KENO model of the DPC is presented in Figure 5. Each model is a single DPC model with water reflection. All the DPC components are neglected except for the stainless steel canister wall. For the NA cases, the basket and neutron absorber panels are modeled, and the neutron absorber is replaced with water. For the DB cases, both the neutron absorber and the basket are replaced with water.

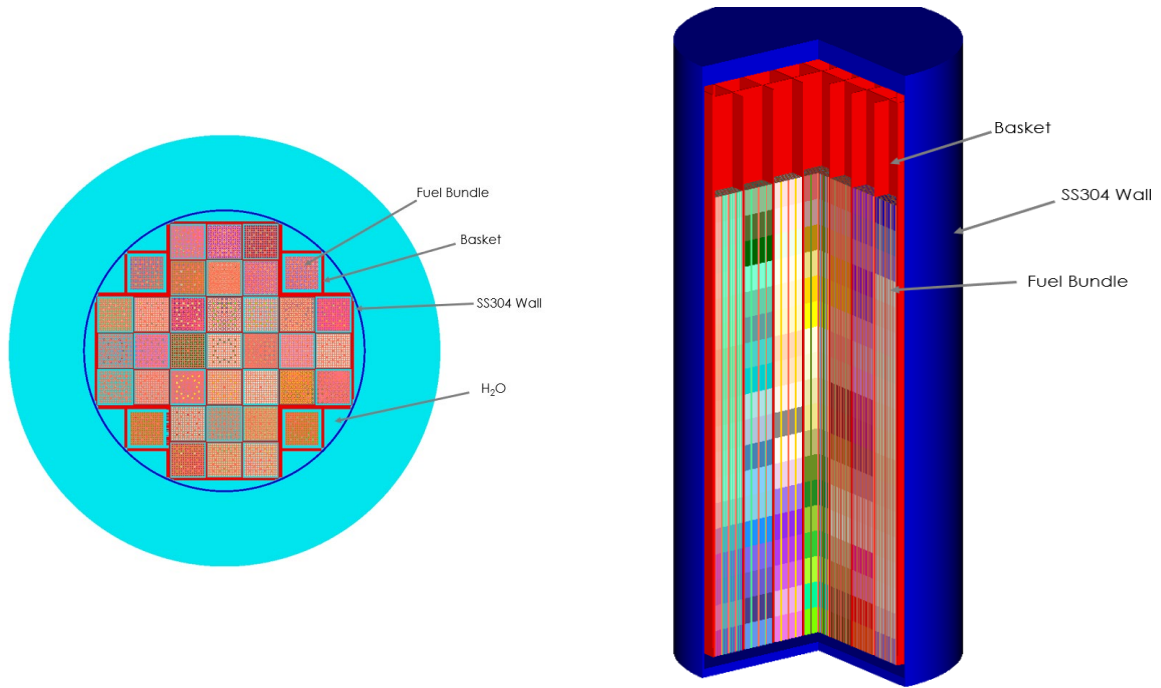


**Figure 5. Cross-sectional view of the DPC basket (left), and a 3D cut-away view of the DPC (right).**

The Zion DPC has 37 basket locations for PWR fuel bundles. These 37 locations are numbered (arbitrarily) sequentially for use in studies in this report, as shown in Figure 6.

		1	2	3		
	4	5	6	7	8	
9	10	11	12	13	14	15
16	17	18	19	20	21	22
23	24	25	26	27	28	29
	30	31	32	33	34	
		35	36	37		

**Figure 6. Arbitrarily numbered basket locations in the Zion DPCs.**

Generically, the  $15 \times 15$  PWR fuel bundles inside the Zion DPCs have 21 guide tube locations which can receive an insert rod. Figure 7 shows

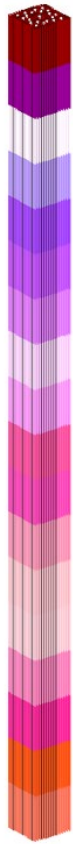


**Figure 8. Isometric view of a single  $15 \times 15$  PWR showing guide tube locations (left), and 3D model of a single PWR fuel bundle with 18 axial nodal sections for as-loaded spent fuel isotopic compositions.**

the guide tube locations and the axial zones for spent fuel compositions and for fresh fuel compositions, when applicable. Inside the DPC basket, the  $15 \times 15$  pin PWR bundles are modeled with axially zoned spent fuel compositions specific to each bundle as based on UNF-ST&DARDS depletion calculations and bounding axial burnup profiles from Bhat et al. [3]. However, specific cases in this report also model all fuel axial nodes as 5 wt% enriched fresh fuel. For criticality analysis, fresh fuel is often used to bound problems and is similarly useful for the studies presented in this report. Fresh fuel is also of particular interest for this problem because fresh fuel cases remove variations of the spatial dependency of reactivity in loading patterns. Therefore, it is useful to compare the reactivity trends between fresh and as-loaded DPC models to determine whether the as-loaded configurations introduce alternative trends. Analysis, of the DPC layout shown in Figure 8 is expected to show that the neutron flux is maximized in the inner regions of the cask. This is the case for a cask loaded with fresh fuel, but the as-loaded patterns may shift the location of maximum reactivity as a result of varied fuel depletion throughout the DPC.

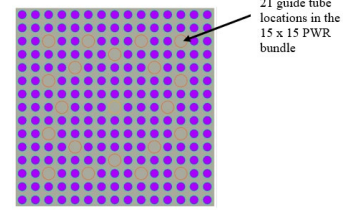


**Figure 7. Cross-sectional diagram of a  $15 \times 15$  PWR bundle.**

Additionally, the maximum reactivity of a DPC may have a strong correlation with the total fissile mass in conjunction with radial distribution and axial variations. The total fissile mass per DPC in the NA dataset is provided in Figure 9 and Figure 10 for the DB dataset, with comparisons added from Walker's results [2] for models with no inserts. The comparison of the data shown in Figure 9 indicates good agreement between total DPC fissile mass and maximum reactivity. This trend is independent of radial distribution and axial variation.

Although the results shown in Figure 9 and Figure 10 indicate a strong correlation between total DPC fissile mass and maximum DPC reactivity, some correlation to radial distribution and axial variation also exists. The

radial distribution of the Zion as-loaded DPC total fuel bundle fissile mass per DPC is shown in Figure 11, and the axial variation was shown in Figure 12. As expected, the radial distribution of total fuel bundle fissile mass varies significantly across the population of DPCs, whereas the axial variation shows the light-water reactor cosine power shape with the end effect, as expected.

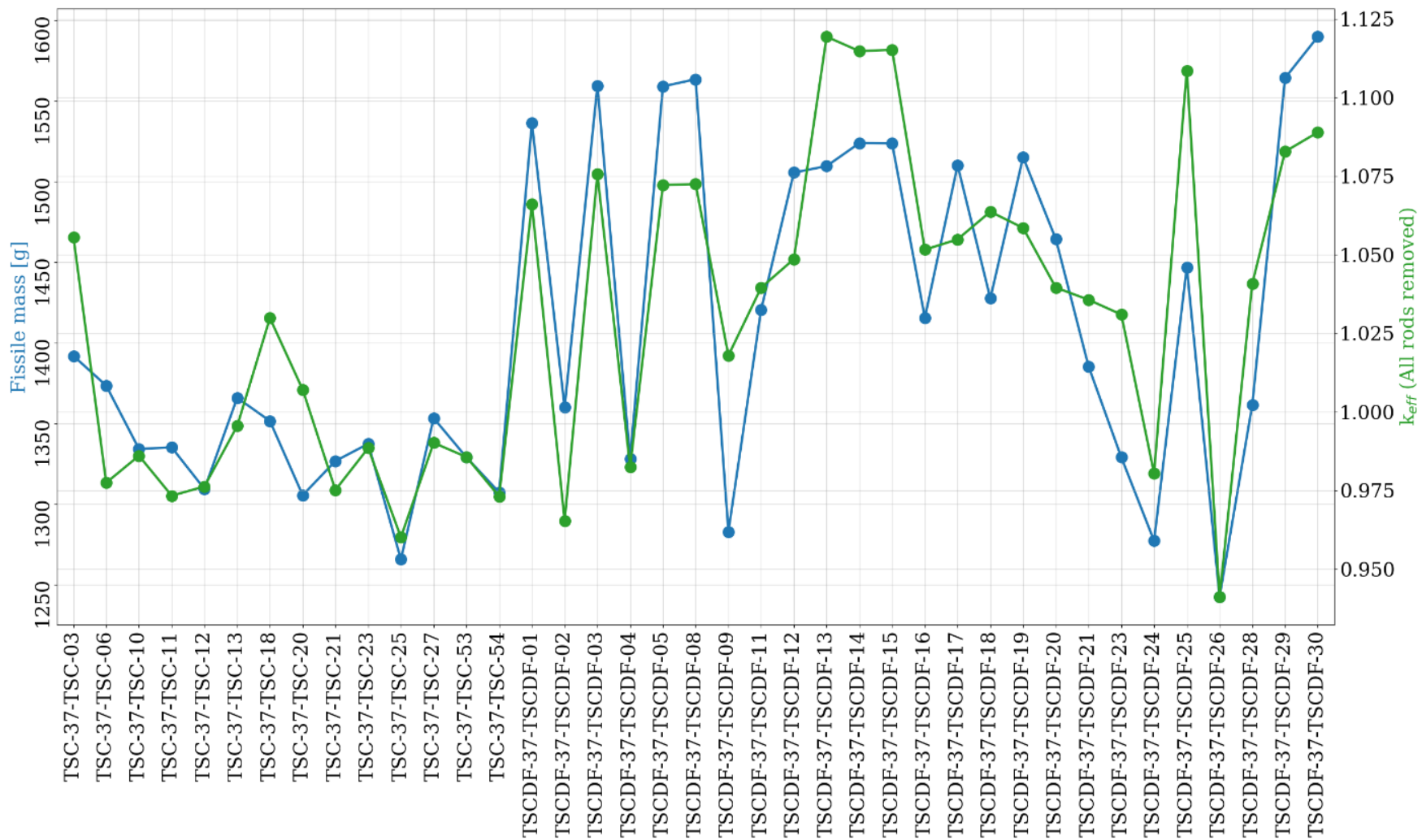


Figure 9. Total DPC fissile mass in the DPCs in the NA dataset compared to un-rodded results from Walker [2].

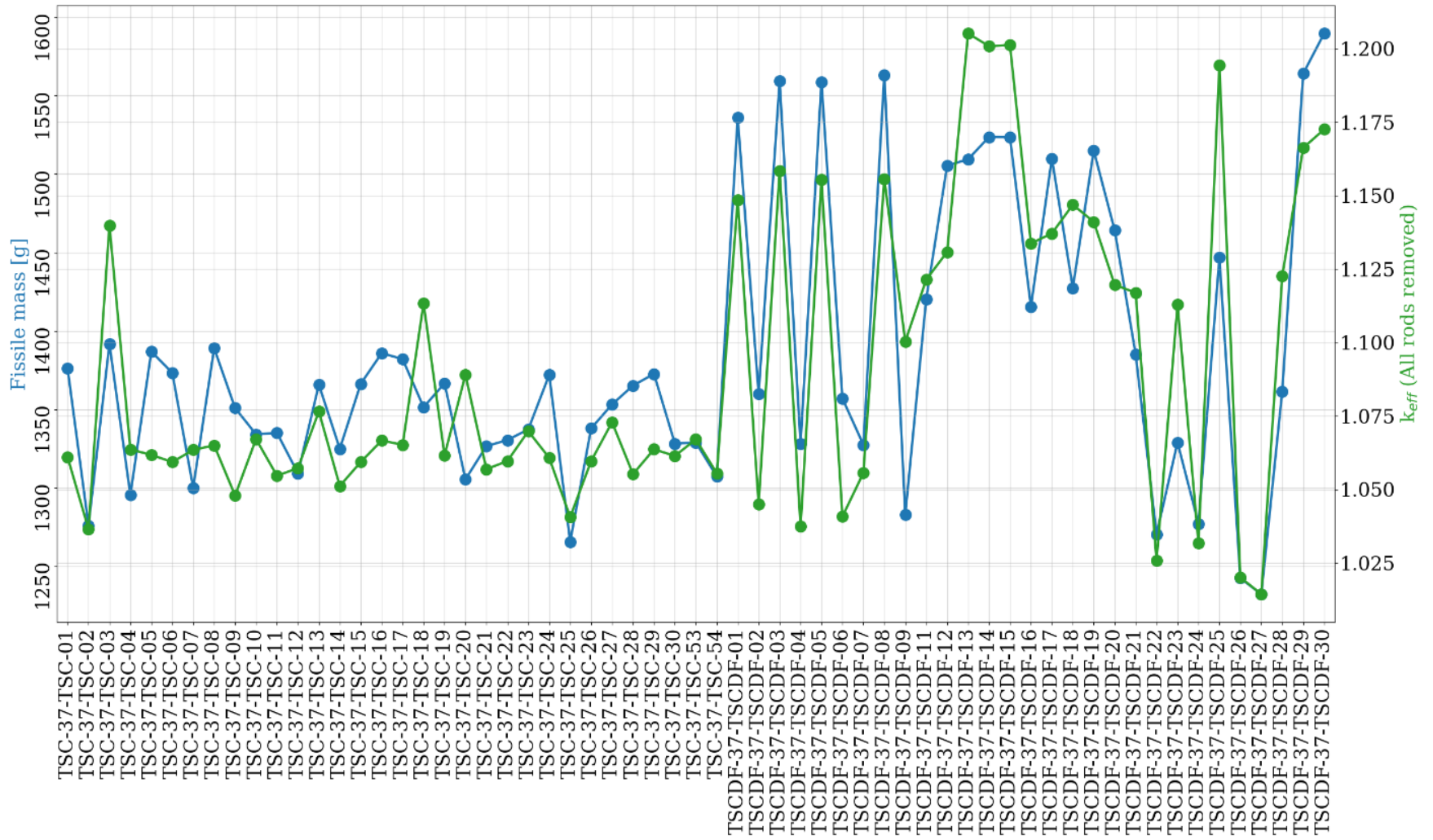


Figure 10. Total DPC fissile mass in the DPCs in the DB dataset compared to un-rodded results from Walker [2].



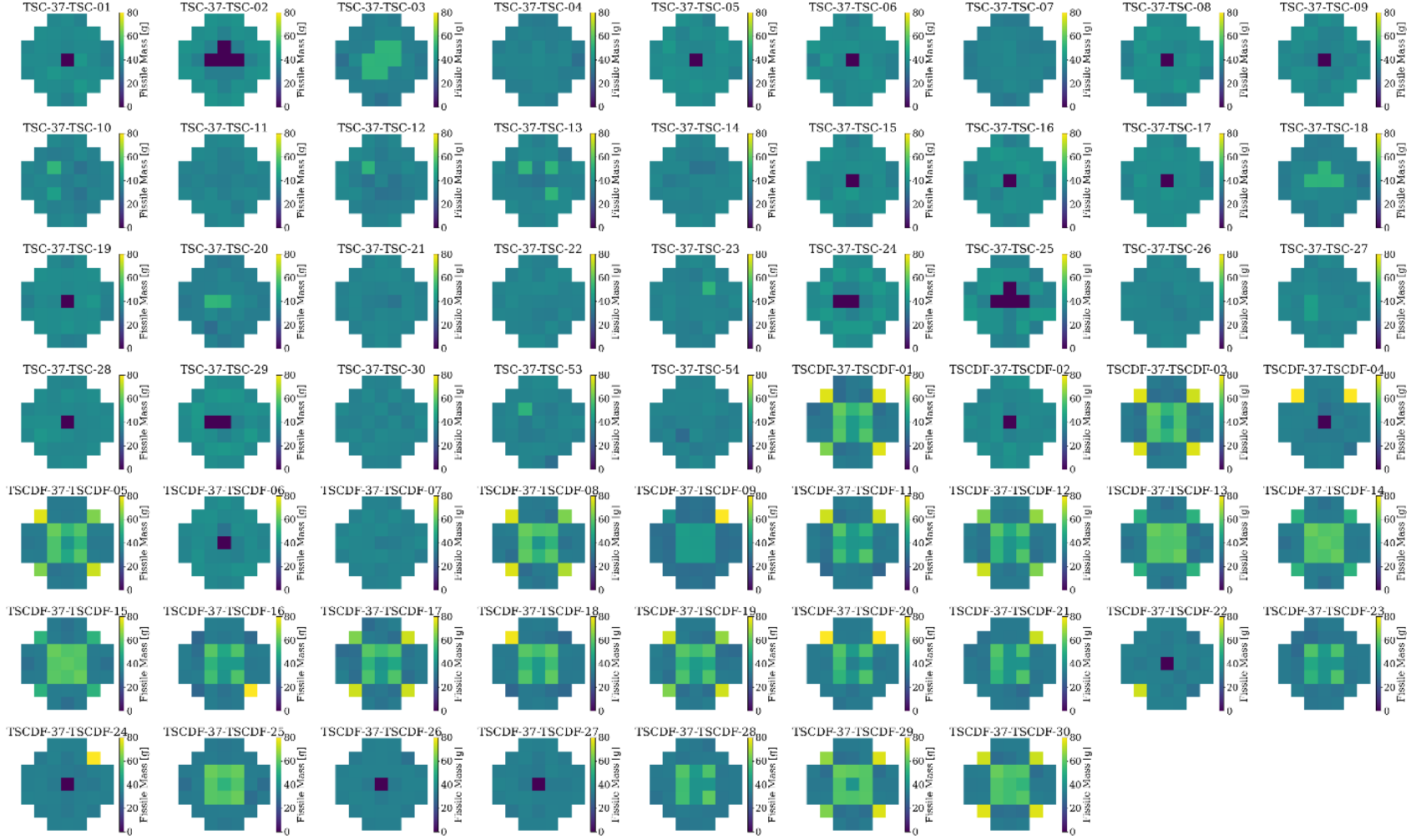
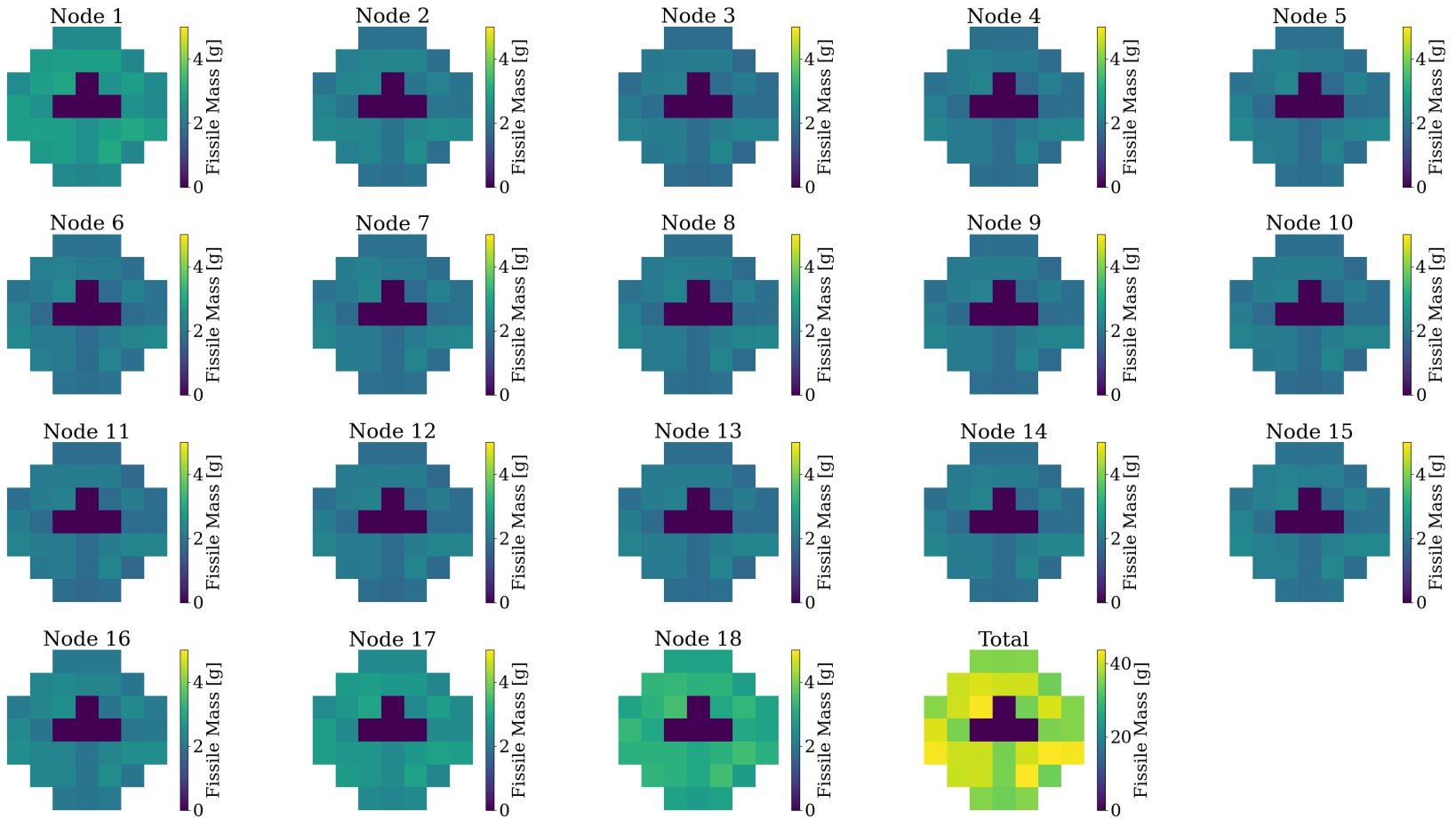


Figure 11. Radial distribution of total fuel bundle fissile mass in the DPCs in the DB dataset. Darker colors indicate low fissile mass bundles, and lighter colors represent higher fissile mass bundles.

TSC-37-TSC-25 Fissile content



**Figure 12.** Example of the axial distribution of total radial fuel bundle fissile mass in in the DPC. Darker colors indicate low fissile mass bundles, and lighter colors represent higher fissile mass bundles. Node 1 is at the bottom of the bundle.

## 2.2 DCRA DESIGN

The DCRA design is considered open-ended for the purposes of this report. However, to make comparisons between designs already in use (e.g., the RCCAs in Walker [2]) and the materials typically used for criticality control (e.g., B<sub>4</sub>C), four materials were selected for this study.

### 2.2.1 DCRA Characteristics

The DCRA was modeled as a uniform composition, continuous along the axial length of the fuel bundle. Each rod design was considered either to be either *small* at a radius of 0.37 cm, or *large* at a radius of 0.64 cm.

The materials and the rod dimensions were selected to support exploration of specific issues related to potential future DCRA design, as detailed below:

- **Insertion challenges.** Full insertion of any type of rod into a spent nuclear fuel bundle can be challenging; however, as evidenced by Walker [2], insertion is performed on a regular basis. Some of the potential challenges are operational: because of material fatigue and geometric changes in the guide tubes, rods may encounter physical restrictions during insertion. Therefore, it may be beneficial for future DCRA design to include options to accommodate rod size, as well as information related to effectiveness for this parameter.
- **Overall weight.** DPCs have overall weight limits and/or restrictions. Therefore, DCRA studies must cover a range of material types and densities to provide information related to effectiveness for this parameter.
- **Variability in future design.** The regulatory process to approve any potential future design may be best served by not limiting requirements to any material type. Rather, requirements should be based on a parameter such as the masses of specific nuclides or absorption cross sections. Therefore, DCRA studies should address a range of material types and densities to provide information on effectiveness for this parameter.
- **Insertion depth.** It is well understood that as PWR fuel depletes, the top of the fuel becomes the dominant region of reactivity. Therefore, one might assume that a DCRA design would only require partial insertion to be effective. Although this is fundamentally sound thinking for intact fuel, this approach may not actually account for the reactivity of the spent fuel's lower nodes, which are often only slightly less reactive than the top. More importantly, partial insertion does not account for extreme fuel damage and rod failures over long time frames and unspecified degradation mechanisms, which can result in fuel pellet or debris piles at the gravitational bottom of the system. Therefore, in this work, the DCRA's are modeled as full length, which relies on the assumption that they will remain intact indefinitely and will provide neutron absorption to fuel which may or may not remain intact.<sup>3</sup>
- **Mechanical properties.** Evaluation of mechanical properties or suitability of the selected DCRA materials for repository environments is not within the scope of this report. This report outlines the feasibility of DCRA's and provides a basis for development of a full methodology to evaluate them for post-closure criticality. Future work should include these mechanical and material considerations as part of the ongoing effort.

---

<sup>3</sup> To this end, future evaluations should explore the impact of fuel pellet rearrangements.

DCRA material characterization is provided in Table 2 and Figure 13.

**Table 2. Characterization of the DCRA**

DCRA material	Density (g/cc)	Mass per rod (grams) (small/large)	Description
AIC (control rod material): Ag 80% Cd 5% In 15%	5.09 <sup>4</sup>	Small rod = 801 Large rod = 2396	Same material as RCCAs used by Walker [2]. <sup>5</sup> Material is used because it is already being placed in existing casks, providing a baseline for comparisons to other materials.
B <sub>4</sub> C	2.52	Small rod = 396 Large rod = 1186	Typical neutron absorber used for non-disposal configurations. Material is used for comparisons because it is a very common neutron absorber but is expected to degrade quickly in post-closure analysis.
WB <sub>2</sub> (tungsten boride): W 89.47 % B 10.52 %	15.3	Small rod = 2407 Large rod = 7201	High-density material selected for potentially favorable mechanical properties. This material density <sup>6</sup> bounds the actual density of the AIC.
TiB <sub>2</sub> (titanium boride) T 68.924% B 31.07 %	4.52	Small rod = 711 Large rod = 2127	Moderate density material selected for potentially favorable mechanical properties while being significantly less dense than WB <sub>2</sub> .

<sup>4</sup> Note that Walker [2] changes the material density of the RCCA from 9.9 to 5.09, which is retained in this report.

<sup>5</sup> Note that Walker [2] uses a material density of approximately 50%, which is very conservative and bounds any possible degradation from use during reactor operations.

<sup>6</sup> Material density impacts the total weight being added to the DPC.

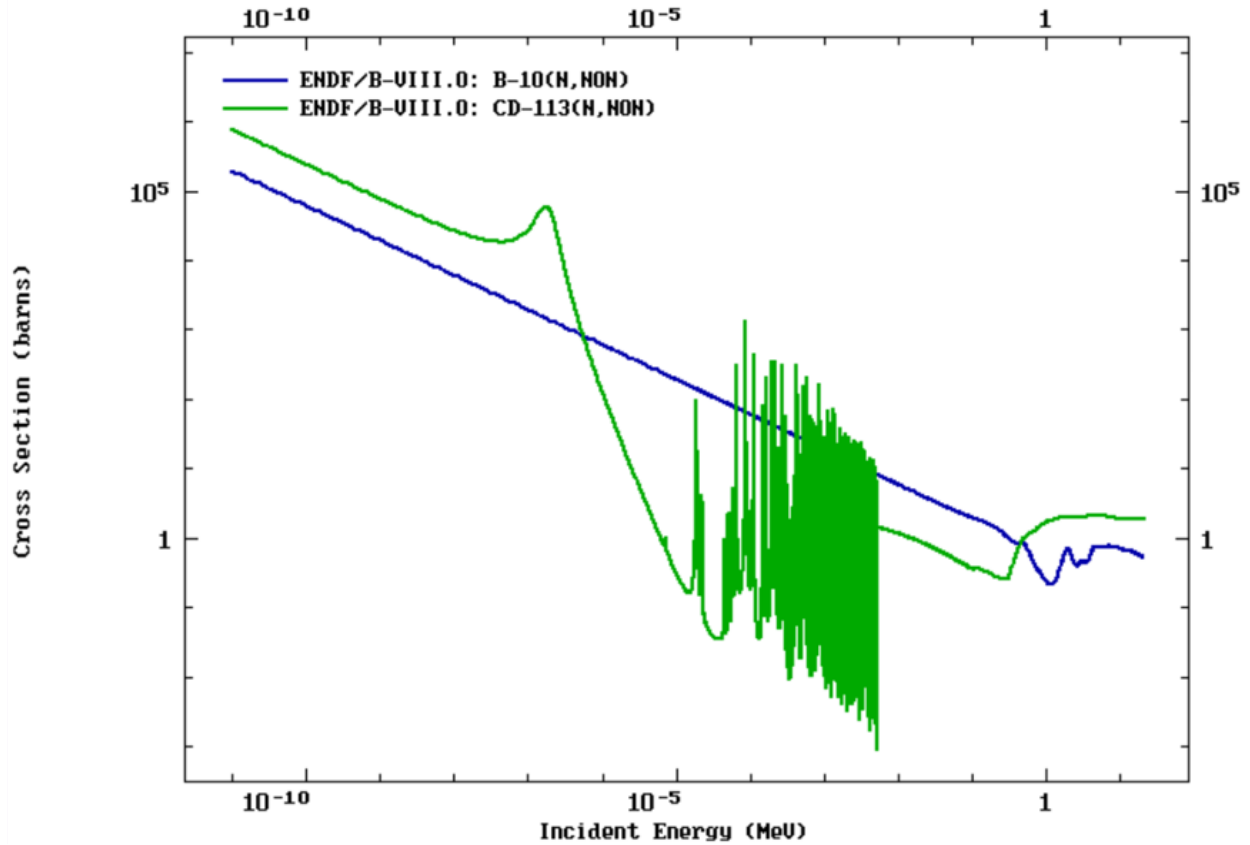


Figure 13. Comparison of cross sections of neutron-absorbing isotopes in DCRA materials.

### 2.2.2 DCRA Effectiveness Considerations

As mentioned in Section 2.2.1, the regulatory approval for use of any potential DCRA design must account for a wide range of parameters. Because the approval process for post-closure criticality is not yet known, this provides information that can be used to form the basis for defining those criteria. One simple way to address characterization of DCRAs is to require specific materials and design characteristics, but another option could be based on neutron absorption criteria per unit mass. For example, analyzing the amount of B-10 per cubic centimeter could be used as a potential demonstration. This type of option allows for the maximum design flexibility.

## 2.3 FEASIBILITY STUDY METHODOLOGY

The KENO models generated by Walker [2] are used as the starting point so that reactivity comparisons can be made where desirable. For each of the NA and DB models, the inserts added by Walker [2] were removed by filling the guide tubes with water. This created an empty template that was made available to the analysis script that performs parametric sweeps, which will fill the now-empty guide tube locations with variations of the DCRA materials used in this analysis.

### 2.3.1 Basket Zones and Fuel Bundle Subzones

The 37 basket locations shown in Figure 6 are arbitrarily divided into zones, as shown in Figure 14.

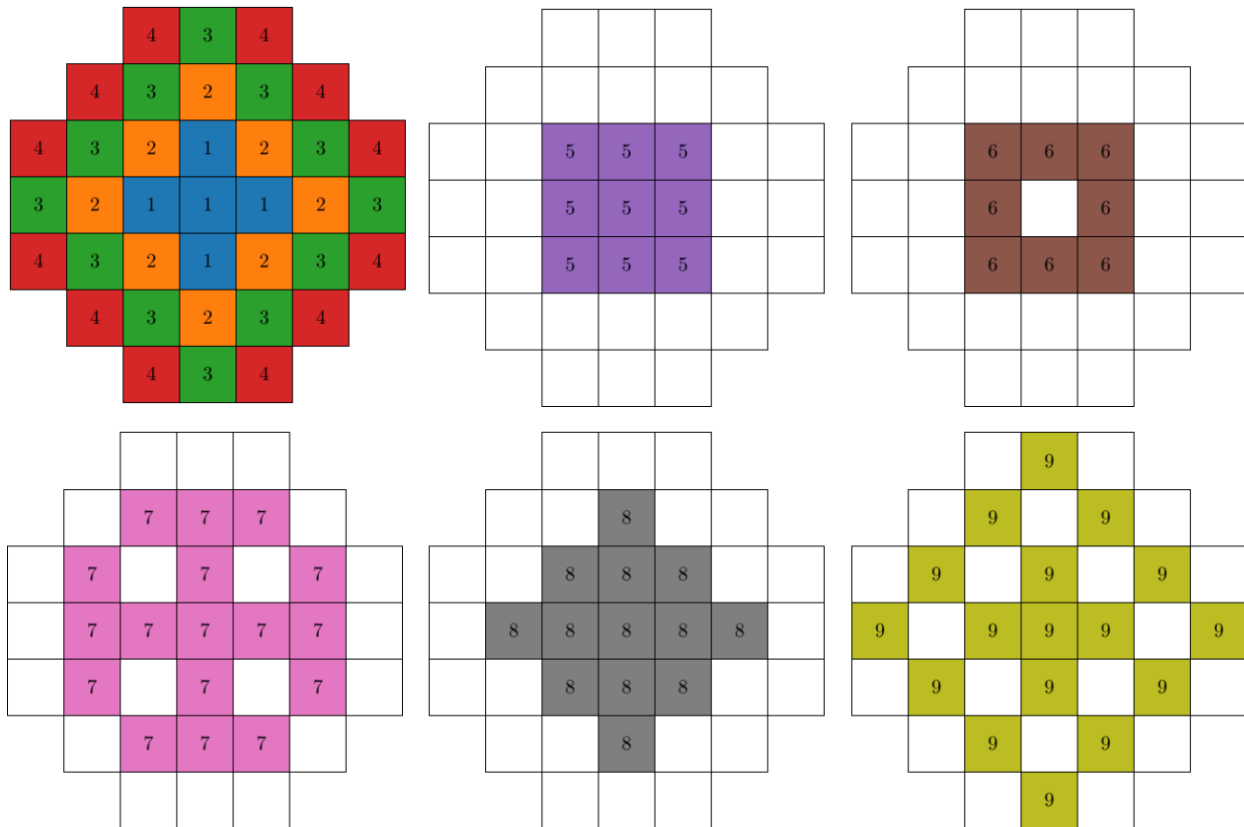


**Figure 14. Location of basket zones.** Note that Zones 1 to 4 are shown together in the figure for convenience but are not included in the same models.

In addition to the zones shown in Figure 14, additional models are used in which all 37 basket locations have DCRA's, which is called *zone 0*. The variations of fuel loading zones are used to evaluate trends for both the as-loaded spent fuel and the fresh fuel models. The variety of zones and fuel compositions allows for an evaluation of the impact that inserting DCRA's within various locations within the cask has on reactivity. Because multiple spent fuel as-loaded cases are being evaluated, the impact from different spent fuel loading patterns can also be explored and compared to impacts caused by fresh fuel loading patterns.

For each location within a basket zone, the fuel bundle guide tube locations are further subdivided into arbitrarily selected subzones in which each bundle within that zone uses the same subzone pattern. Subzones are used to explore the reactivity effect of inserting rods in different patterns within the fuel bundle to explore the overall reactivity impact of the fuel bundle subzone loading patterns. It is of interest to explore how variations in mass of neutron absorbers from various numbers and arrangements of the DCRA's impacts the results. These studies were completed with both fresh and as-loaded compositions using the subzones shown in Figure 15.

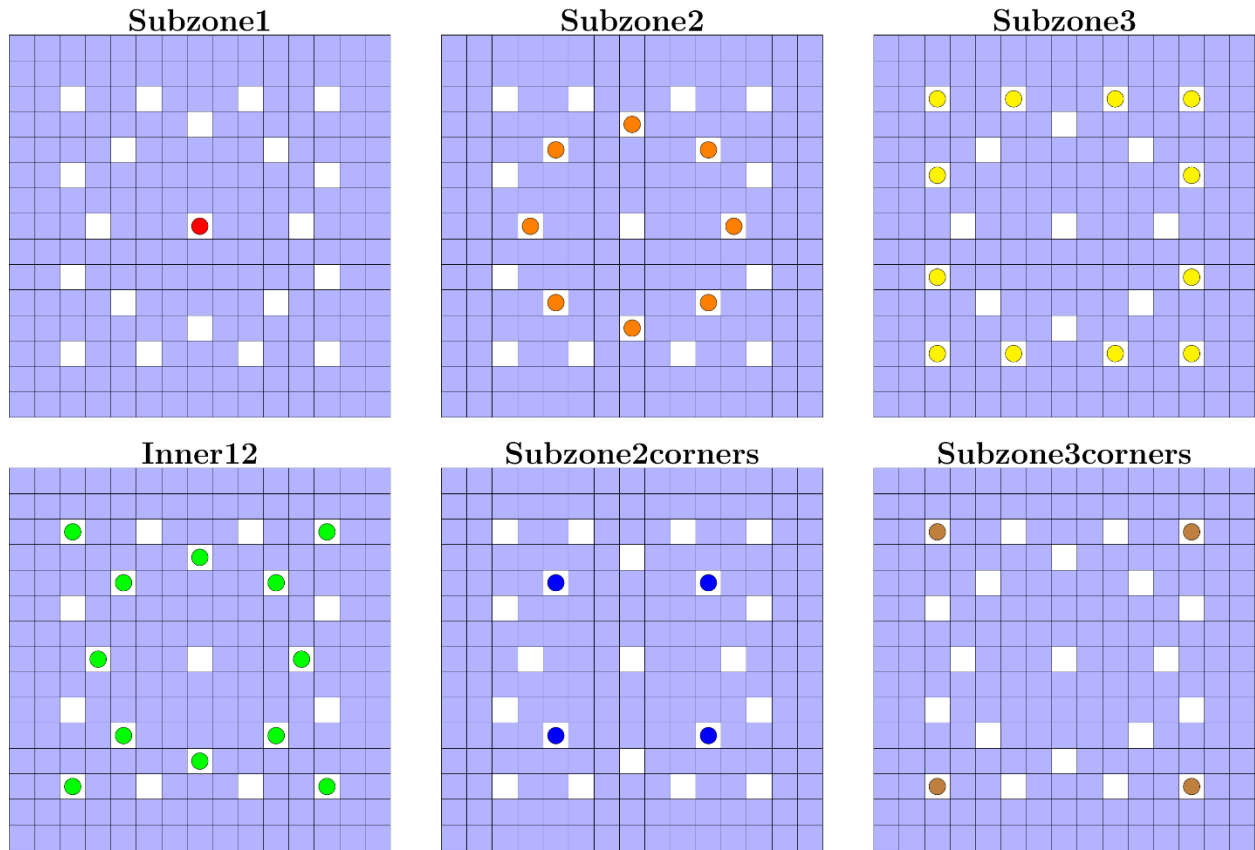


Figure 15. Layout of the various subzones.

Each zone and subzone combination has a unique total number of rods. For each DCRA material and rod size, each zone and subzone combination has a potentially different total DCRA mass. It is important to evaluate the total mass with respect to overall DPC weight limits and neutron absorber mass effectiveness. Information related to the total number of rods is provided in Table 3, and Table 4 through Table 6 present the mass of DCRA materials being compared to the AIC material from Walker [2].

Table 3. Distribution of the number of insert rods by zone and subzone

Zone	Number of locations	Subzone					
		2	2 corners	3	3 corners	Inner 12	All rods
		Rods per subzone					
		8	4	12	4	12	21
		Total number of rods per zone					
0	37	296	148	444	148	444	777
1	5	40	20	60	20	60	105
2	8	64	32	96	32	96	168
3	12	96	48	144	48	144	252
4	12	96	48	144	48	144	252
5	9	72	36	108	36	108	189
6	8	64	32	96	32	96	168
7	17	136	68	204	68	204	357
8	13	104	52	156	52	156	273
9	17	136	68	204	68	204	357

**Table 4. Total mass of B<sub>4</sub>C DCRA's per zone and subzone combination and rod radius**

zone	Number of locations	DCRA with B <sub>4</sub> C (small radius rod = 0.37 cm)						DCRA with B <sub>4</sub> C (large radius rod = 0.64 cm)					
		subzone						subzone					
		2	2 corners	3	3 corners	inner 12	all rods	2	2 corners	3	3 corners	inner 12	all rods
		total zone mass (kg)						total zone mass (kg)					
0	37	4,342	2,171	6,512	2,171	6,512	11,397	12,990	6,495	19,485	6,495	19,485	34,098
1	5	79	40	119	40	119	208	1,755	878	2,633	878	2,633	4,608
2	8	203	101	304	101	304	533	2,809	1,404	4,213	1,404	4,213	7,373
3	12	457	228	685	228	685	1,199	4,213	2,106	6,319	2,106	6,319	11,059
4	12	457	228	685	228	685	1,199	4,213	2,106	6,319	2,106	6,319	11,059
5	9	257	128	385	128	385	674	3,160	1,580	4,739	1,580	4,739	8,294
6	8	203	101	304	101	304	533	2,809	1,404	4,213	1,404	4,213	7,373
7	17	917	458	1,375	458	1,375	2,406	5,968	2,984	8,952	2,984	8,952	15,667
8	13	536	268	804	268	804	1,407	4,564	2,282	6,846	2,282	6,846	11,980
9	17	917	458	1,375	458	1,375	2,406	5,968	2,984	8,952	2,984	8,952	15,667

**Table 5. Total mass of WB<sub>2</sub> DCRA's per zone and subzone combination and rod radius**

Zone	Number of locations	DCRA with WB <sub>2</sub> (small radius rod = 0.37 cm)						DCRA with WB <sub>2</sub> (large radius rod = 0.64 cm)					
		Subzone						Subzone					
		2	2 corners	3	3 corners	Inner 12	All rods	2	2 corners	3	3 corners	Inner 12	All rods
		total zone mass (kg)						total zone mass (kg)					
0	37	26,359	13,180	39,539	13,180	39,539	69,193	78,866	39,433	118,299	39,433	118,299	207,024
1	5	481	241	722	241	722	1,264	10,658	5,329	15,986	5,329	15,986	27,976
2	8	1,232	616	1,848	616	1,848	3,235	17,052	8,526	25,578	8,526	25,578	44,762
3	12	2,773	1,386	4,159	1,386	4,159	7,278	25,578	12,789	38,367	12,789	38,367	67,143
4	12	2,773	1,386	4,159	1,386	4,159	7,278	25,578	12,789	38,367	12,789	38,367	67,143
5	9	1,560	780	2,339	780	2,339	4,094	19,184	9,592	28,776	9,592	28,776	50,357
6	8	1,232	616	1,848	616	1,848	3,235	17,052	8,526	25,578	8,526	25,578	44,762
7	17	5,565	2,782	8,347	2,782	8,347	14,607	36,236	18,118	54,354	18,118	54,354	95,119
8	13	3,254	1,627	4,881	1,627	4,881	8,542	27,710	13,855	41,565	13,855	41,565	72,738
9	17	5,565	2,782	8,347	2,782	8,347	14,607	36,236	18,118	54,354	18,118	54,354	95,119



**Table 6. Total mass of TiB<sub>2</sub> DCRA's per zone and subzone combination and rod radius**

Zone	Number of locations	DCRA with TiB <sub>2</sub> (small radius rod = 0.37 cm)						DCRA with TiB <sub>2</sub> (large radius rod = 0.64 cm)					
		Subzone						Subzone					
		2	2 corners	3	3 corners	Inner 12	All rods	2	2 corners	3	3 corners	Inner 12	All rods
		total zone mass (kg)						total zone mass (kg)					
0	37	7,787	3,894	11,681	3,894	11,681	20,441	23,299	11,650	34,949	11,650	34,949	61,160
1	5	142	71	213	71	213	373	3,149	1,574	4,723	1,574	4,723	8,265
2	8	364	182	546	182	546	956	5,038	2,519	7,556	2,519	7,556	13,224
3	12	819	410	1,229	410	1,229	2,150	7,556	3,778	11,335	3,778	11,335	19,836
4	12	819	410	1,229	410	1,229	2,150	7,556	3,778	11,335	3,778	11,335	19,836
5	9	461	230	691	230	691	1,209	5,667	2,834	8,501	2,834	8,501	14,877
6	8	364	182	546	182	546	956	5,038	2,519	7,556	2,519	7,556	13,224
7	17	1,644	822	2,466	822	2,466	4,315	10,705	5,352	16,057	5,352	16,057	28,101
8	13	961	481	1,442	481	1,442	2,523	8,186	4,093	12,279	4,093	12,279	21,489
9	17	1,644	822	2,466	822	2,466	4,315	10,705	5,352	16,057	5,352	16,057	28,101

### 2.3.2 Analysis Dataset Sequence

The analysis dataset sequence was developed as the analysis progressed and reactivity trends were observed. The objective was to establish the potential effectiveness of DCRA's and estimate the feasibility of their use with respect to their ability to maintain subcriticality under the current worst-case scenarios from UNF-ST&DARDS and from the NA and DB models. The sequence of dataset generation is shown in Table 7.

**Table 7. Characterization of the calculation sets generated by the analysis**

Calculation set	Model(s) type	Zone(s) (locations)	Subzones	Fuel type	DCRA(s)	DCRA rod radius (cm)
1	TSCDF-37- TSCDF-25  NA version	0 (37) 1 (4) 2 (8) 3 (12) 4 (12)	No rods (0) 2 (8) 2 corners (4) 3 (12) 3 corners (4) inner 12 (12) all rods (21)	As-loaded Fresh	AIC B <sub>4</sub> C WB <sub>2</sub> TiB <sub>2</sub>	Small (0.37) Large (0.64)
2	NA dataset	0 (37) 1 (4) 2 (8)	No rods (0) 2 (8) 2 corners (4) inner 12 (12) all rods (21)	As-loaded	WB <sub>2</sub>	Small (0.37) Large (0.64)
3	NA dataset DB dataset	5 (9) 6 (8)	No rods (0) inner 12 (12) all rods (21)	As-loaded Fresh	WB <sub>2</sub>	Small (0.37) Large (0.64)
4	DB dataset	0 (37)	No rods (0) all rods (21)	As-loaded Fresh	WB <sub>2</sub>	Large (0.64)
5	NA dataset DB dataset	7 (17) 8 (13) 9 (17)	No rods (0) inner 12 (12) all rods (21)	As-loaded Fresh	WB <sub>2</sub>	Small (0.37) Large (0.64)
6	TSCDF-37- TSCDF-25  NA version	5 (9) 6 (8) 7 (17) 8 (13) 9 (17)	No rods (0) 2 (8) 2 corners (4) 3 (12) 3 corners (4) inner 12 (12) all rods (21)	As-loaded Fresh	AIC B <sub>4</sub> C WB <sub>2</sub> TiB <sub>2</sub>	Small (0.37) Large (0.64)
7	NA dataset DB dataset	0 (37) 1 (4) 2 (8) 5 (9) 6 (8) 7 (17) 8 (13) 9 (17)	No rods (0) 2 (8) 2 corners (4) 3 (12) inner 12 (12) all rods (21)	As-loaded Fresh	WB <sub>2</sub>	Small (0.37) Large (0.64)

### 2.3.3 Characteristics of the Initial Utility Program

The utility program was written in python, and it can read KENO input created by UNF-ST&DARDS and used by Walker [2] and replace the as-loaded materials and rods (if present in a guide tube) with a different rod loading and pattern. Based on the consistent numbering scheme in the Walker [2] inputs, the modified assemblies may be arbitrarily selected and modified. The loaded rod materials, sizes, and loading patterns are easily modified in the utility program, which enables rapid generation of parametric variations of the models. In addition to modifying the rod geometry and materials, the utility program can change the fuel material in the DPC from as-loaded to fresh fuel. Each new input takes approximately the same runtime as the original Walker [2] input.

Within the utility program, rod materials, rod geometry, rod loading patterns (subzones), and assembly zones are easy to define or modify, which enables an automated way to evaluate the impact of a pre-parameter. An accompanying processing function can read the output files generated by running the models to easily create the comparison plots shown in this report. The program generates new inputs in categorized directories organized by selected parameters, which makes it possible to skip previously generated/processed combinations (i.e., avoids duplicating work).

While the utility program is effective for the purposes in this report, it could easily be expanded to work for a wider range of parameters and features. Possible features for enhancing the python utility program include the following:

- Implementing options for rod geometries other than cylindrical (e.g., annular)
- Implementing options for modifying the water composition
- Implementing more rod materials
- Implementing an option to modify the default rod density
- Implementing more options for fuel material replacement than 5% enriched fresh fuel (e.g., other enrichments or compositions)
- Utilizing other PWR cask designs and fuel designs
- Integrating with UNF-ST&DARDS or remaining as stand alone
- Adding functionality for BWR DPCs and fuel with different insert designs specific to BWR fuel

In addition to the example modifications shown above, a feature could be added to automatically generate an optimal rod loading pattern for a selected input by incorporating heuristics, optimization, and machine learning techniques. In this case, *optimal* should be defined and could have multiple options. This type of method would first determine the most impactful rod locations and would then fill those locations with the number of rods needed to meet a specified criticality goal. The optimization routine could incorporate constraints such as the cost of materials and manufacturing or weight of rod materials. It could also incorporate functionality to select from a set of various post-closure criticality scenario models (e.g., NA, DB, pellet piles).

### 3. RESULTS

The primary focus of this study is to evaluate the potential applicability of variations of DCRA zones and subzone combinations to establish the potential for using standard zone/subzone patterns for all DPCs in a dataset and/or using zone/subzone patterns tailored to DPC specific needs. Both approaches have advantages and disadvantages. For example, the standard zone/subzone approach would necessarily involve larger numbers of DCRAAs, which would increase weight and cost. However, this approach may be more accepted by end users and regulators because of the larger inherent margin they would typically provide. For the tailored zone/subzone approach, each DPC would only include the number and location of DCRAAs needed to preclude subcriticality, thus reducing the weight and cost of the DCRAAs while increasing the technical rigor needed for end users and regulators. These results provide some initial guidance on next steps for both approaches.

The results of the calculations are presented to show the reactivity impact that DCRAAs have with respect to the following parameters:

- Insert rod material (AIC, B<sub>4</sub>C, WB<sub>2</sub> and TiB<sub>2</sub>)
- Insert rod size (small or large)
- Insert rod pattern in a bundle (subzones)
- Number and location of bundles with rods of the same pattern (zones)
- Trend comparison between fresh and as-loaded isotopic compositions
- Trend comparison between as-loaded DPCs
- Trend comparison between NA and DB models

#### 3.1 REACTIVITY TRENDS

The reactivity trends seen in the results of the calculations are discussed below. The results of the calculation sets characterized in Table 7 and are coalesced into figures and tables as needed.

##### 3.1.1 Trends Related to Insert Rod Material, Rod Size, and Subzones

The reactivity trends associated with DCRA material and rod size for various subzones and zones (see Figure 15 and Figure 14, respectively) are plotted as  $k_{\text{eff}}$  vs. absorber mass (both total DCRA mass and important isotope mass separately). Results are provided for as-loaded isotopic compositions in the TSCDF-37-TSCDF-25 DPC and for the fresh fuel case using the TSCDF-37-TSCDF-25 DPC layout. A single DPC was selected based on a higher-than-average reactivity from Walker [2] to evaluate the initial set of parameters being evaluated in this report. This DPC was arbitrarily selected for the studies in this section from among the NA results in Figure 3 because it has a  $k_{\text{eff}}$  of approximately 1.1: one of the primary functions of the DCRA is to maintain DPC subcriticality; therefore, using one of the most reactive NA DPCs is instructive to that end. However, as can be seen in Figure 16, the fissile mass per fuel bundle is not evenly distributed, as is expected for every as-loaded DPC. The DPC seen in Figure 16 is also one of a small number of DPCs with completely empty cells because there was less fuel than needed to fill the DPC after emptying the spent fuel pool.

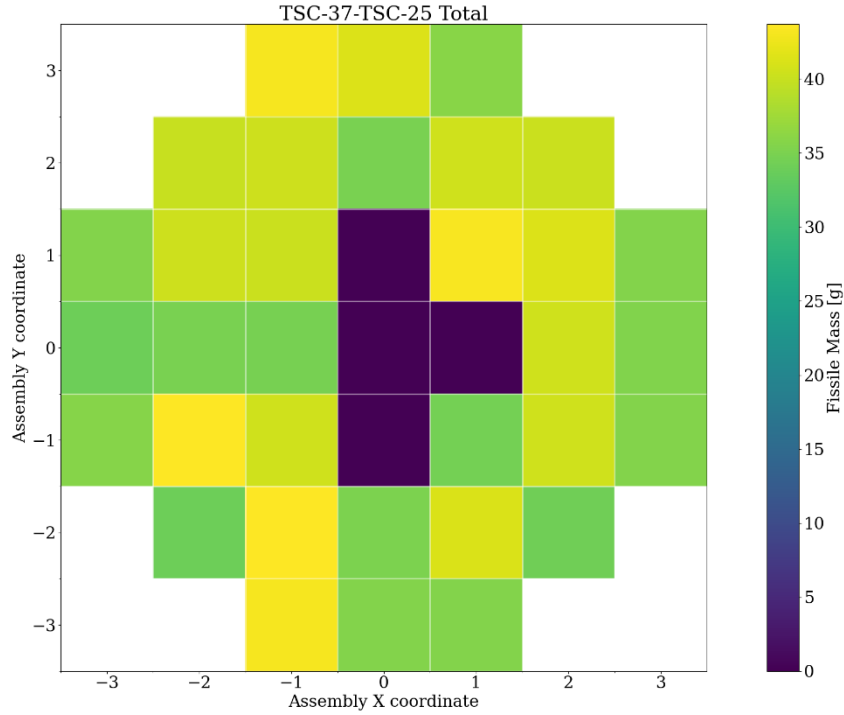


**Figure 16. Total fissile isotope distribution per basket location for NA model TSCDF-37-TSCDF-25.**

An additional visualization of the axial fissile mass distribution per fuel bundle of the fuel in the TSCDF-37-TSCDF-25 DPC is provided in Figure 17. Note that in Figure 17, the numbered zones in the key refer to the same basket locations that are presented in Figure 14 for zone 1 to zone 4 as a means of providing information about the location of those axial nodes in the basket. The dark purple cells indicate the empty locations in the partially filled DPC.

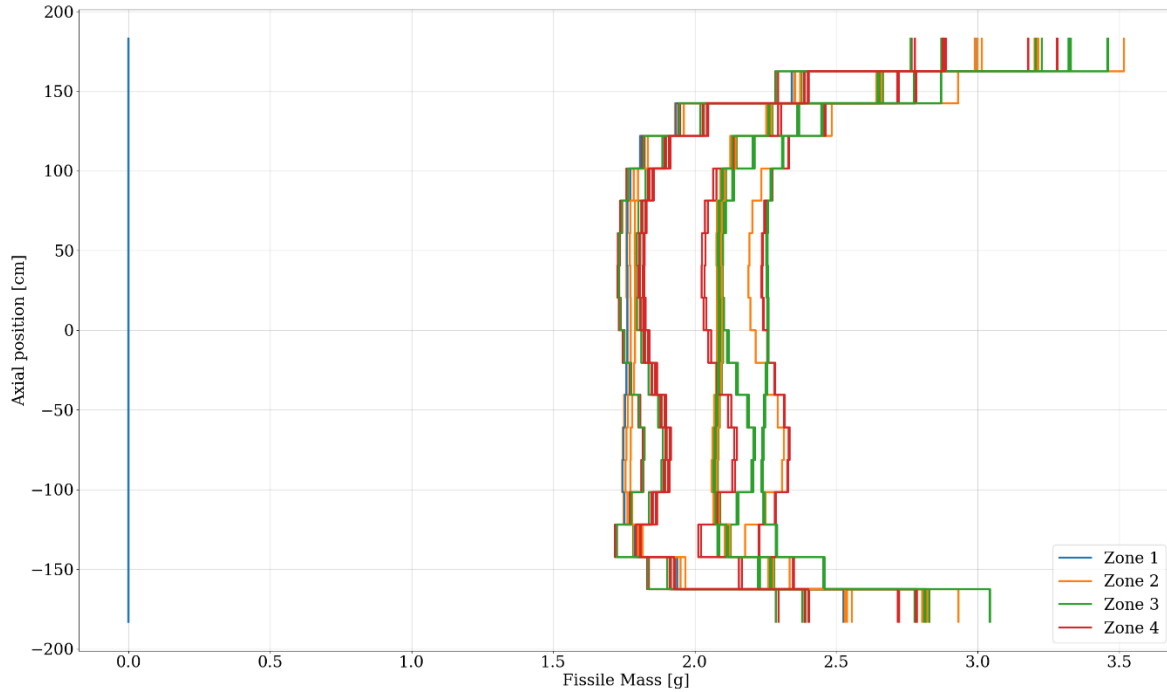


**Figure 17. Axial distribution of the fissile isotope distribution per bundle for NA model TSCDF-37-TSCDF-25.**

In this section, for results of studies using NA model TSCDF-37-TSCDF-25, each DCRA material is presented first with as-loaded fuel compositions, and then it is presented with fresh fuel compositions, followed by a delta-k of fresh-to-spent fuel. Additional plots and results are provided as discussed below.

The results for DCRA with AIC are provided in Figure 18 through Figure 20, the results for DCRA with  $B_4C$  are provided in Figure 21 through Figure 23, the results for DCRA with  $WB_2$  are provided in Figure 24 through Figure 26, and the results for DCRA with  $TiB_2$  are provided in Figure 27 through Figure 29. The calculations provide results for zones 0 through 9 and for subzones with no rods, subzone 2, subzone 2 corners, subzone 3, subzone 3 corners, inner 12 and all rods (see Figure 15). The reactivity trends seen in the results presented in Figure 18 through Figure 20 show the following:

- Trends are relatively consistent between fresh and spent fuel for all DCRA materials.
  - This trend is expected because all DCRA materials are thermal absorbers.
- The fresh fuel cases show that increasing absorber mass reduces reactivity less effectively than in the spent fuel cases.
- The delta-k plots of fresh-to-spent fuel show that Zones 1, 5, 6, and 8 exhibit a delta-k that is 5–10% greater than in the other zones. This indicates that the spent fuel results for those zones have a greater impact on reactivity than in the other zones. These zones are centrally located in the DPC, which suggests that because these zones are in or next to the very high fissile content location seen in Figure 16 in basket location 13 (per diagram shown in Figure 6), they have a greater impact on the as-loaded isotopic compositions for this particular DPC.

- The reactivity impact of the rod size between fresh and spent fuel shows consistency.
  - This is expected because the main difference between the two models is the axial variation in spent fuel, which is not impacted by full-length DCRA. Furthermore, the as-loaded isotopic compositions are average compositions radially among the fuel rods in each axial node, thus limiting the impact of pin-specific spent fuel compositions.
- The total mass of the absorber has a significant impact.
  - Increasing the radius of the absorber does not increase the effectiveness when the total mass is equivalent rod size.
- The total mass of the absorber has a major impact when placed towards the center of the DPC.
  - The trend is almost linear, and using a linear trend would be conservative.
- Absorber effectiveness increases when the absorber mass distribution includes more rods.
  - This trend is seen by matching the total mass with the number of rods used. Larger radius absorbers will result in less rods than smaller radius rods of equivalent total mass. This demonstrates how the economy of neutron absorption can be improved with a given mass.
- The impact of subzones is somewhat minimal. The primary difference based on subzone selection is the number of rods used within the subzone.
- Zones 3 and 4 are of lesser importance. This result is expected because these zones are used to evaluate the exterior regions of the DPC. The absorption of neutrons in this region has less impact because the probability of leaking is higher. However, some care should be taken because some DPCs have failed fuel zones on the exterior of the basket, and these locations may include underburned bundles.

The results presented in Figure 30 compare the delta-k of the DCRA with AIC to the other DCRA materials using subzone all rods (21). This comparison is of interest because the current practice of using RCCAs in DPCs is common, so understanding how DCRA compare with RCCAs is important. The result of this comparison shows that although zones 3 and 4 have no real difference or impact and reactivity, as expected<sup>7</sup>, the AIC material is the most effective across all zones and rod sizes. For most zones and rod sizes, this difference is less than 5% delta-k, providing some confidence that materials other than AIC may also prove very effective as DCRA.

The results presented in Figure 31 compare the delta-k of the fresh fuel to that of as-loaded spent fuel isotopic compositions for all DCRA materials using subzone for all rods (21). This plot essentially summarizes the results in this section regarding the similarity of DCRA materials in neutron maintenance and zone impacts.

It should be noted that the discussion related to reactivity trends presented in Figure 18 through Figure 31 are only directly applicable conclusively to a single DPC layout—the TSCDF-37-TSCDF-25 with the NA configuration. Additional study results are provided for the full NA dataset in Section 3.1.2.

---

<sup>7</sup> Note that the material density is about half theoretical density; however, increasing the density closer to actual does little to further reduce reactivity since maximum blackness is already achieved, per Walker [2].

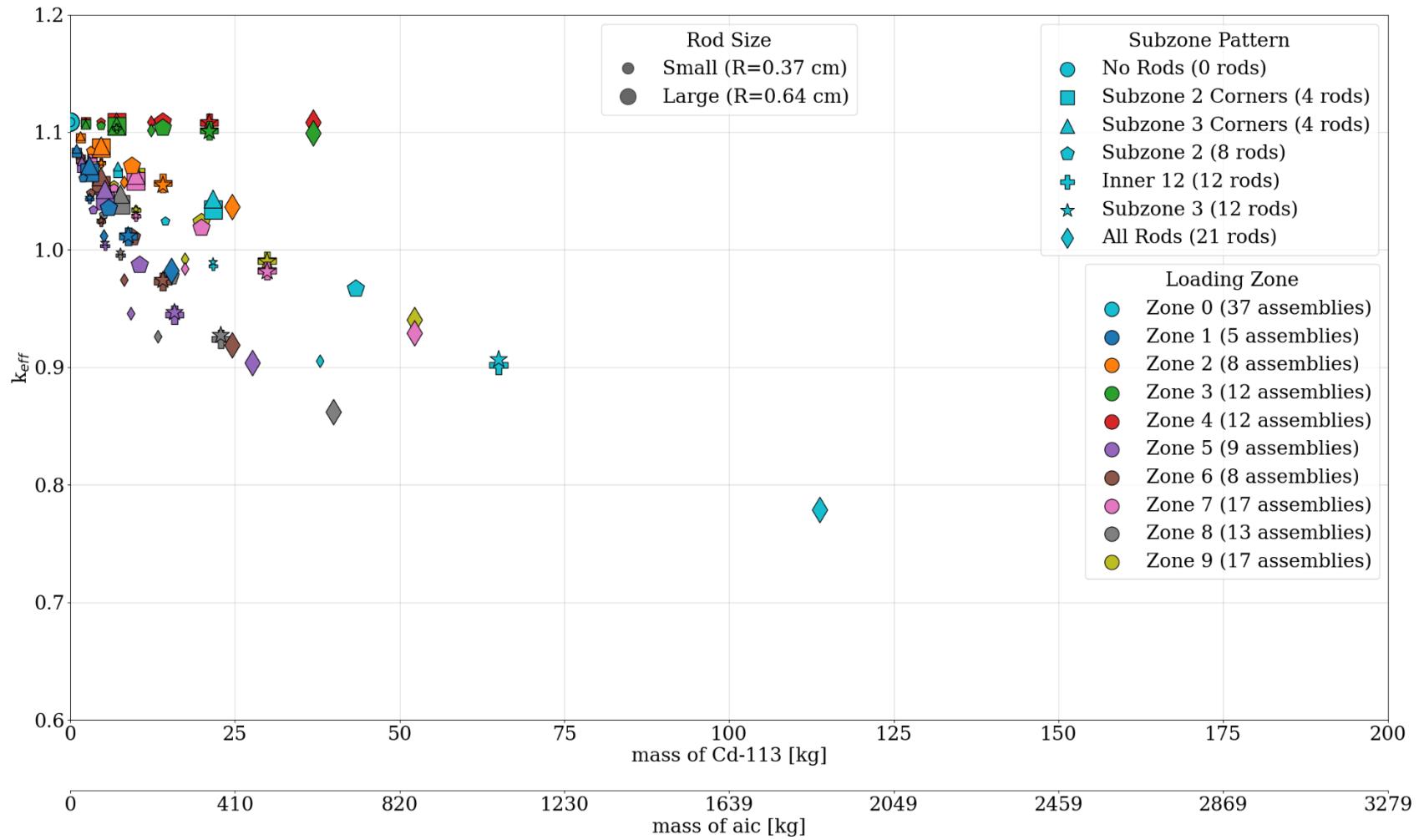
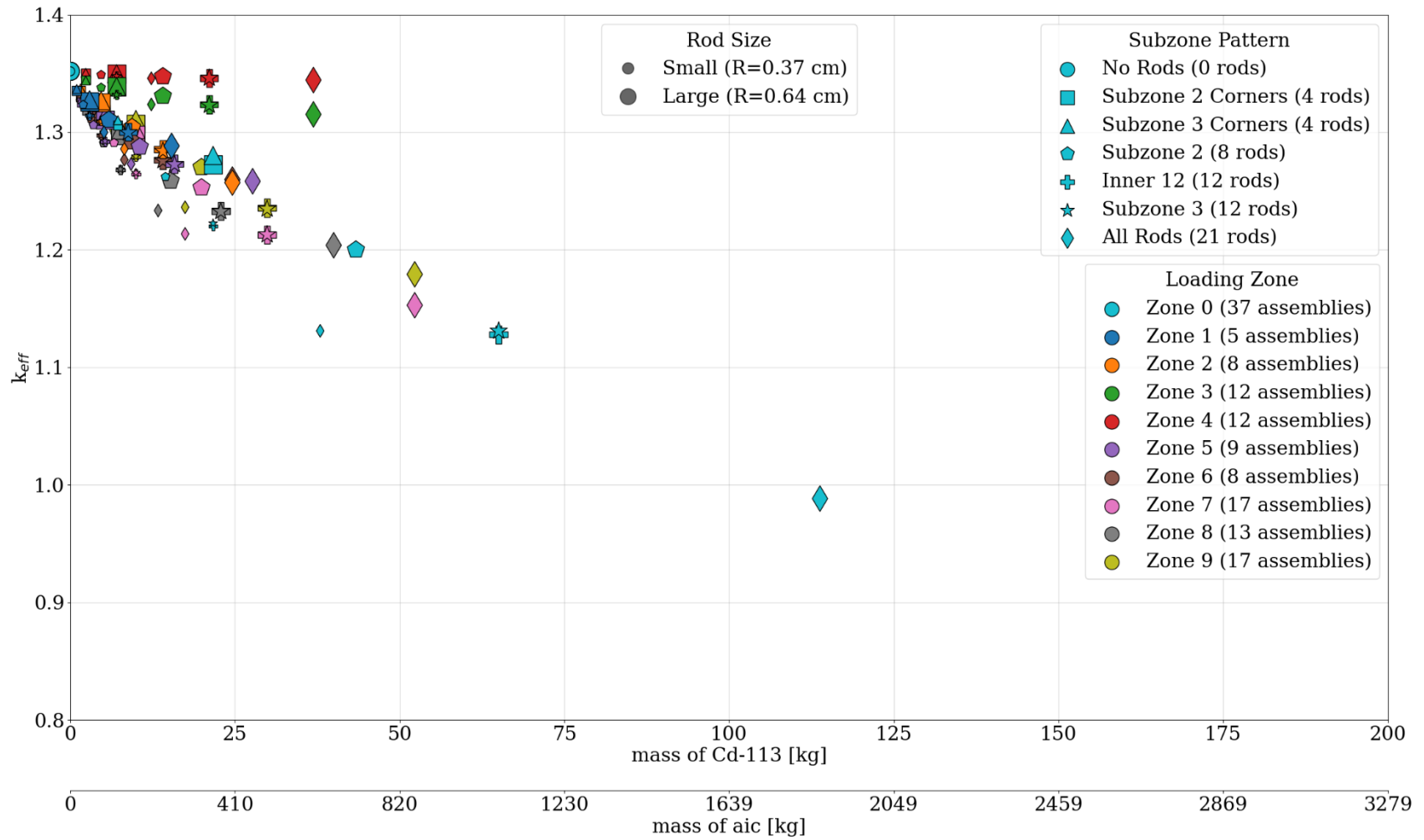


Figure 18. Results of NA model TSCDF-37-TSCDF-25 with DCRA material AIC and as-loaded spent fuel isotopic compositions.





**Figure 19. Results of NA model TSCDF-37-TSCDF-25 with DCRA material AIC and fresh fuel isotopic compositions.**

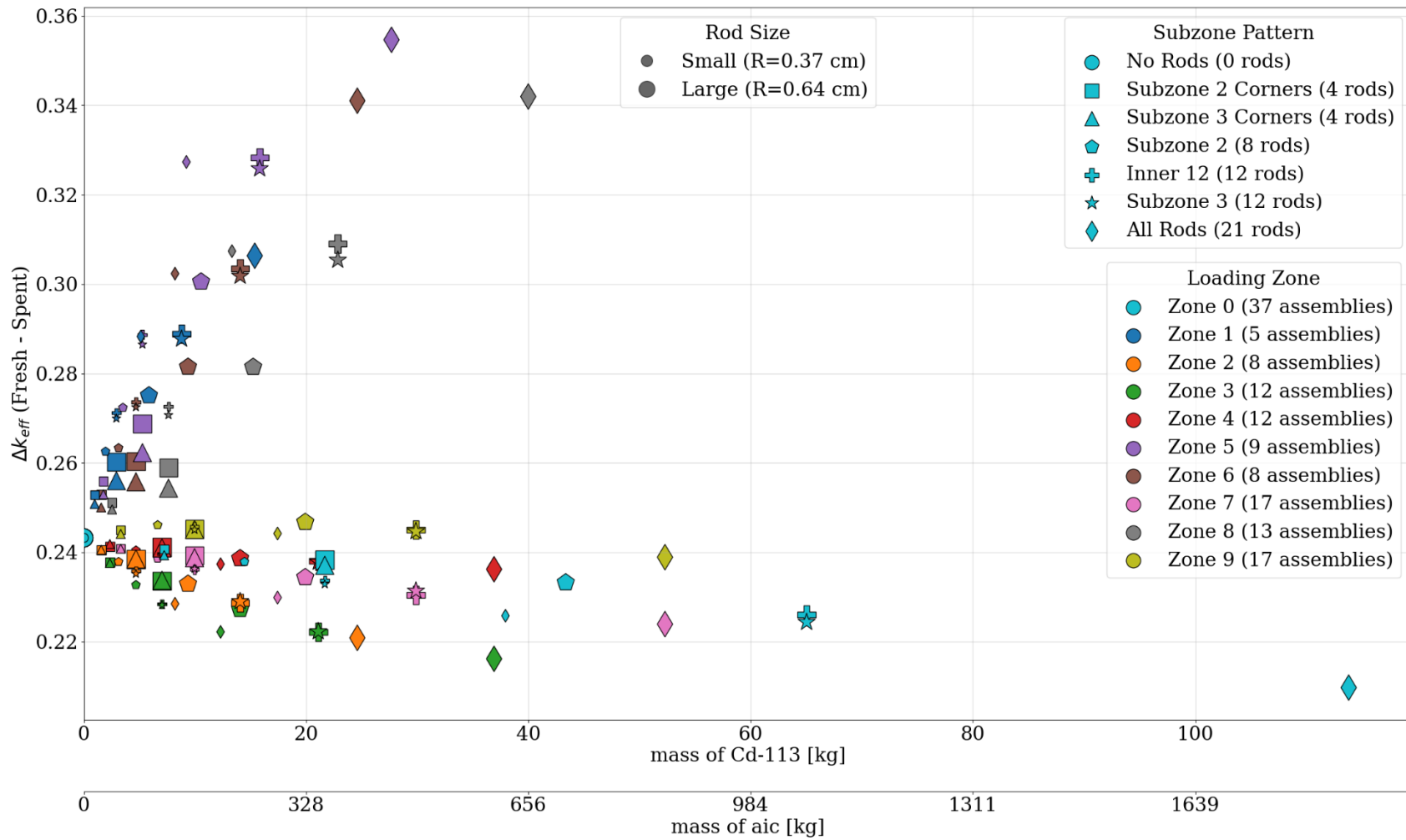


Figure 20. Delta-k of fresh vs. spent fuel isotopic compositions for NA model TSCDF-37-TSCDF-25 with DCRA material AIC.

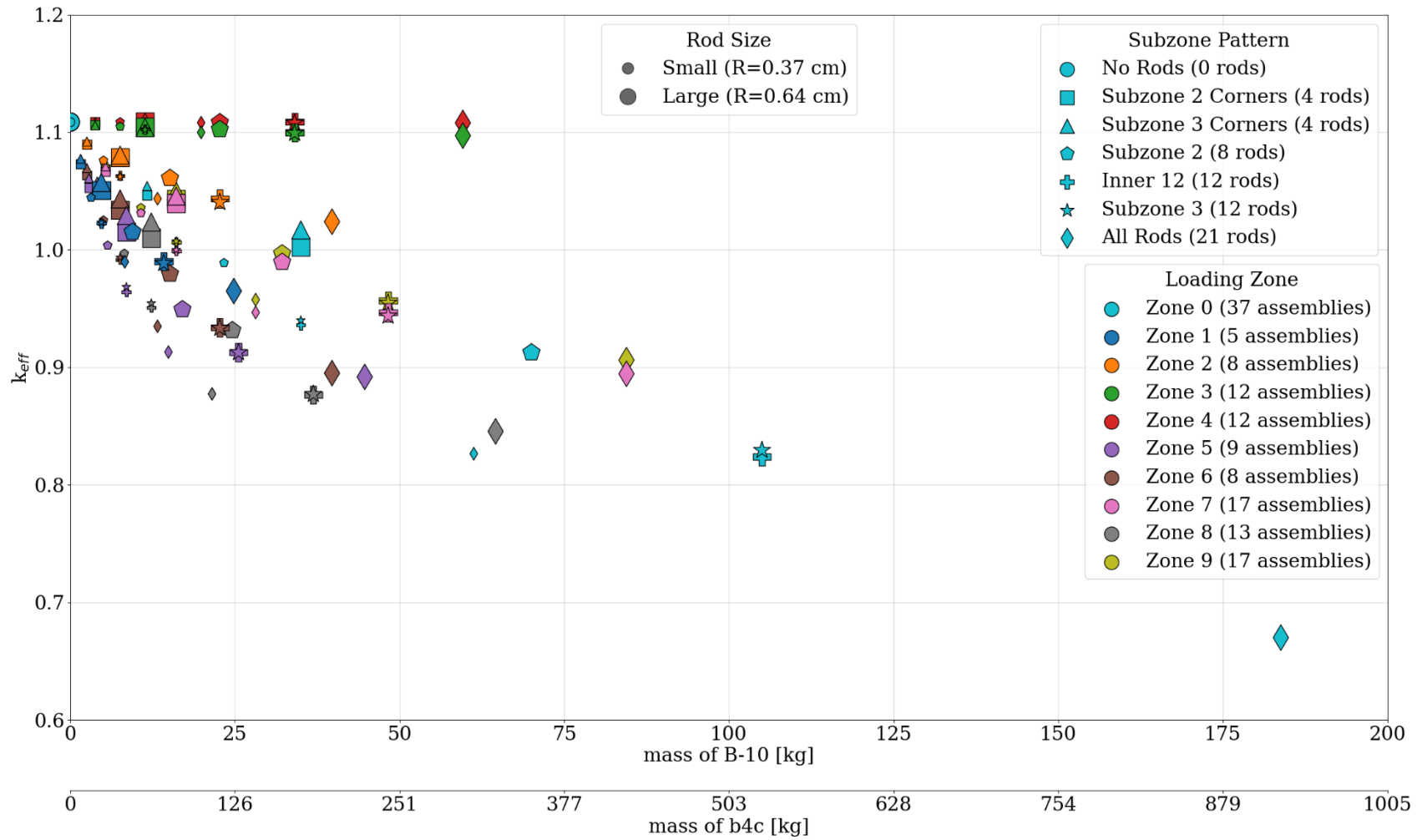


Figure 21. Results of NA model TSCDF-37-TSCDF-25 with DCRA material B<sub>4</sub>C and as-loaded spent fuel isotopic compositions.

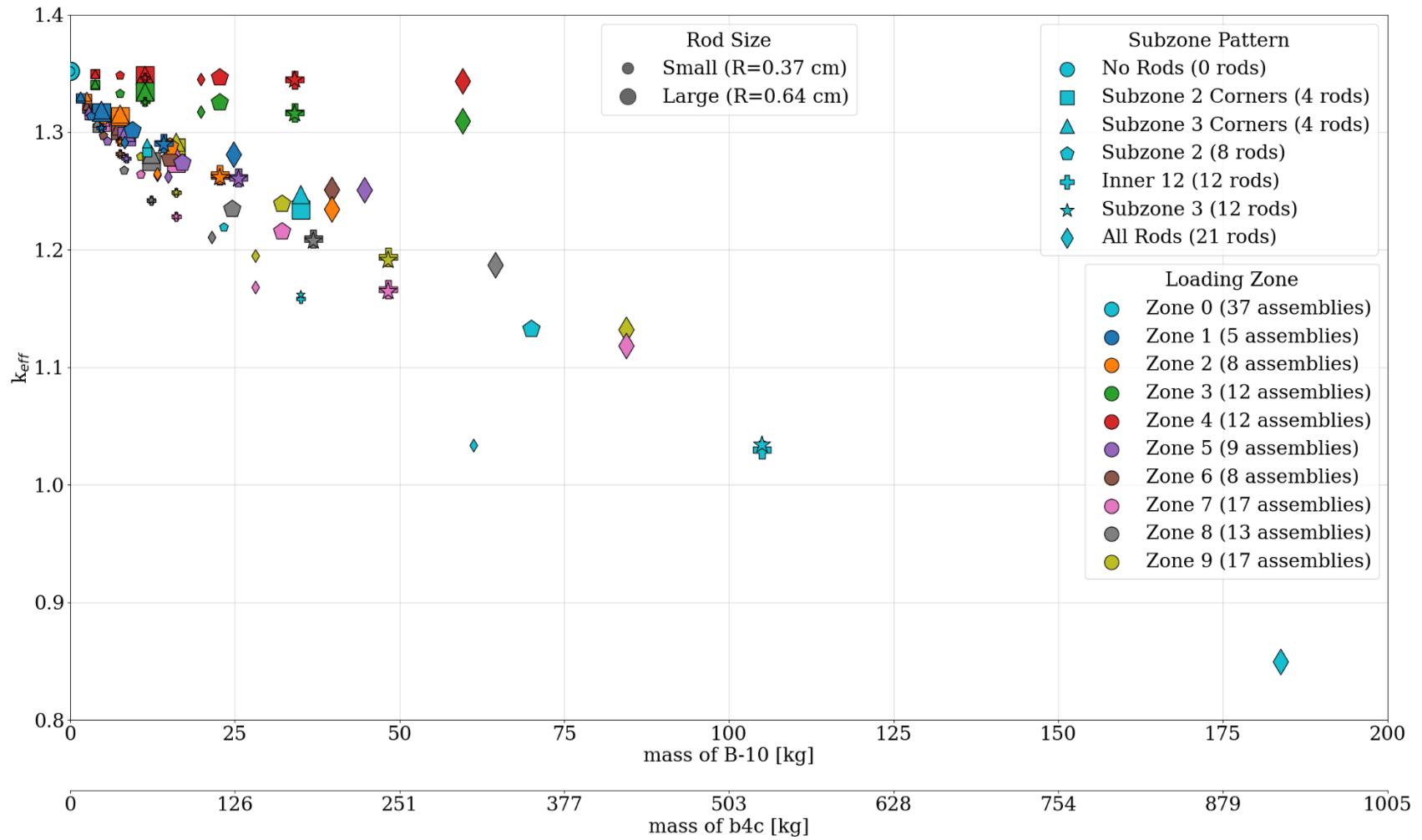


Figure 22. Results of NA model TSCDF-37-TSCDF-25 with DCRA material B<sub>4</sub>C and fresh fuel isotopic compositions.

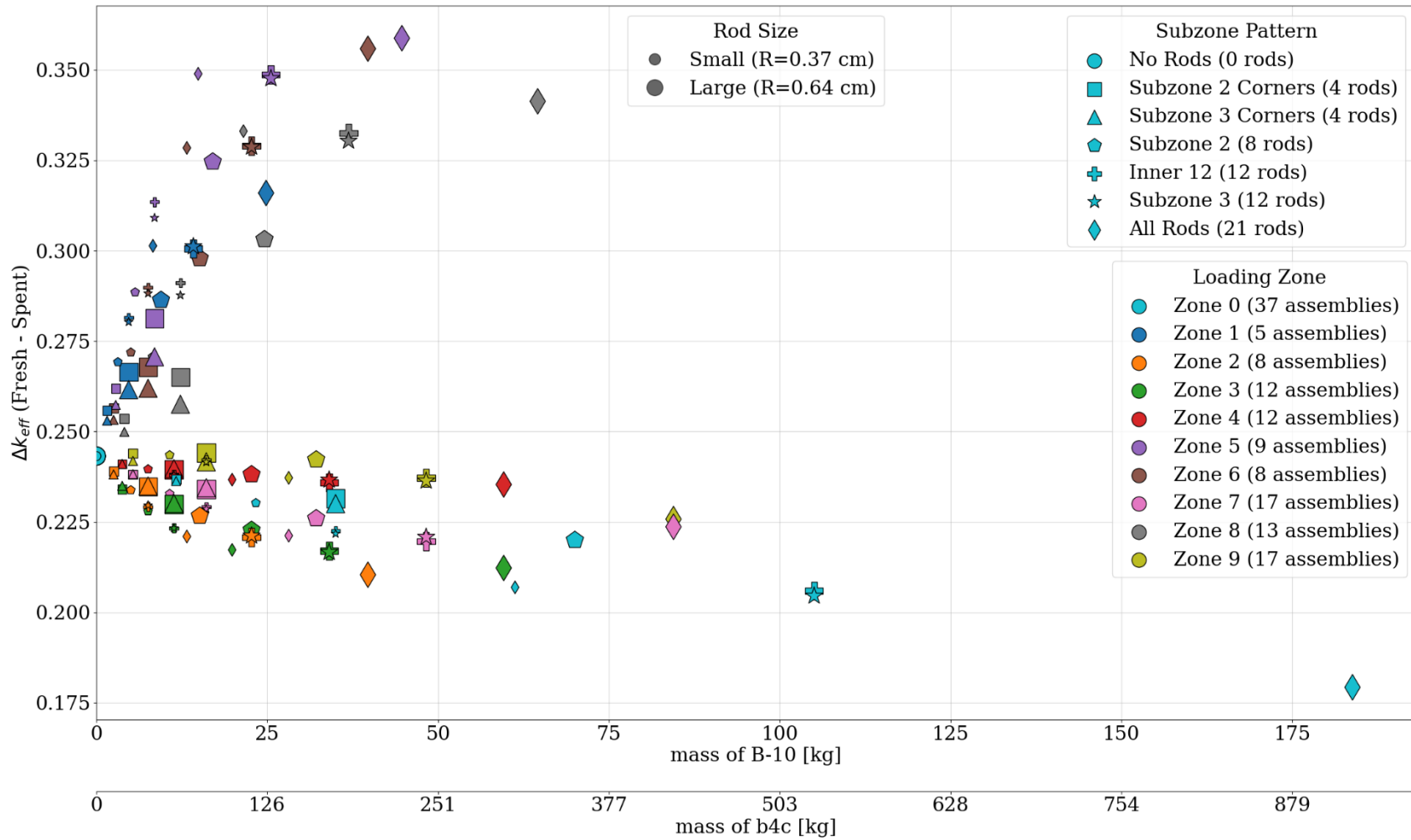


Figure 23. Delta-k of fresh vs. spent fuel isotopic compositions for the NA model TSCDF-37-TSCDF-25 with DCRA material B<sub>4</sub>C.

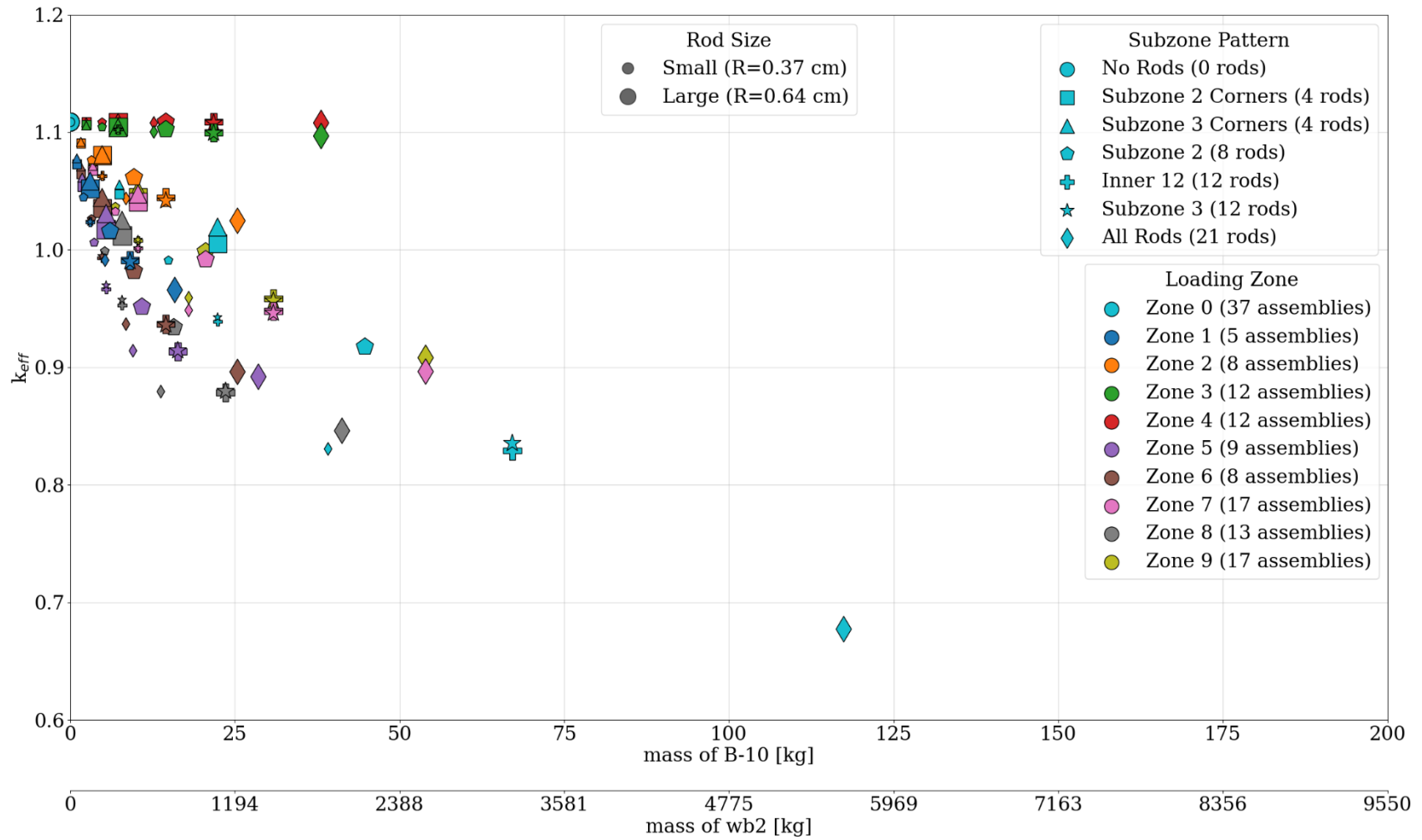


Figure 24. Results of NA model TSCDF-37-TSCDF-25 with DCRA material WB<sub>2</sub> and as-loaded spent fuel isotopic compositions.

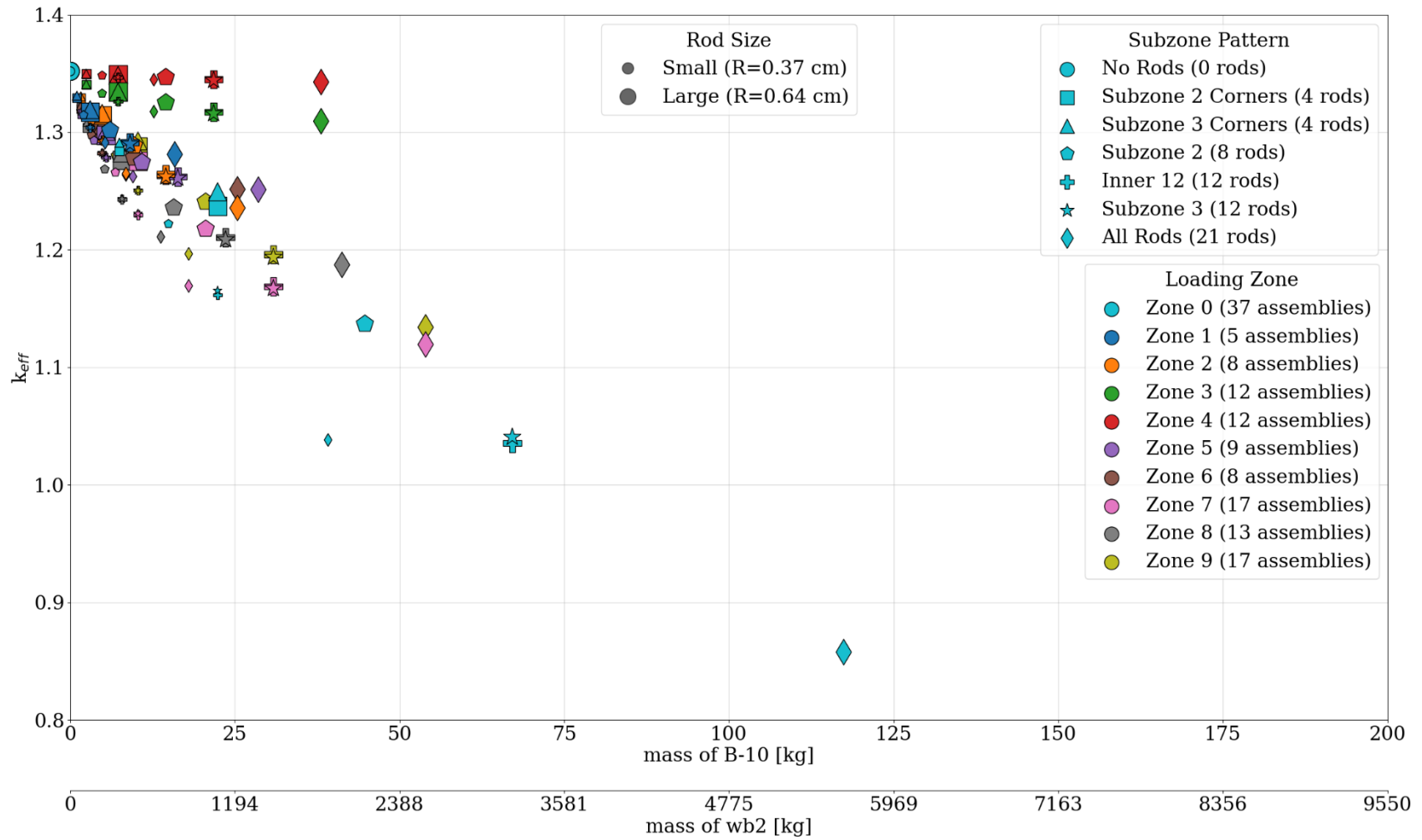


Figure 25. Results of NA model TSCDF-37-TSCDF-25 with DCRA material  $WB_2$  and fresh fuel isotopic compositions.

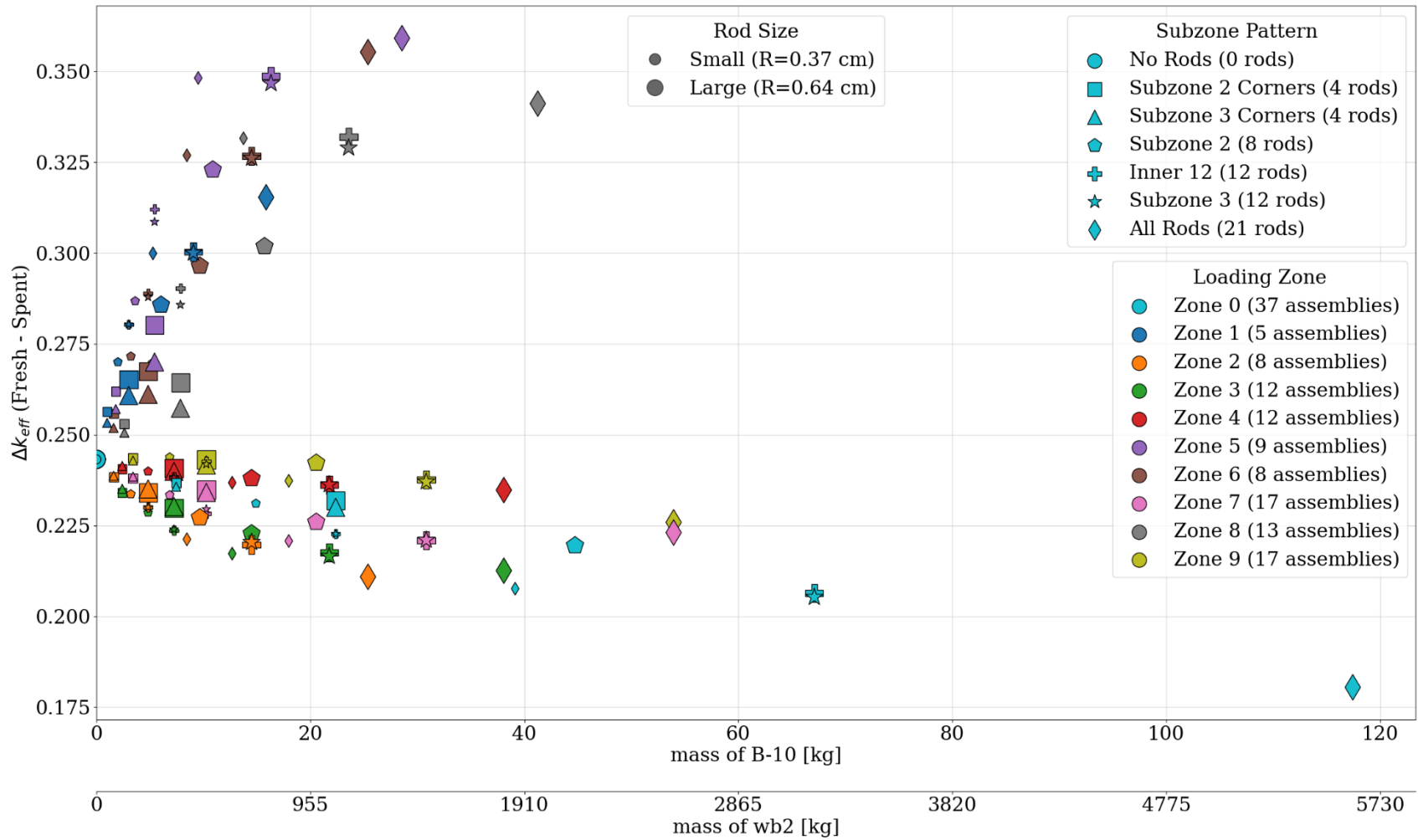


Figure 26. Delta-k of fresh vs. spent fuel isotopic compositions for the NA model TSCDF-37-TSCDF-25 with DCRA material WB<sub>2</sub>.



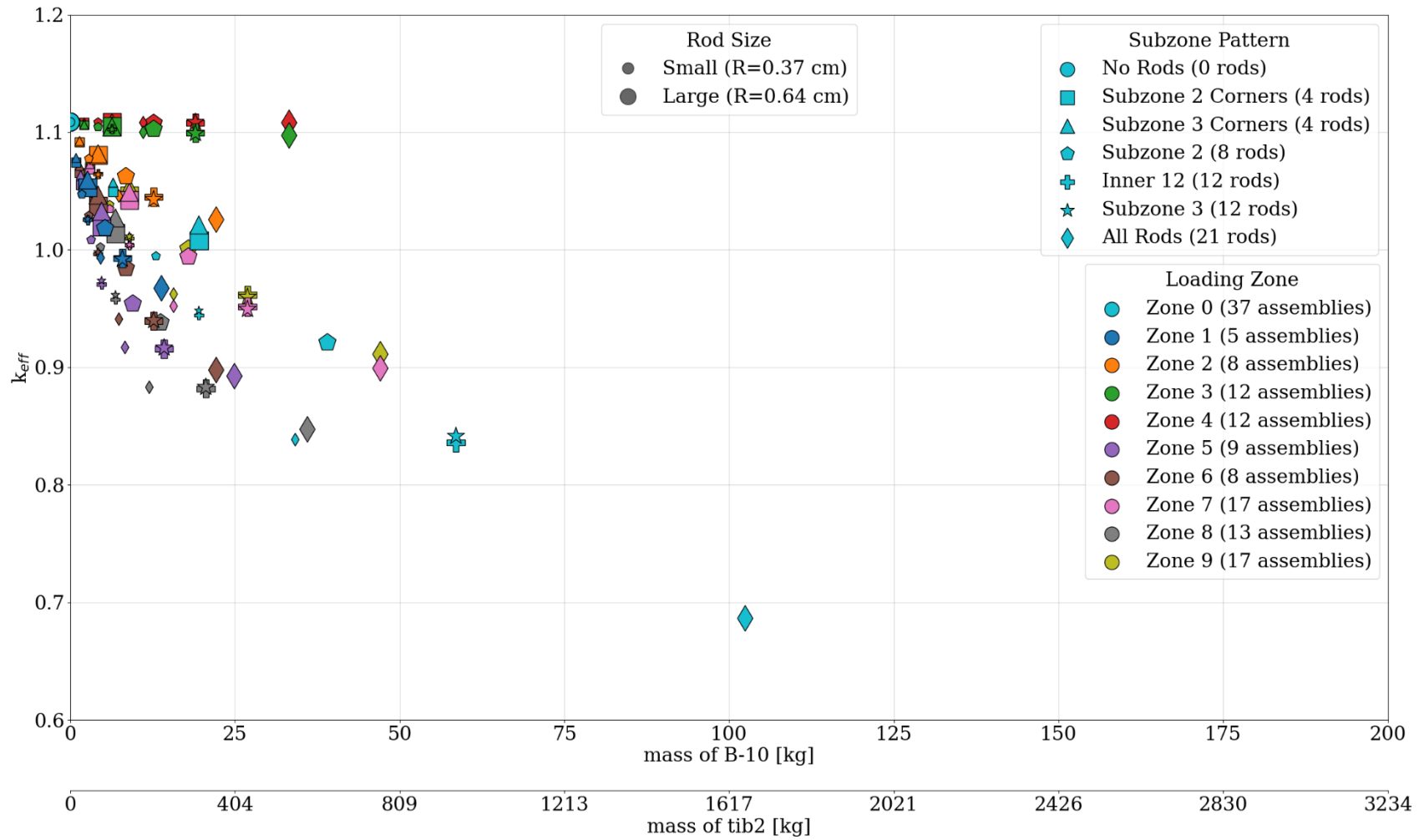


Figure 27. Results of NA model TSCDF-37-TSCDF-25 with DCRA material  $TiB_2$  and as-loaded spent fuel isotopic compositions.

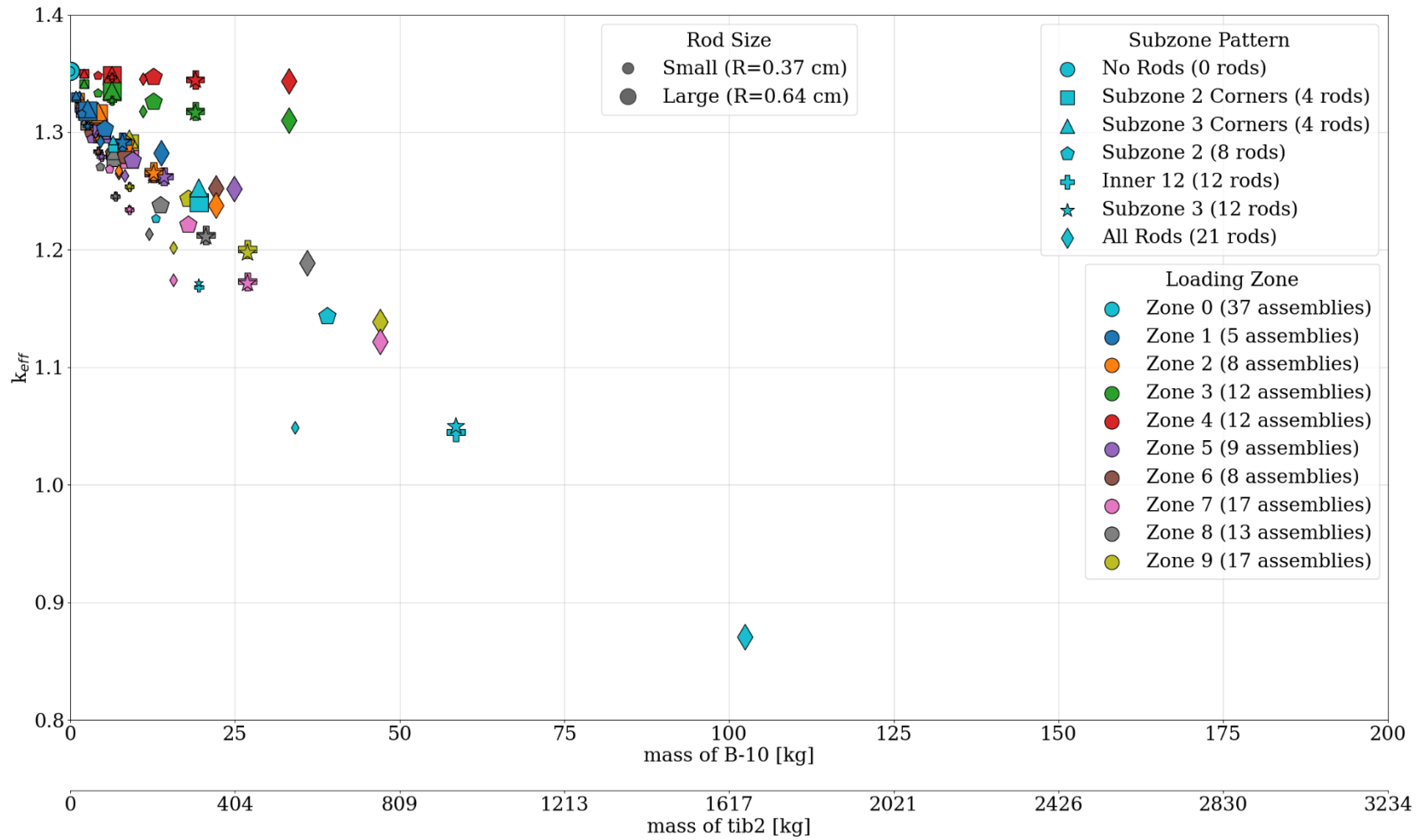


Figure 28. Results of NA model TSCDF-37-TSCDF-25 with DCRA material  $TiB_2$  and fresh fuel isotopic compositions.

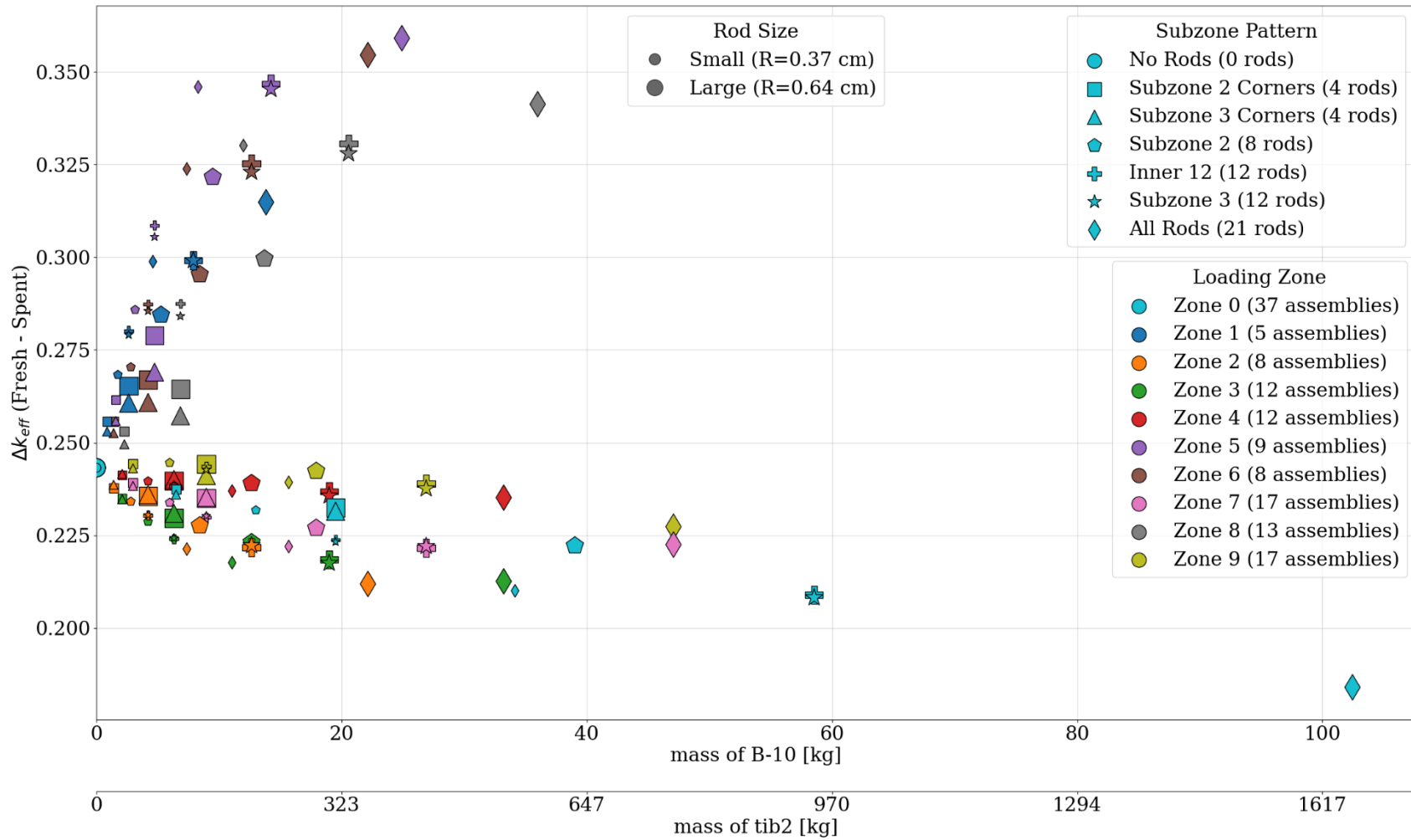
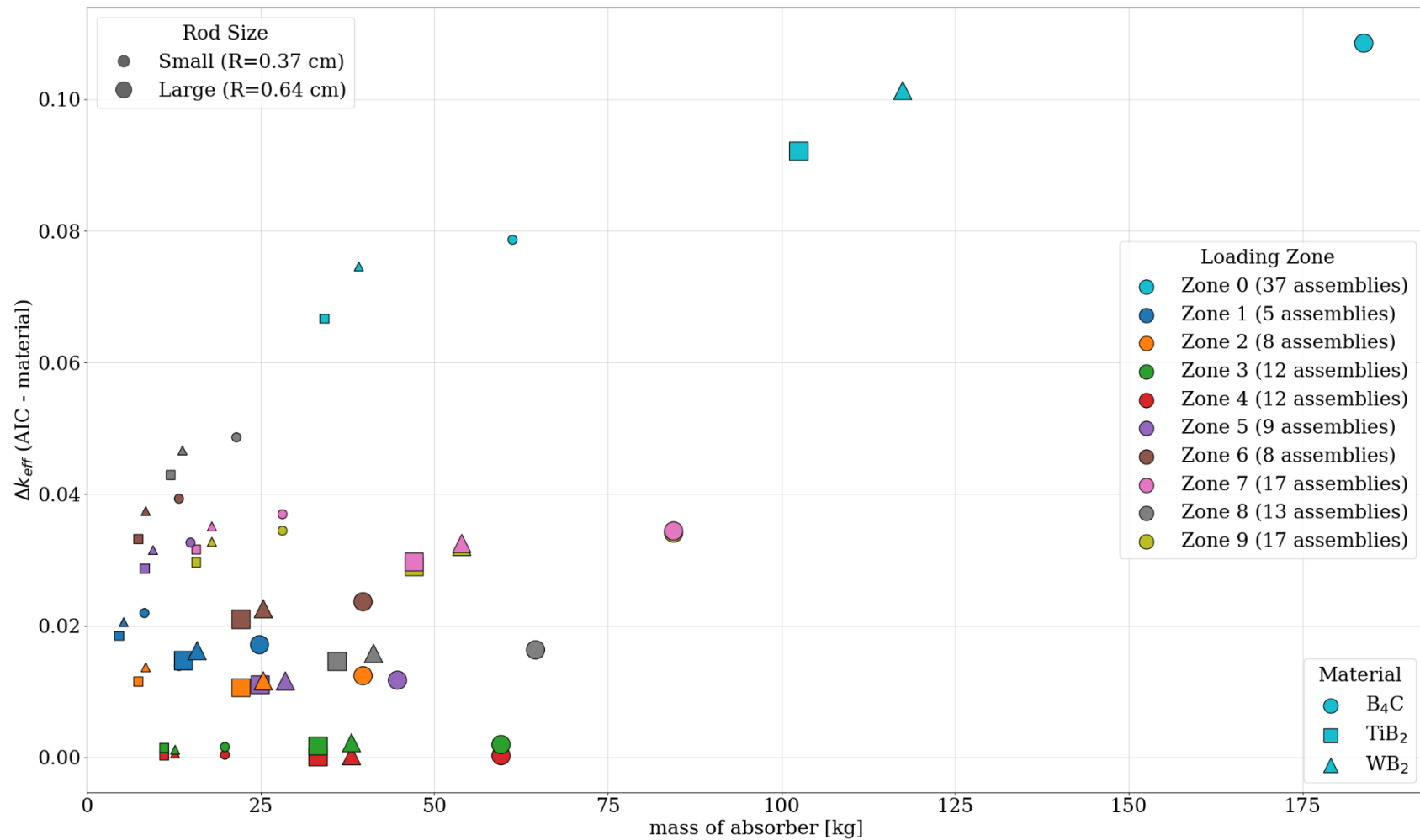
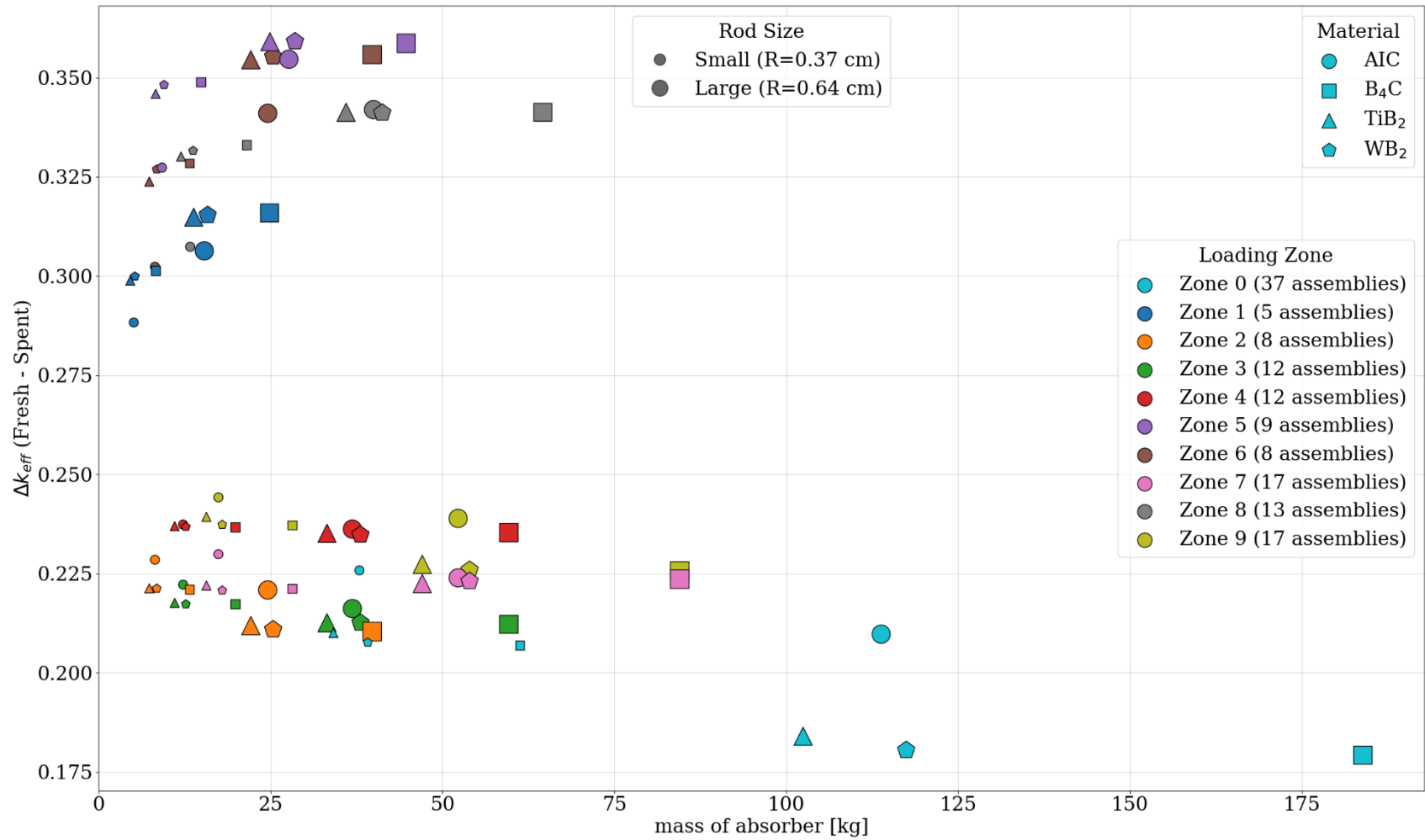


Figure 29. Delta-k of fresh vs. spent fuel isotopic compositions for the NA model TSCDF-37-TSCDF-25 with DCRA material TiB<sub>2</sub>.



**Figure 30. Delta-k of AIC to  $B_4C$ ,  $TiB_2$  and  $WB_2$  DCRA materials, respectively, for spent fuel isotopic compositions for the NA model TSCDF-37-TSCDF-25 for subzone, all rods (21).**



**Figure 31. Comparison of the delta-k results for NA case TSCDF-37-TSCDF-25 with subzone, all rods (21) of fresh-to-spent fuel isotopic compositions for the DCRA materials in all zones.**

### 3.1.2 Results for all NA datasets

The initial results presented in Section 3.1.1 only account for a single as-loaded DPC, which is the TSCDF-37-TSCDF-25 DPC layout selected based on a higher-than-average reactivity from Walker [2]. This DPC was selected to explore the reactivity of various parameter sweeps. As discussed in Section 3.1.1, one of the important conclusions of the initial studies shows that the as-loaded spent fuel isotopic compositions within the various as-loaded DPCs can be expected to impact the relative effectiveness of the study zones and subzones. Although this was expected, the initial studies were performed to initialize the reactivity effect of the basic parameters being considered. In this section, additional calculations are presented for the full NA dataset so that the reactivity trends can be evaluated for all the variations in as-loaded DPCs while focusing on a subset of the previously evaluated parameters. The behavior of various subzone and zone combinations among the as-loaded DPCs is of specific interest with respect to the trends described in Section 3.1.1. It is also important to identify any consistent trends in comparison to those in the fresh fuel cases. Furthermore, it is of interest to evaluate whether the zone and subzone combination with lower DCRA mass totals can maintain subcriticality for some as-loaded configuration and not others because of the variation in loading patterns.

This section presents results for calculations using subzones 2, 2 corners, inner 12, and all rods (21) (see Figure 15). Zone 3 and 4 were not considered because the results given in Section 3.1.1 show these to be low importance DPC regions, although this may not be the case for DPCs with under-burned failed fuel containers. Additionally, because of the general similarity in the results for various DCRA materials, WB<sub>2</sub> was arbitrarily selected for the remaining calculations (see Figure 30 and Figure 31).

The results of the calculations discussed in this section are presented in Figure 32 through Figure 51 and in Table 8 and Table 9. Results for all NA datasets are provided on each plot for all zones except 3 and 4 and for the base model (as-loaded inserts from Zion: the Walker models [2]) and with all rods removed (the UNF-ST&DARDS generated model).

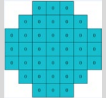
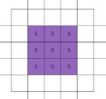
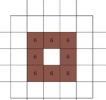
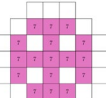
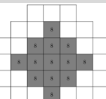
For each subzone, the first plot shows results for the small diameter rods, and the second plot shows results for the large diameter rods. The third plot for each subzone is a delta-k plot of large-to-small diameter rods. Additional plots are included as needed.

The results for subzone 2 are provided in Figure 32 through Figure 34, subzone 2 corners in Figure 35 through Figure 37, and Figure 38 is provided to compare subzone 2 with subzone 2 corners. The results for subzone inner 12 are provided in Figure 40 through Figure 45, including additional delta-k comparisons. The results for subzone all rods (21) is provided in Figure 46 through Figure 51, including additional delta-k comparisons. The results are also summarized and compared to three subcritical limits in Table 8 and Table 9. The reactivity trends seen in the results presented in Table 8 and Table 9 and Figure 32 through Figure 51 show the following:

- Multiple combinations of zones and subzones yield a subcritical configuration for most DPCs.
- The reactivity difference between small and large rods ranges from 1–3 % for most DPCs for most zone and subzone combinations. Some DPCs show much smaller or larger trends.
  - Note that for these delta-k plots, based on the results presented in Section 3.1.1, the large diameter DCRA rods are typically better at maintaining subcriticality (larger rod means lower k), so the figures which compare the reactivity between the large-to-small DCRA rod results are really a comparison between lower k to higher k results, leading to an expectation of negative delta-k results.

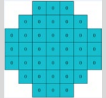
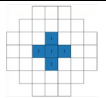
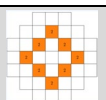
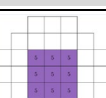
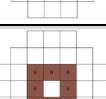
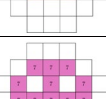
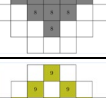
- The impact of large vs. small rods is not uniform among DPCs. This result suggests that as-loaded isotopic compositions which yield variations on locations within the DPC with regions of maximum reactivity are more variable than what might be expected based on a simple neutron leakage assumption. This conclusion suggests that each DPC could utilize a DPC-specific zone/subzone combination to minimize the total mass of absorber and/or the number of DCRA's.
- The reactivity differences resulting from rod size across the various DPCs essentially evaporate for zone 0, which uses the subzone in every location. Some DPCs and zones 8 and 9 approach the same  $\Delta k$  as zone 0. It can be concluded that there is a subset of basket locations for a DPC which can yield the same subcritical impacts as the full basket, or there is an optimum arrangement of zones and subzones which yield the same impact as applying the subzone to the entire DPC.
  - The selection of zone is an important parameter and can impact the amount of absorber needed. For example, several cases show that zone 5 is almost as effective as or potentially more effective than zone 9. Note that zone 9 requires almost double the number of absorbers needed in zone 5.
- Figure 38 uniquely compares the reactivity effect of subzone 2 and subzone 2 corners. Subzone 2 has twice the number of rods than subzone 2 corners. The same reactivity trends seen in the comparison between rod size (i.e., increased absorber mass decreases reactivity discussed above with respect to Figure 34 and Figure 37) is also seen in the comparison of these two subzones, albeit the reactivity impact is twice that of the reactivity difference because of rod size: a maximum of approximately 4–5%  $\Delta k$  for rod size and approximately 8% for subzone (Figure 38).
  - This trend can be more clearly delineated by comparing an equal mass of absorber from the two subzones, as shown in Figure 39, which compares subzone 2 with small rods to subzone 2 corners with large rods. This comparison yields an equivalent absorber mass comparison between the two subzones. Interestingly, the results show very close agreement in reactivity, with the maximum difference ranging between 1–1.5 %  $\Delta k$ . This result shows that absorber mass may be more important than the number of rods or the rod location.
- Comparison of the subzone inner 12 results presented in Figure 42 (spent fuel rod size comparison) and Figure 43 (fresh fuel rod size comparison) provides additional information related to the reactivity effect of large vs. small DCRA's within the various zones. Figure 44 and Figure 45 provide  $\Delta k$  plots of fresh-to-spent fuel for small and large rods, respectively. Rod size does not show significant trends for the inner 12 subzone.
- The subzone all rods (21) results are presented in Figure 46 through Figure 51 in the same manner as presented for the inner 12 subzone. The reactivity trends between both subzones are consistent.

**Table 8. Summary of the zone and subzone results for the NA datasets with large diameter rod DCRA's with WB<sub>2</sub>**

Zone	Subcritical limit	Subzone 2 (8 rods)	Subzone 2 corners (4 rods)	Subzone 3 (12 rods)	Inner 12 (12 rods)	All rods (21 rods)	Zone layout
Zone 0 (37 assemblies)	0.95	39/39 (100.0%)	23/39 (59.0%)	39/39 (100.0%)	39/39 (100.0%)	39/39 (100.0%)	
Zone 0 (37 assemblies)	1	39/39 (100.0%)	35/39 (89.7%)	39/39 (100.0%)	39/39 (100.0%)	39/39 (100.0%)	
Zone 0 (37 assemblies)	1.03	39/39 (100.0%)	39/39 (100.0%)	39/39 (100.0%)	39/39 (100.0%)	39/39 (100.0%)	
Zone 1 (5 assemblies)	0.95	6/39 (15.4%)	2/39 (5.1%)	13/39 (33.3%)	12/39 (30.8%)	14/39 (35.9%)	
Zone 1 (5 assemblies)	1	29/39 (74.4%)	22/39 (56.4%)	39/39 (100.0%)	39/39 (100.0%)	39/39 (100.0%)	
Zone 1 (5 assemblies)	1.03	39/39 (100.0%)	33/39 (84.6%)	39/39 (100.0%)	39/39 (100.0%)	39/39 (100.0%)	
Zone 2 (8 assemblies)	0.95	13/39 (33.3%)	8/39 (20.5%)	13/39 (33.3%)	13/39 (33.3%)	16/39 (41.0%)	
Zone 2 (8 assemblies)	1	25/39 (64.1%)	18/39 (46.2%)	32/39 (82.1%)	31/39 (79.5%)	34/39 (87.2%)	
Zone 2 (8 assemblies)	1.03	34/39 (87.2%)	27/39 (69.2%)	35/39 (89.7%)	35/39 (89.7%)	36/39 (92.3%)	
Zone 5 (9 assemblies)	0.95	18/39 (46.2%)	12/39 (30.8%)	22/39 (56.4%)	22/39 (56.4%)	22/39 (56.4%)	
Zone 5 (9 assemblies)	1	39/39 (100.0%)	34/39 (87.2%)	39/39 (100.0%)	39/39 (100.0%)	39/39 (100.0%)	
Zone 5 (9 assemblies)	1.03	39/39 (100.0%)	39/39 (100.0%)	39/39 (100.0%)	39/39 (100.0%)	39/39 (100.0%)	
Zone 6 (8 assemblies)	0.95	17/39 (43.6%)	11/39 (28.2%)	21/39 (53.8%)	19/39 (48.7%)	22/39 (56.4%)	
Zone 6 (8 assemblies)	1	39/39 (100.0%)	30/39 (76.9%)	39/39 (100.0%)	39/39 (100.0%)	39/39 (100.0%)	
Zone 6 (8 assemblies)	1.03	39/39 (100.0%)	35/39 (89.7%)	39/39 (100.0%)	39/39 (100.0%)	39/39 (100.0%)	
Zone 7 (17 assemblies)	0.95	19/39 (48.7%)	14/39 (35.9%)	28/39 (71.8%)	24/39 (61.5%)	33/39 (84.6%)	
Zone 7 (17 assemblies)	1	39/39 (100.0%)	28/39 (71.8%)	39/39 (100.0%)	39/39 (100.0%)	39/39 (100.0%)	
Zone 7 (17 assemblies)	1.03	39/39 (100.0%)	35/39 (89.7%)	39/39 (100.0%)	39/39 (100.0%)	39/39 (100.0%)	
Zone 8 (13 assemblies)	0.95	22/39 (56.4%)	16/39 (41.0%)	22/39 (56.4%)	22/39 (56.4%)	22/39 (56.4%)	
Zone 8 (13 assemblies)	1	39/39 (100.0%)	35/39 (89.7%)	39/39 (100.0%)	39/39 (100.0%)	39/39 (100.0%)	
Zone 8 (13 assemblies)	1.03	39/39 (100.0%)	39/39 (100.0%)	39/39 (100.0%)	39/39 (100.0%)	39/39 (100.0%)	
Zone 9 (17 assemblies)	0.95	17/39 (43.6%)	13/39 (33.3%)	23/39 (59.0%)	23/39 (59.0%)	33/39 (84.6%)	
Zone 9 (17 assemblies)	1	36/39 (92.3%)	26/39 (66.7%)	39/39 (100.0%)	39/39 (100.0%)	39/39 (100.0%)	
Zone 9 (17 assemblies)	1.03	39/39 (100.0%)	35/39 (89.7%)	39/39 (100.0%)	39/39 (100.0%)	39/39 (100.0%)	



**Table 9. Summary of the zone and subzone results for the NA datasets with small diameter rod DCRA's with WB<sub>2</sub>**

Zone	Subcritical Limit	Subzone 2 (8 rods)	Subzone 2 corners (4 rods)	Subzone 3 (12 rods)	Inner 12 (12 rods)	All rods (21 rods)	Zone layout
Zone 0 (37 assemblies)	0.95	28/39 (71.8%)	16/39 (41.0%)	38/39 (97.4%)	39/39 (100.0%)	39/39 (100.0%)	
Zone 0 (37 assemblies)	1	38/39 (97.4%)	27/39 (69.2%)	39/39 (100.0%)	39/39 (100.0%)	39/39 (100.0%)	
Zone 0 (37 assemblies)	1.03	39/39 (100.0%)	35/39 (89.7%)	39/39 (100.0%)	39/39 (100.0%)	39/39 (100.0%)	
Zone 1 (5 assemblies)	0.95	2/39 (5.1%)	1/39 (2.6%)	6/39 (15.4%)	6/39 (15.4%)	13/39 (33.3%)	
Zone 1 (5 assemblies)	1	23/39 (59.0%)	18/39 (46.2%)	28/39 (71.8%)	28/39 (71.8%)	39/39 (100.0%)	
Zone 1 (5 assemblies)	1.03	34/39 (87.2%)	28/39 (71.8%)	39/39 (100.0%)	39/39 (100.0%)	39/39 (100.0%)	
Zone 2 (8 assemblies)	0.95	10/39 (25.6%)	3/39 (7.7%)	13/39 (33.3%)	13/39 (33.3%)	13/39 (33.3%)	
Zone 2 (8 assemblies)	1	19/39 (48.7%)	16/39 (41.0%)	24/39 (61.5%)	24/39 (61.5%)	31/39 (79.5%)	
Zone 2 (8 assemblies)	1.03	29/39 (74.4%)	24/39 (61.5%)	33/39 (84.6%)	33/39 (84.6%)	35/39 (89.7%)	
Zone 5 (9 assemblies)	0.95	14/39 (35.9%)	4/39 (10.3%)	17/39 (43.6%)	18/39 (46.2%)	22/39 (56.4%)	
Zone 5 (9 assemblies)	1	35/39 (89.7%)	22/39 (56.4%)	39/39 (100.0%)	39/39 (100.0%)	39/39 (100.0%)	
Zone 5 (9 assemblies)	1.03	39/39 (100.0%)	33/39 (84.6%)	39/39 (100.0%)	39/39 (100.0%)	39/39 (100.0%)	
Zone 6 (8 assemblies)	0.95	12/39 (30.8%)	3/39 (7.7%)	16/39 (41.0%)	17/39 (43.6%)	19/39 (48.7%)	
Zone 6 (8 assemblies)	1	33/39 (84.6%)	21/39 (53.8%)	36/39 (92.3%)	36/39 (92.3%)	39/39 (100.0%)	
Zone 6 (8 assemblies)	1.03	36/39 (92.3%)	32/39 (82.1%)	39/39 (100.0%)	39/39 (100.0%)	39/39 (100.0%)	
Zone 7 (17 assemblies)	0.95	15/39 (38.5%)	8/39 (20.5%)	18/39 (46.2%)	18/39 (46.2%)	24/39 (61.5%)	
Zone 7 (17 assemblies)	1	30/39 (76.9%)	19/39 (48.7%)	35/39 (89.7%)	35/39 (89.7%)	39/39 (100.0%)	
Zone 7 (17 assemblies)	1.03	35/39 (89.7%)	30/39 (76.9%)	39/39 (100.0%)	39/39 (100.0%)	39/39 (100.0%)	
Zone 8 (13 assemblies)	0.95	17/39 (43.6%)	9/39 (23.1%)	18/39 (46.2%)	18/39 (46.2%)	22/39 (56.4%)	
Zone 8 (13 assemblies)	1	36/39 (92.3%)	24/39 (61.5%)	39/39 (100.0%)	39/39 (100.0%)	39/39 (100.0%)	
Zone 8 (13 assemblies)	1.03	39/39 (100.0%)	34/39 (87.2%)	39/39 (100.0%)	39/39 (100.0%)	39/39 (100.0%)	
Zone 9 (17 assemblies)	0.95	14/39 (35.9%)	7/39 (17.9%)	16/39 (41.0%)	16/39 (41.0%)	23/39 (59.0%)	
Zone 9 (17 assemblies)	1	28/39 (71.8%)	19/39 (48.7%)	35/39 (89.7%)	35/39 (89.7%)	39/39 (100.0%)	
Zone 9 (17 assemblies)	1.03	35/39 (89.7%)	29/39 (74.4%)	39/39 (100.0%)	39/39 (100.0%)	39/39 (100.0%)	

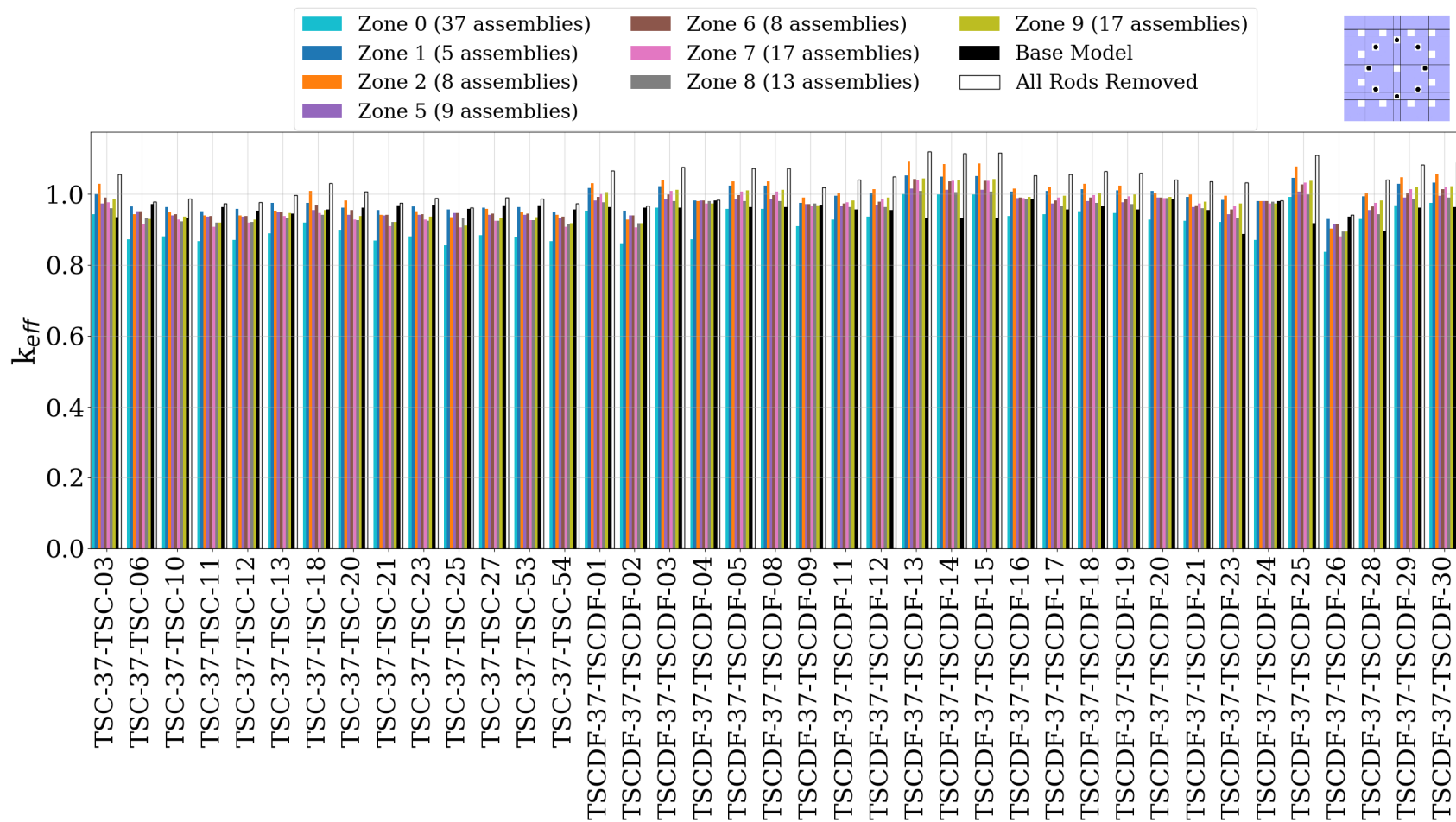


Figure 32. Results of all NA models with DCRA material  $WB_2$  and as-loaded fuel isotopic compositions; subzone 2 with small diameter rods.

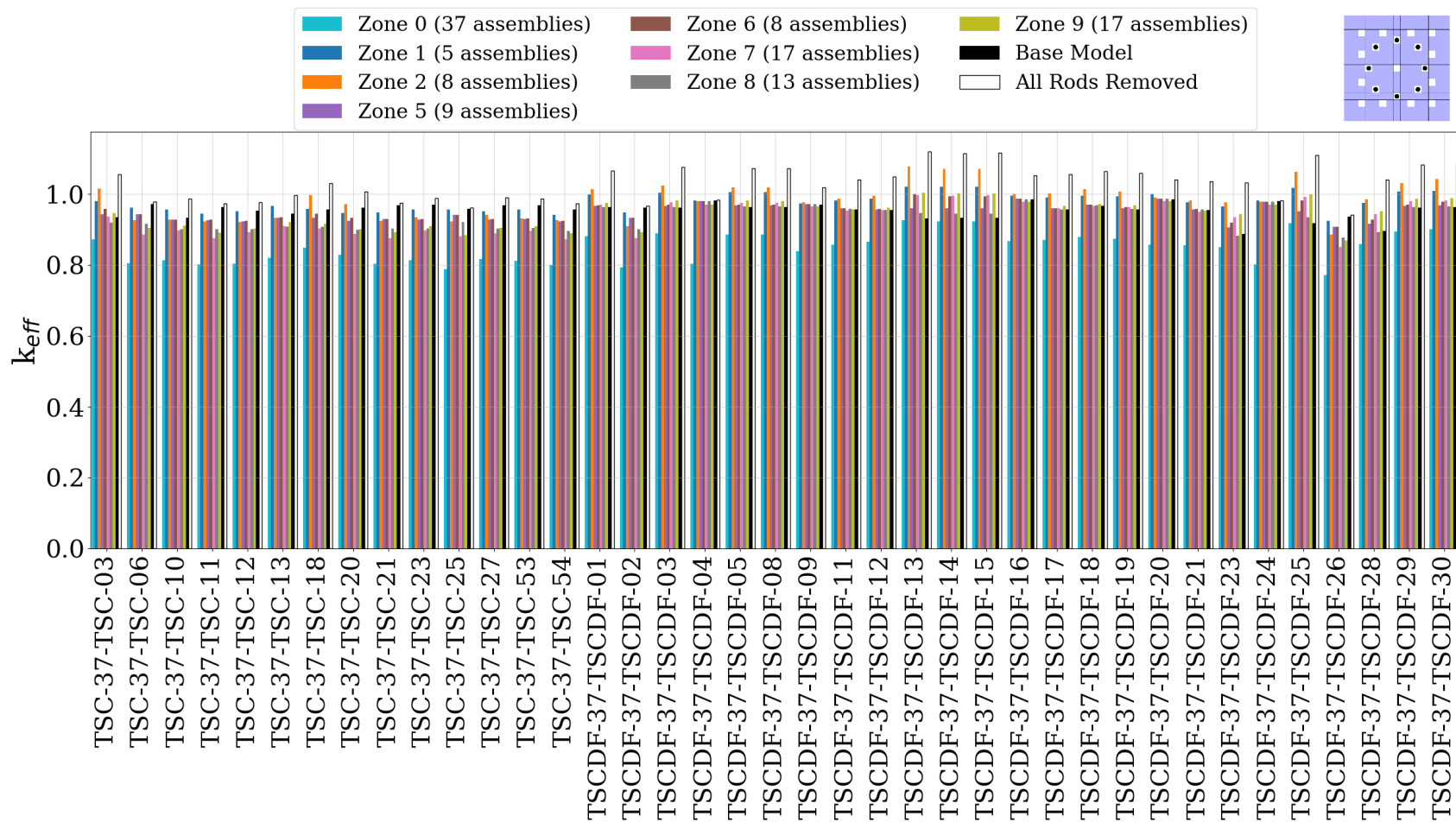
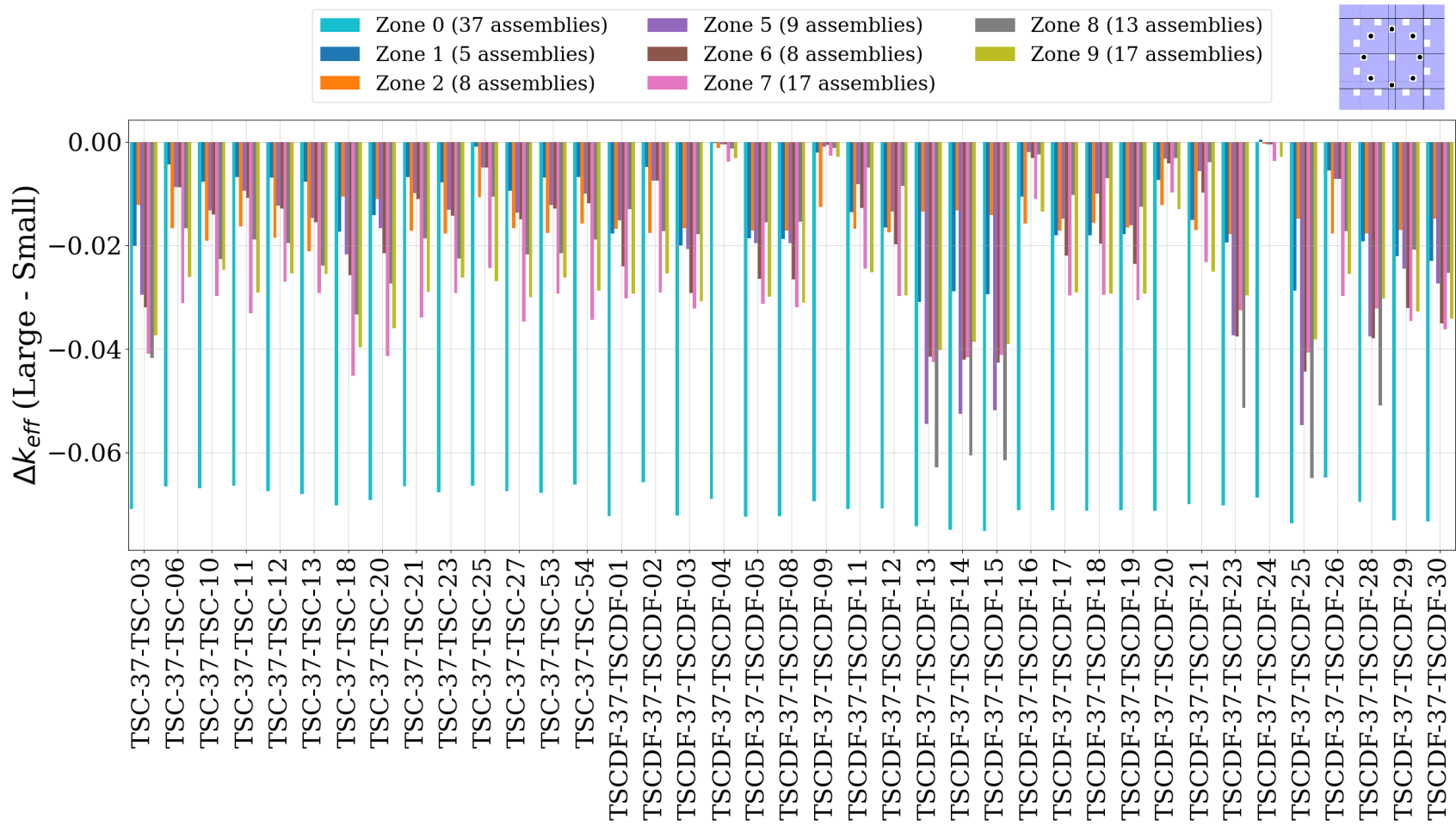


Figure 33. Results of all NA models with DCRA material  $WB_2$  and as-loaded fuel isotopic compositions; subzone 2 with large diameter rods.



**Figure 34. Delta-k of large-to-small diameter rods for all NA models with DCRA material  $WB_2$  and as-loaded fuel isotopic compositions for subzone 2.**

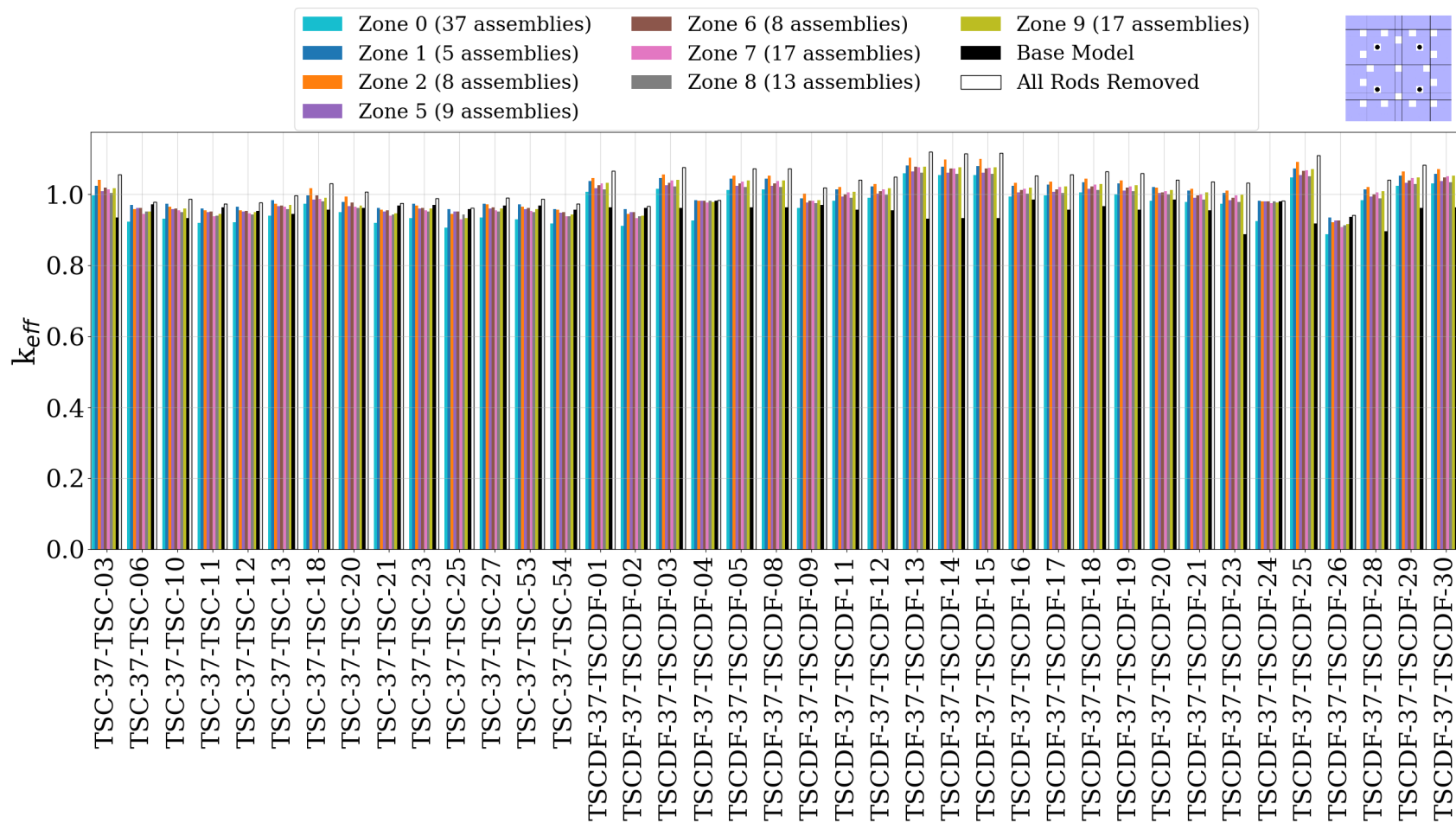


Figure 35. Results of all NA models with DCRA material  $WB_2$  and as-loaded fuel isotopic compositions; subzone 2 corners with small diameter rods.

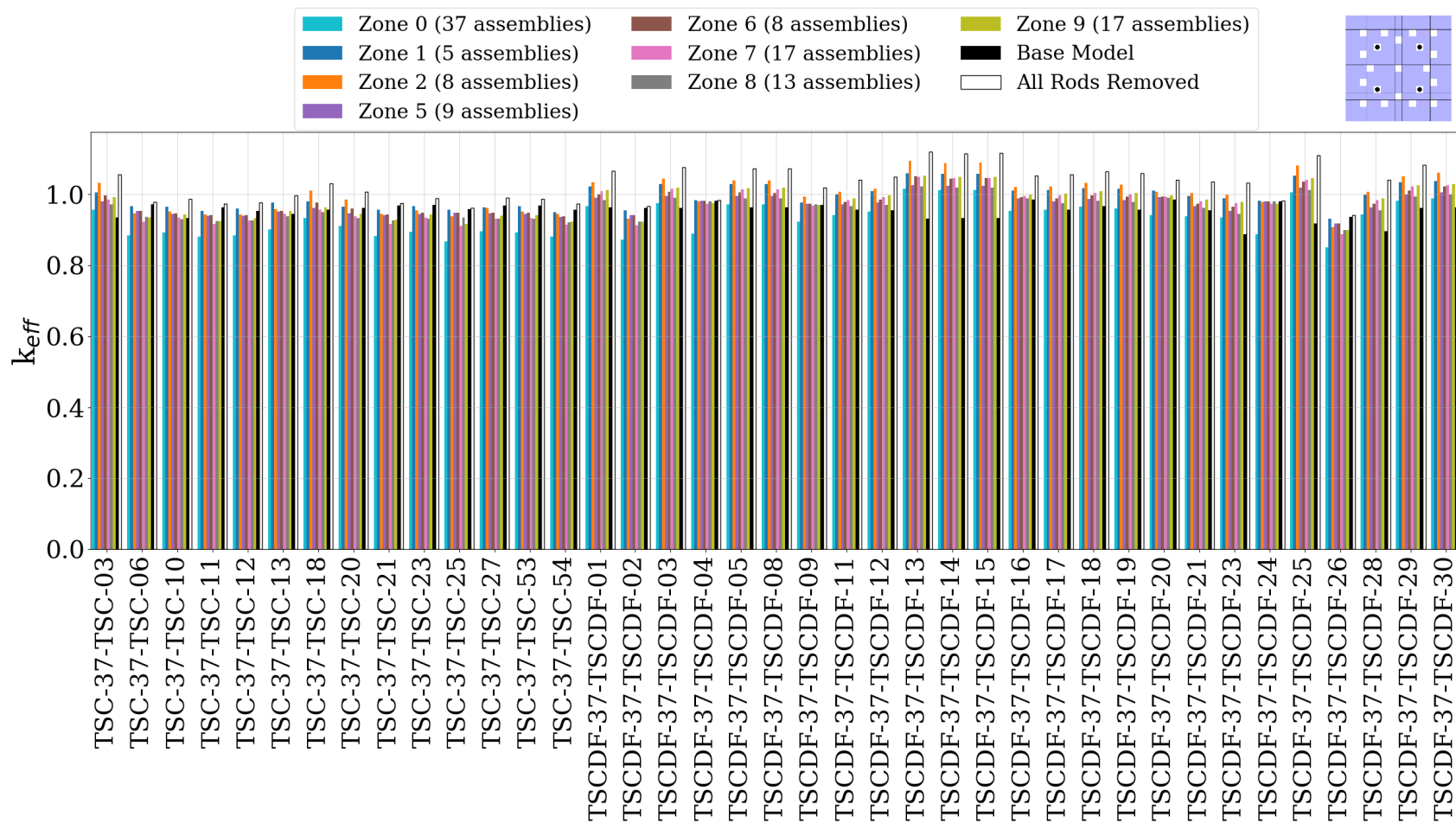


Figure 36. Results of all NA models with DCRA material  $WB_2$  and as-loaded fuel isotopic compositions; subzone 2 corners with large diameter rods.

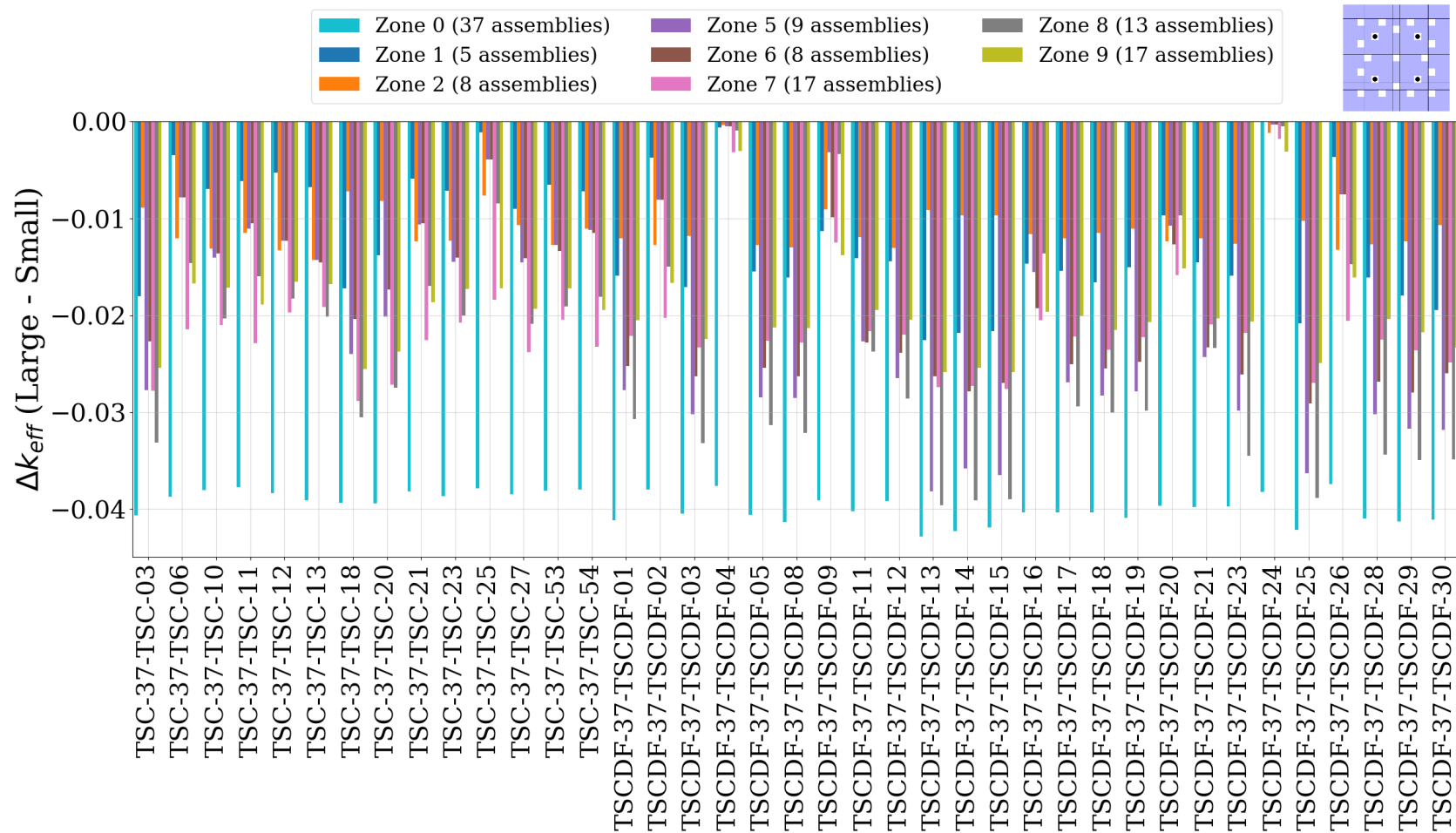
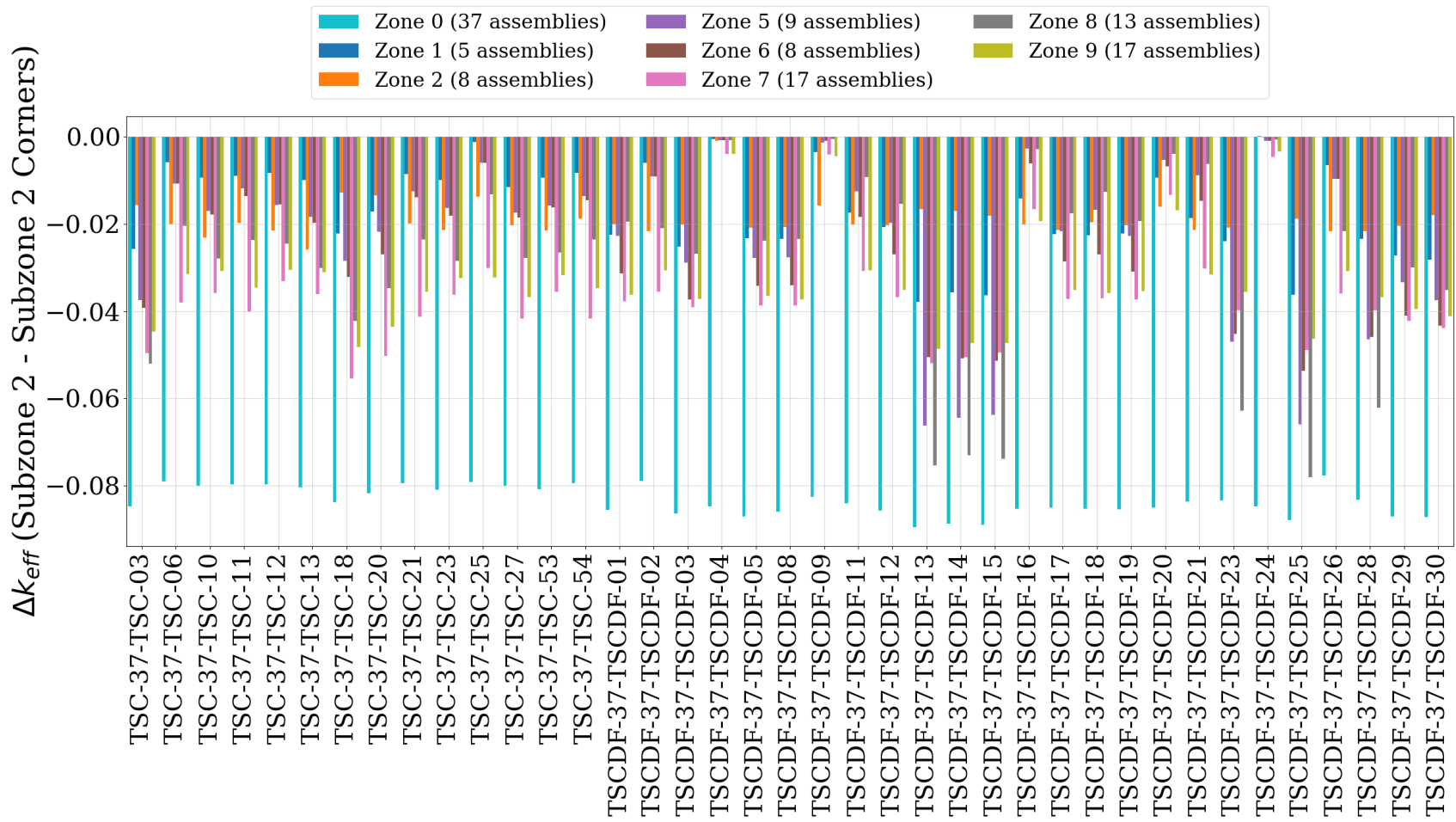


Figure 37. Delta-k of large-to-small diameter rods for all NA models with DCRA material WB<sub>2</sub> and as-loaded fuel isotopic compositions; subzone 2 corners.



**Figure 38. Delta-k of subzone 2 to subzone 2 corners for large diameter rods for all NA models with DCRA material  $WB_2$  and as-loaded fuel isotopic compositions.**



$\Delta k_{eff}$  (Subzone 2 Small- Subzone 2 Corners Large)

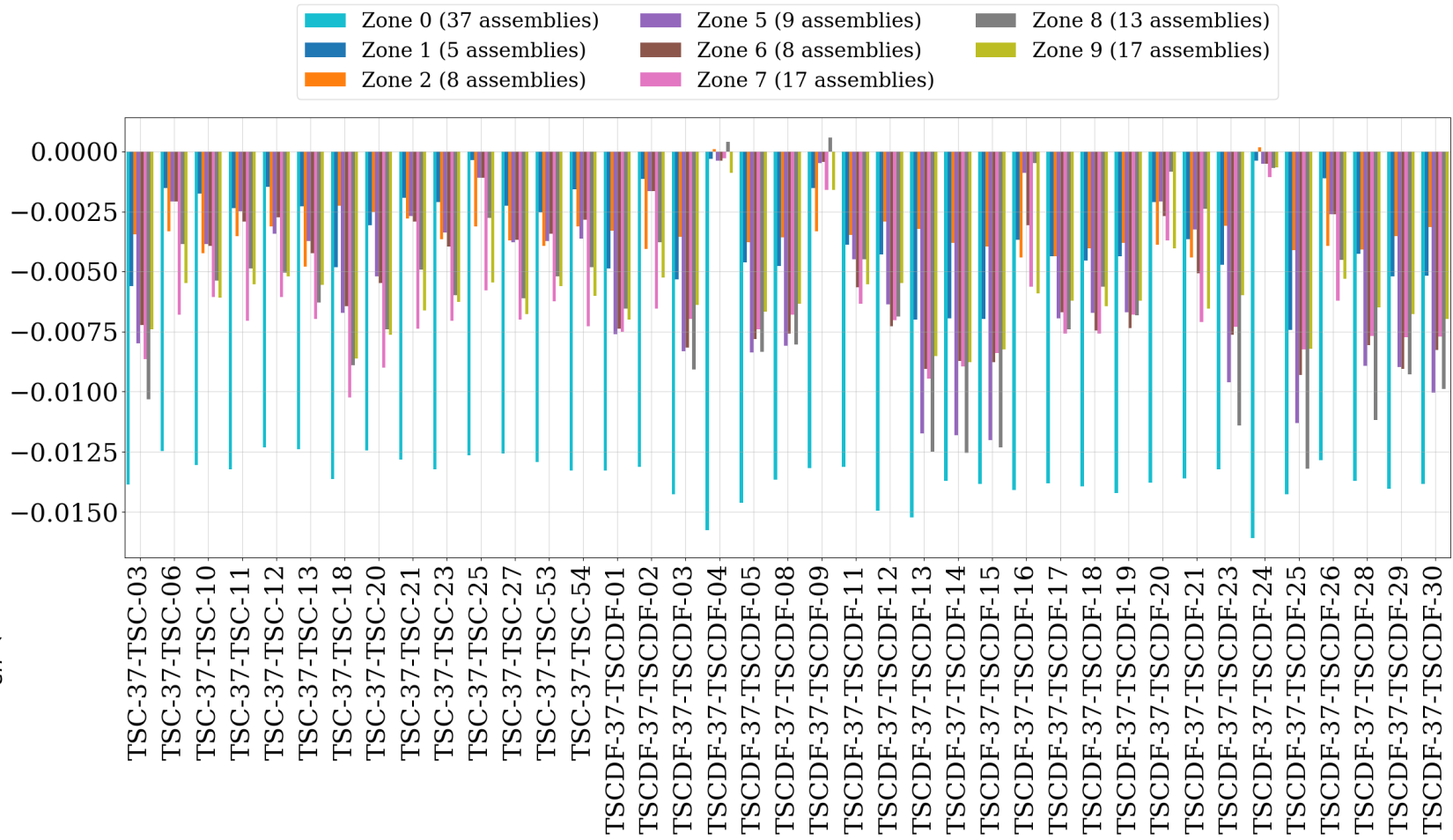


**Figure 39. Delta-k of subzone 2 with small diameter rods to subzone 2 corners with large diameter rods (equal absorber mass) for all NA models with DCRA material  $WB_2$  and as-loaded fuel isotopic compositions.**

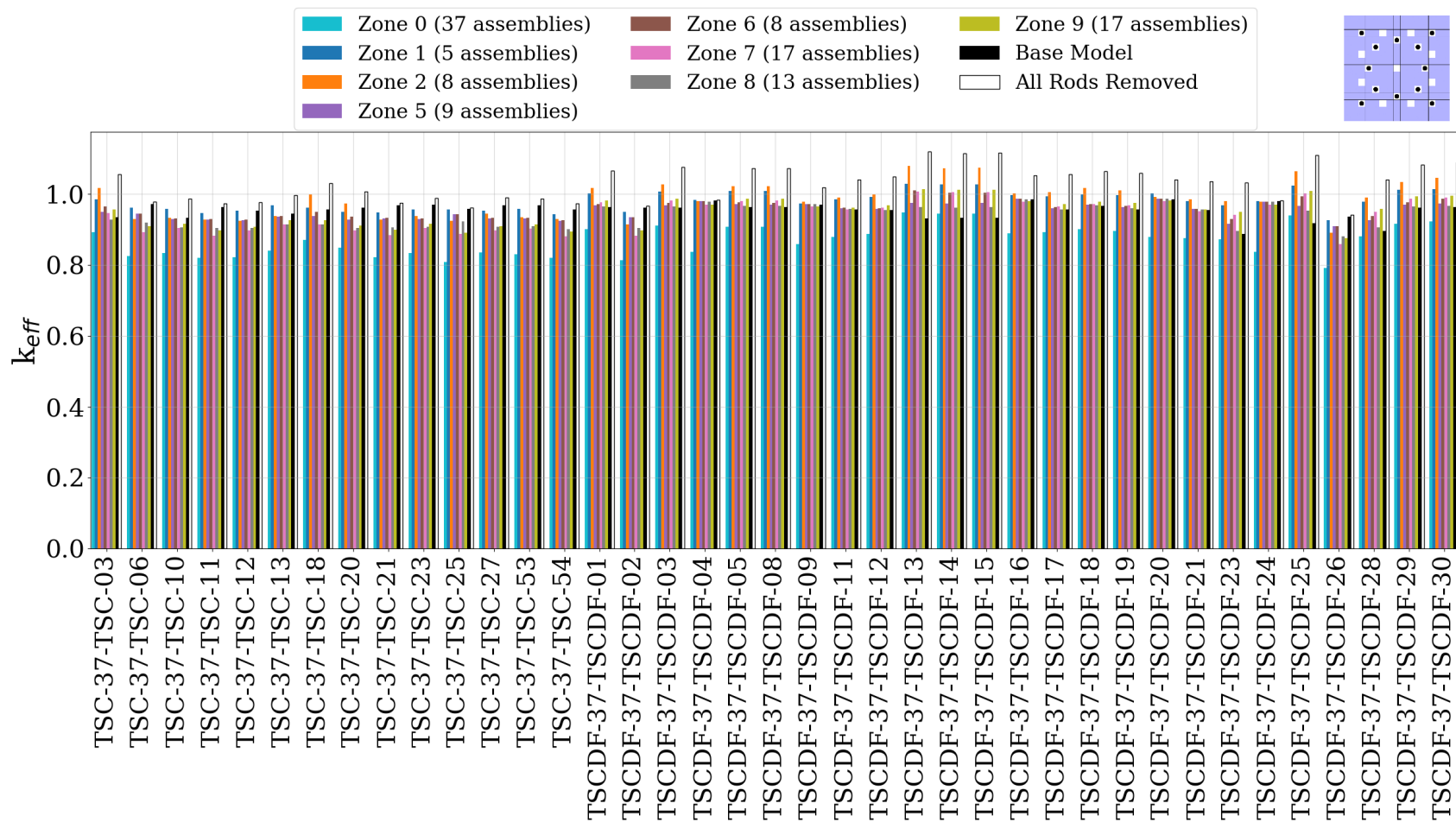


Figure 40. Results of all NA models with DCRA material  $WB_2$  and as-loaded fuel isotopic compositions; subzone inner 12 with small diameter rods.

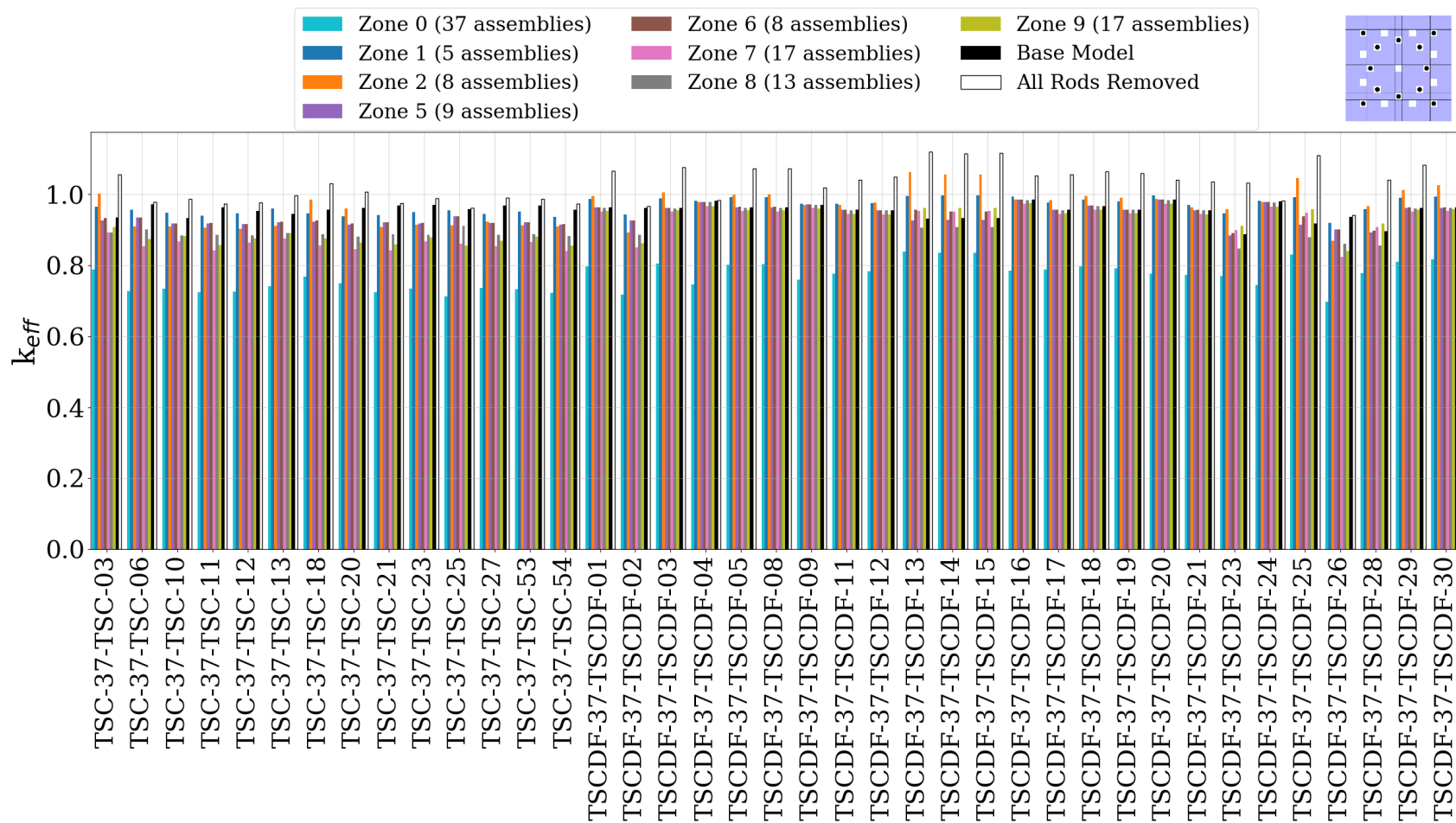
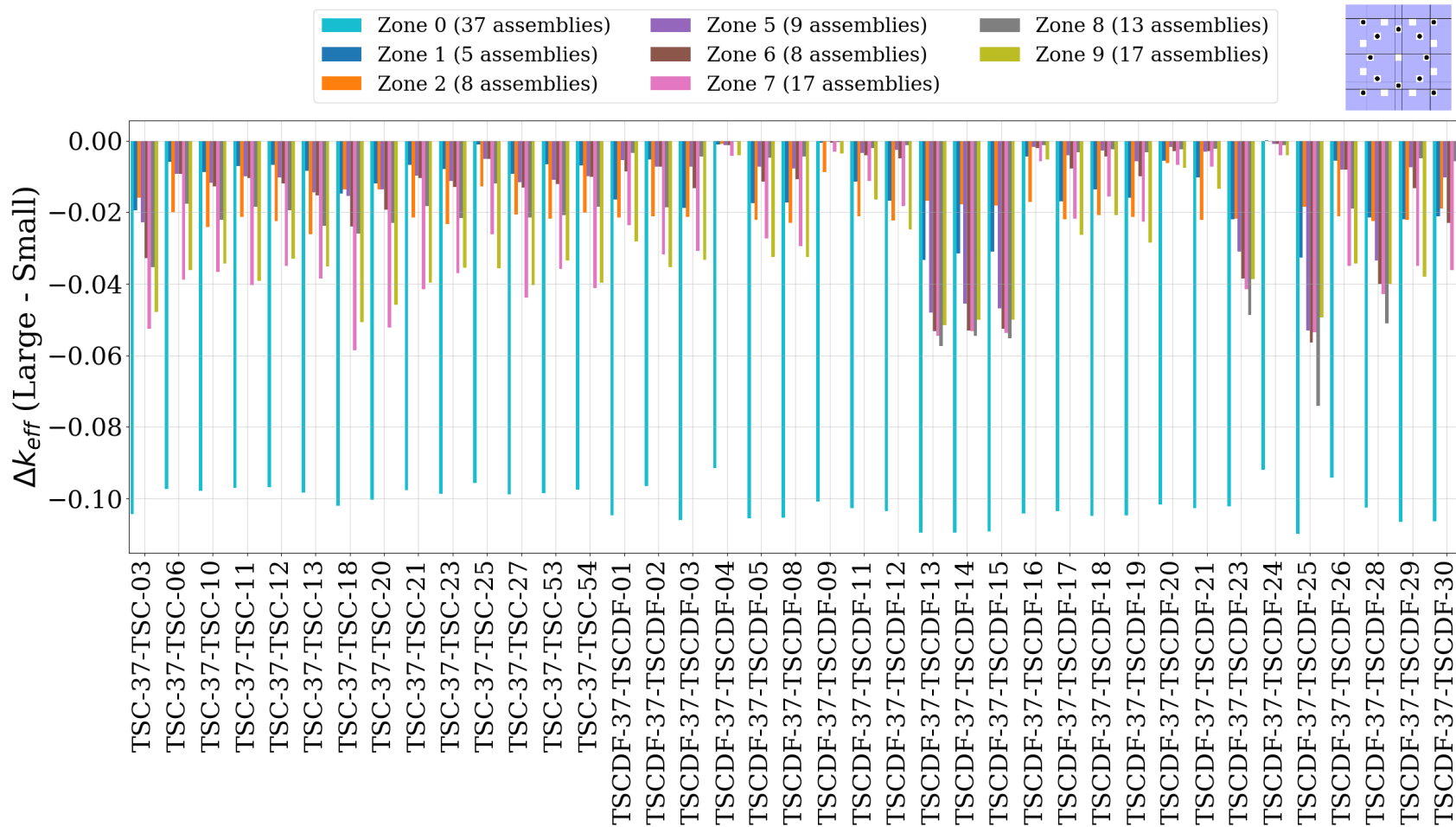
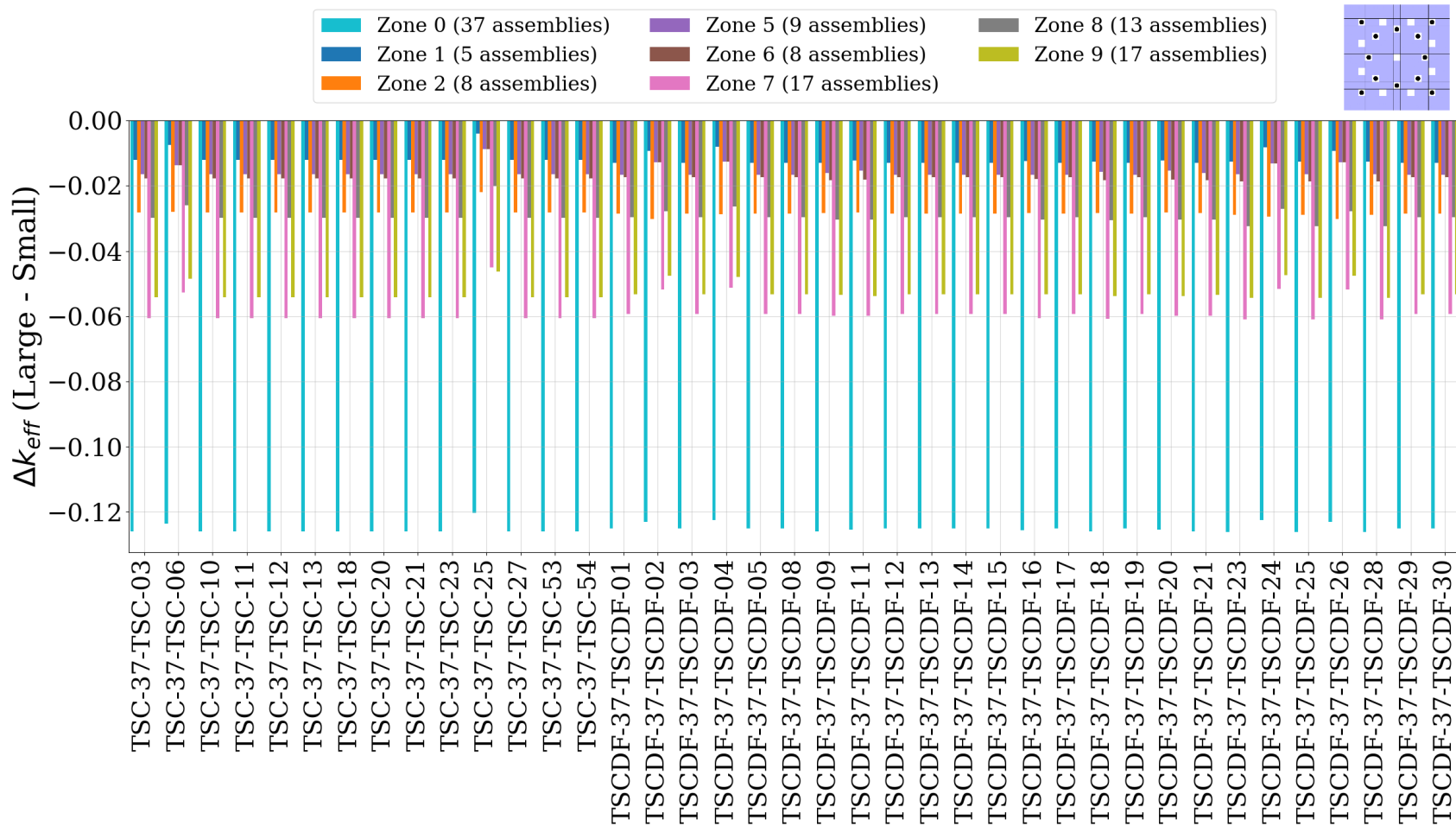


Figure 41. Results of all NA models with DCRA material  $WB_2$  and as-loaded fuel isotopic compositions; subzone inner 12 with large diameter rods.



**Figure 42. Delta-k of large-to-small diameter rods for all NA models with DCRA material  $WB_2$  and as-loaded fuel isotopic compositions for inner 12.**



**Figure 43. Delta-k of large-to-small diameter rods for all NA models with DCRA material  $WB_2$  and fresh fuel isotopic compositions for subzone inner 12.**

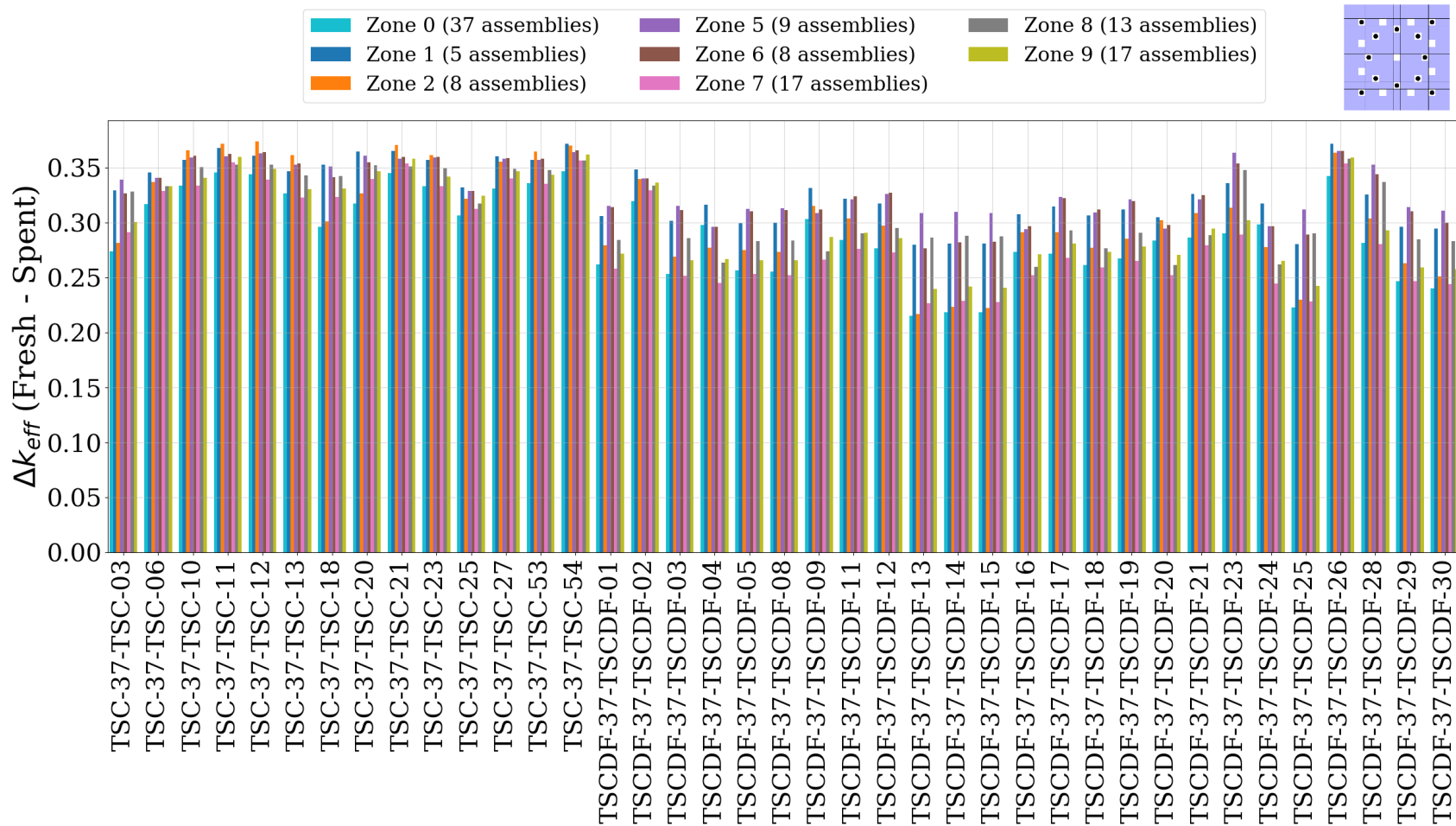


**Figure 44. Delta-k of fresh-to-as-loaded spent fuel isotopic compositions for small diameter rods to small diameter rods for all NA models with DCRA material WB<sub>2</sub> for subzone inner 12.**

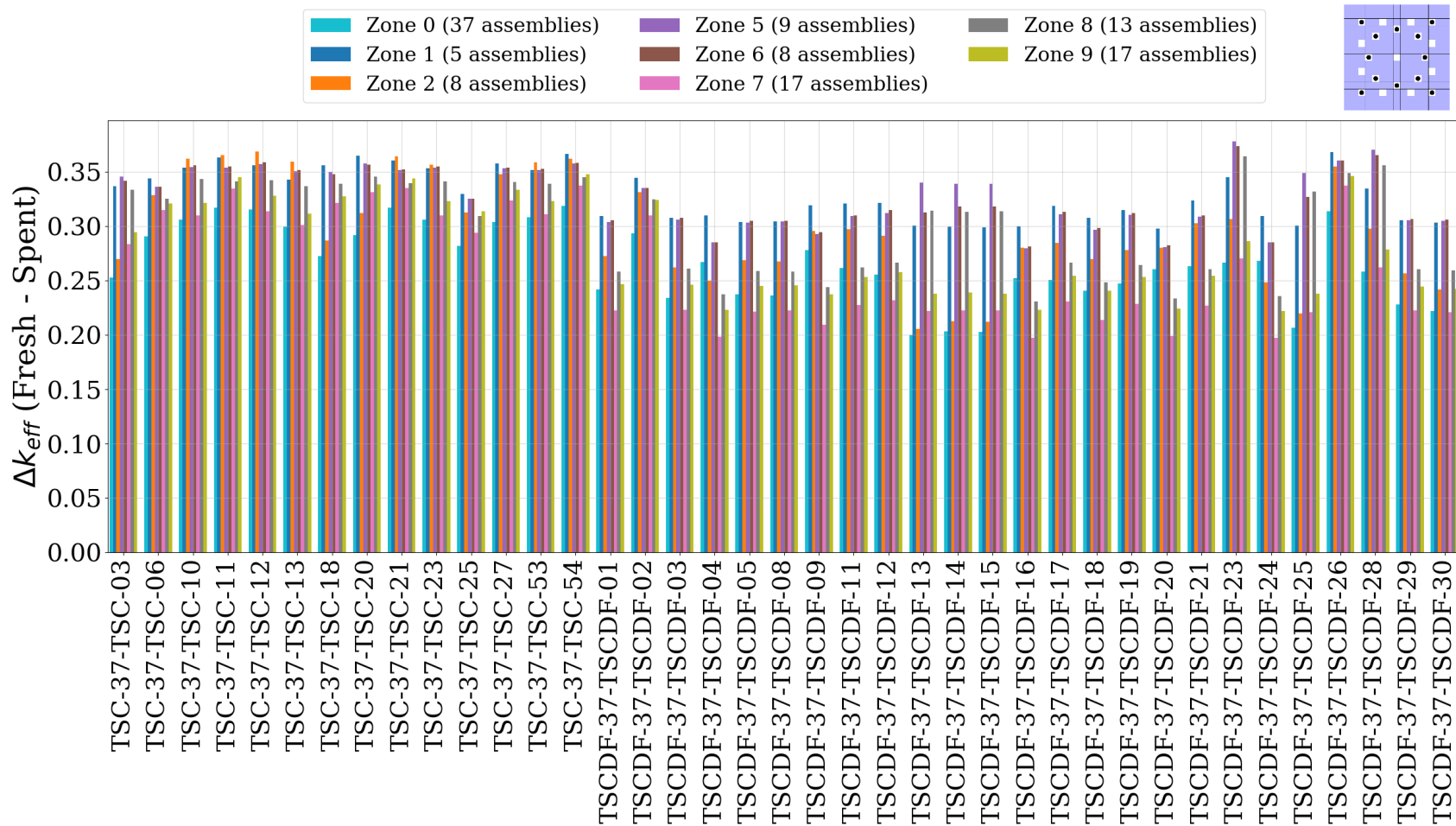


Figure 45. Delta-k of fresh-to-as-loaded spent fuel isotopic compositions for large diameter rods to large diameter rods for all NA models with DCRA material WB<sub>2</sub> for subzone inner 12.

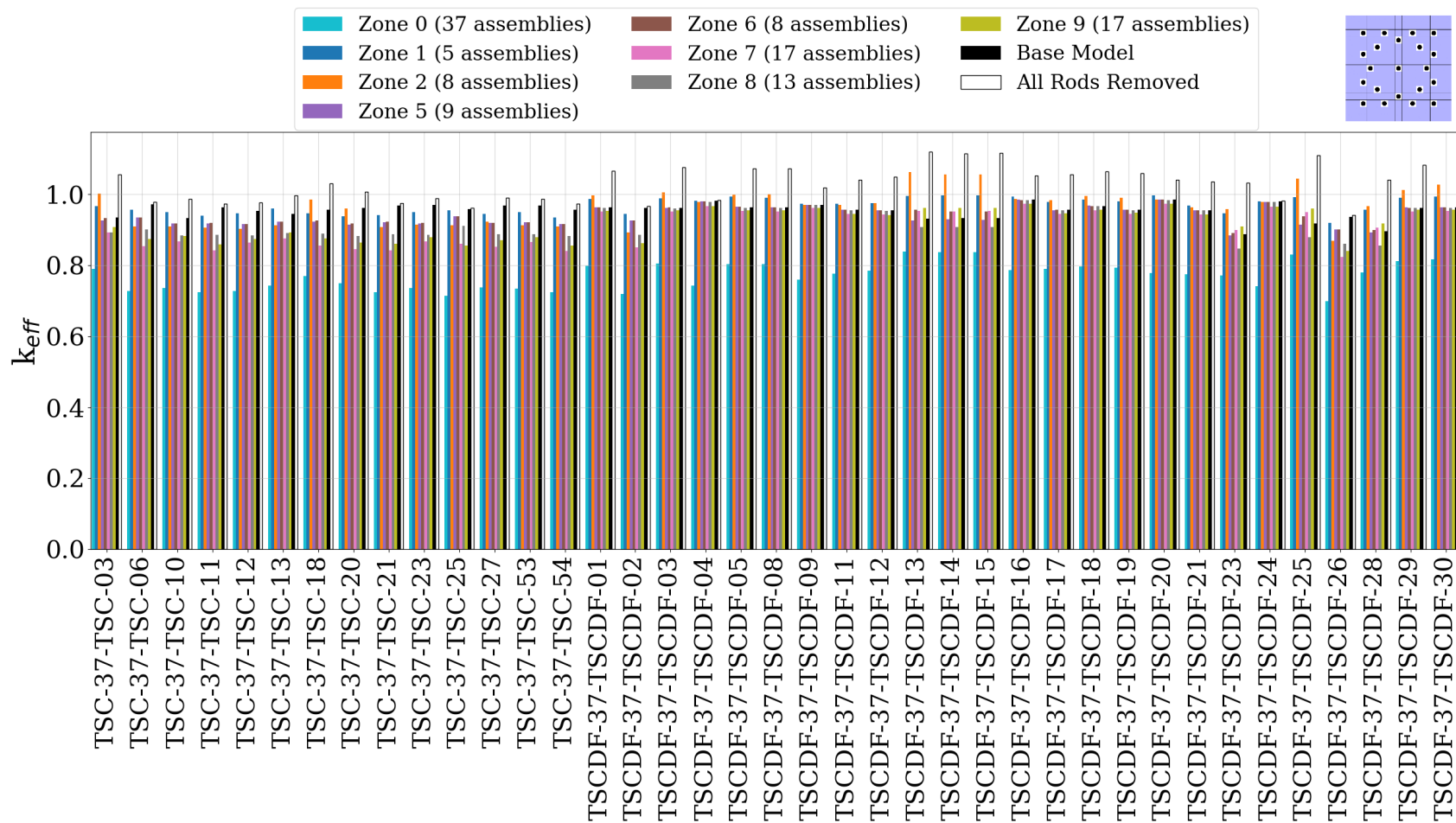


Figure 46. Results of all NA models with DCRA material  $WB_2$  and as-loaded fuel isotopic compositions; subzone all rods (21) with small diameter rods.



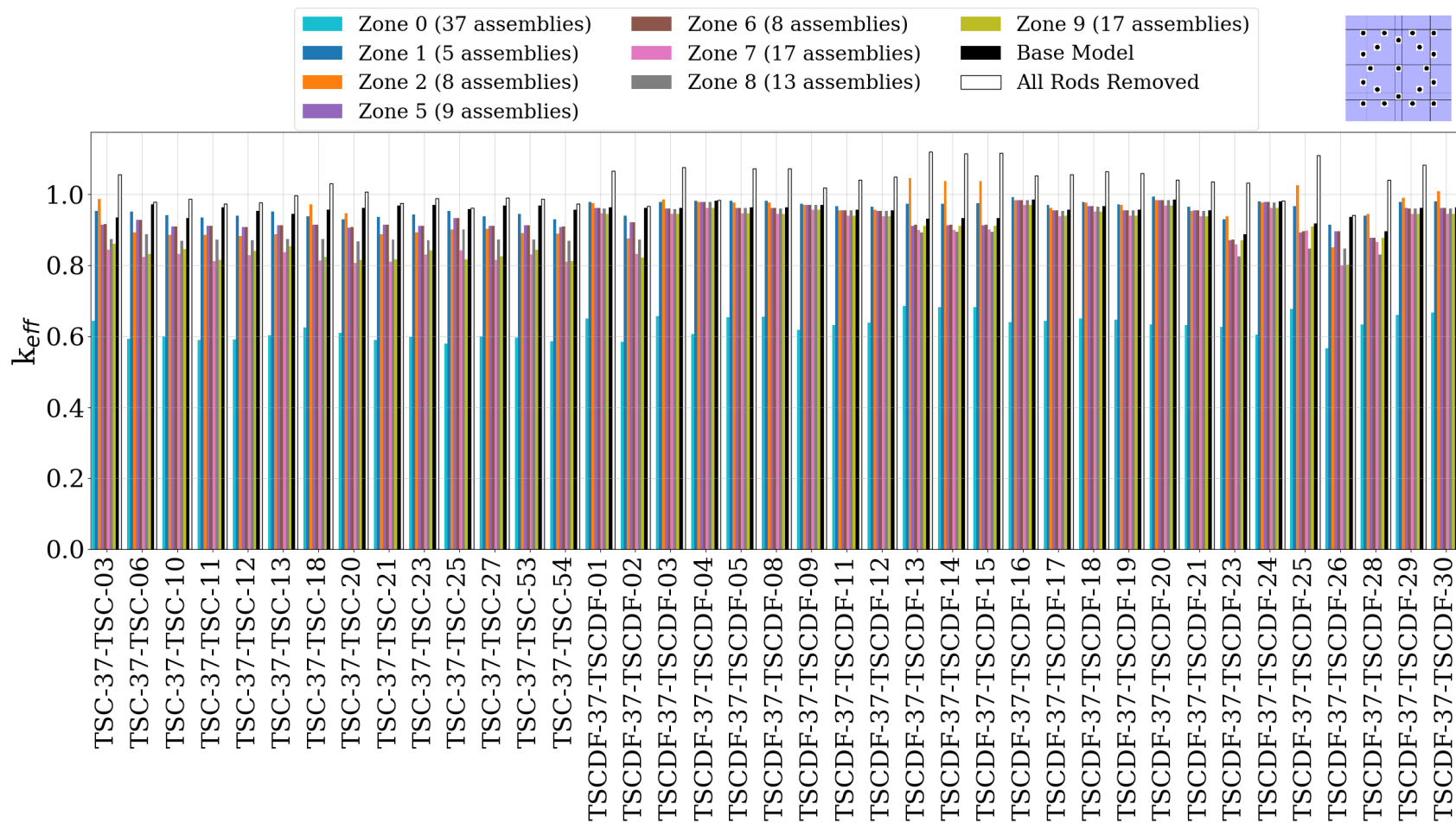
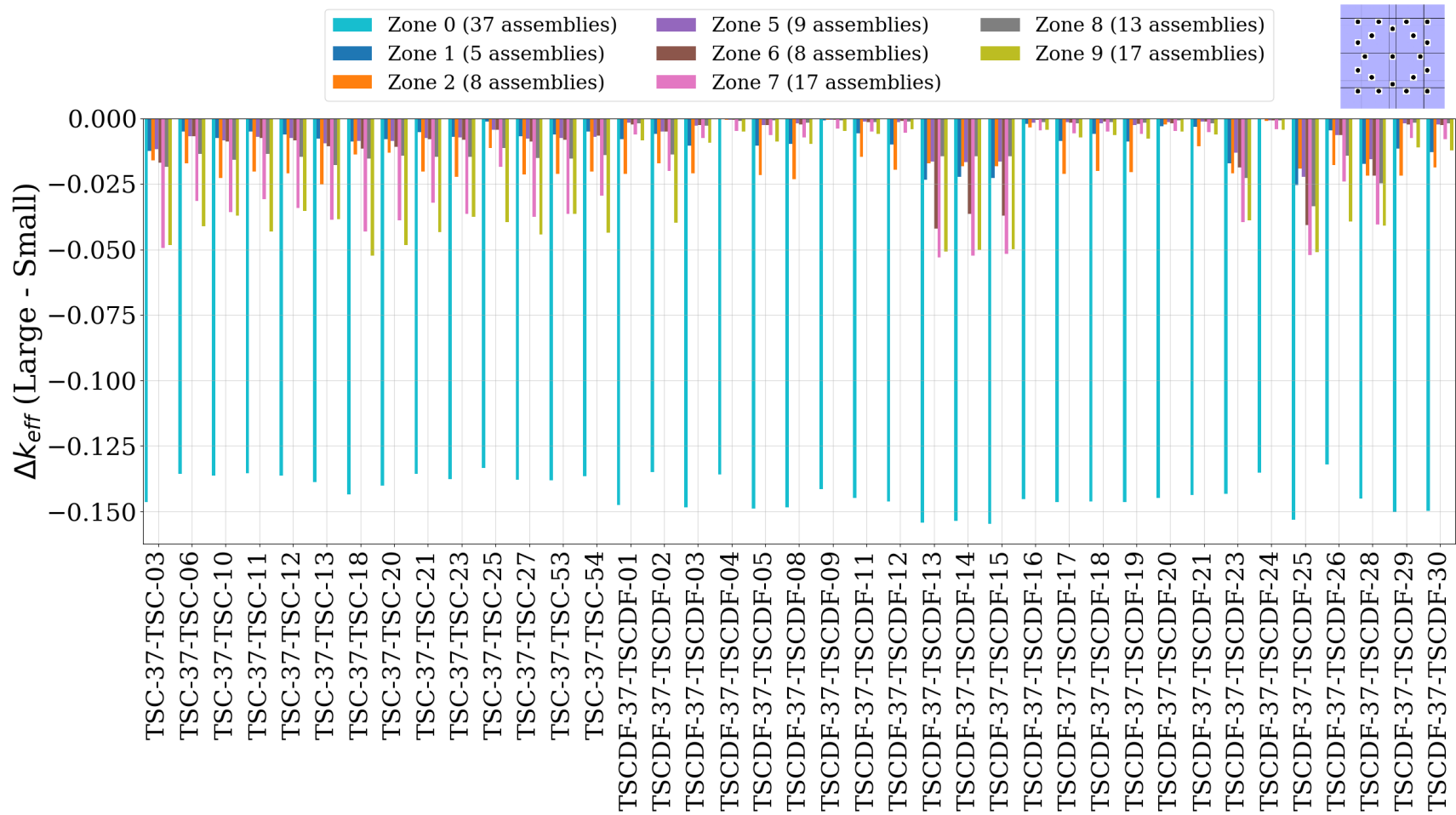


Figure 47. Results of all NA models with DCRA material  $WB_2$  and as-loaded fuel isotopic compositions; subzone all rods (21) with large diameter rods.



**Figure 48. Delta-k of large-to-small diameter rods for all NA models with DCRA material WB<sub>2</sub> and as-loaded fuel isotopic compositions for subzone all rods (21).**

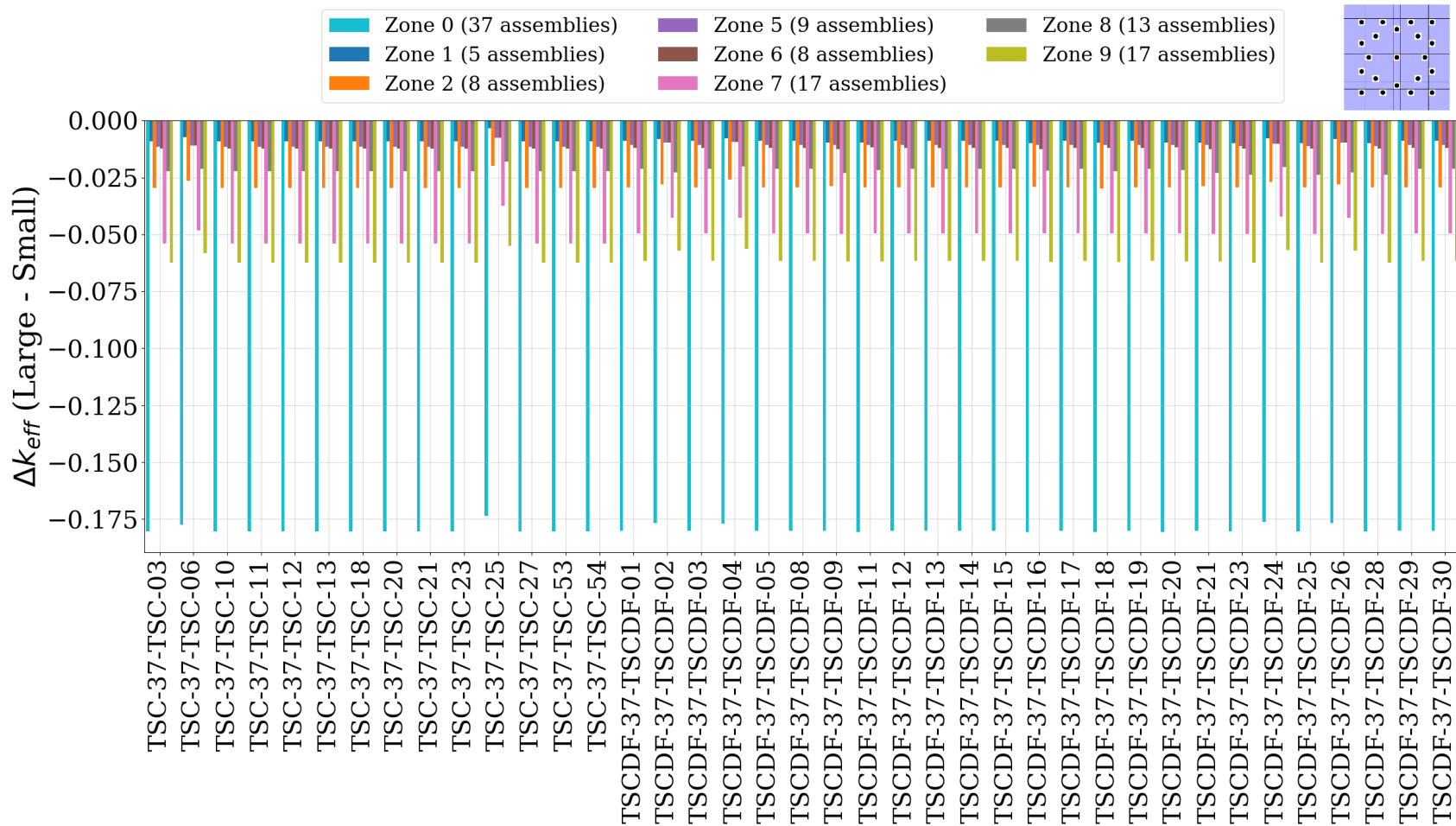


Figure 49. Delta-k of large-to-small diameter rods for all NA models with DCRA material WB<sub>2</sub> and fresh fuel isotopic compositions for subzone all rods (21).

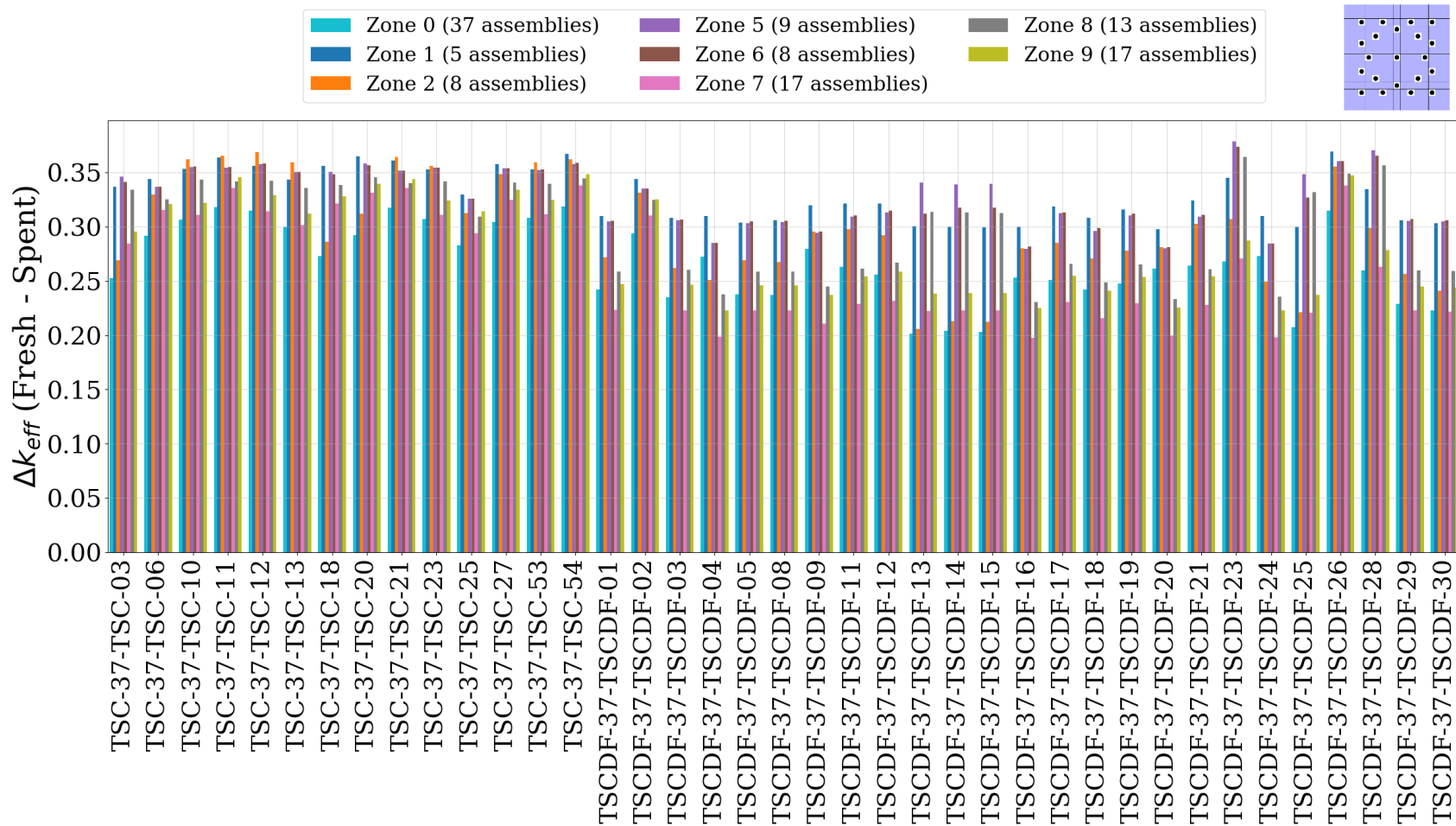
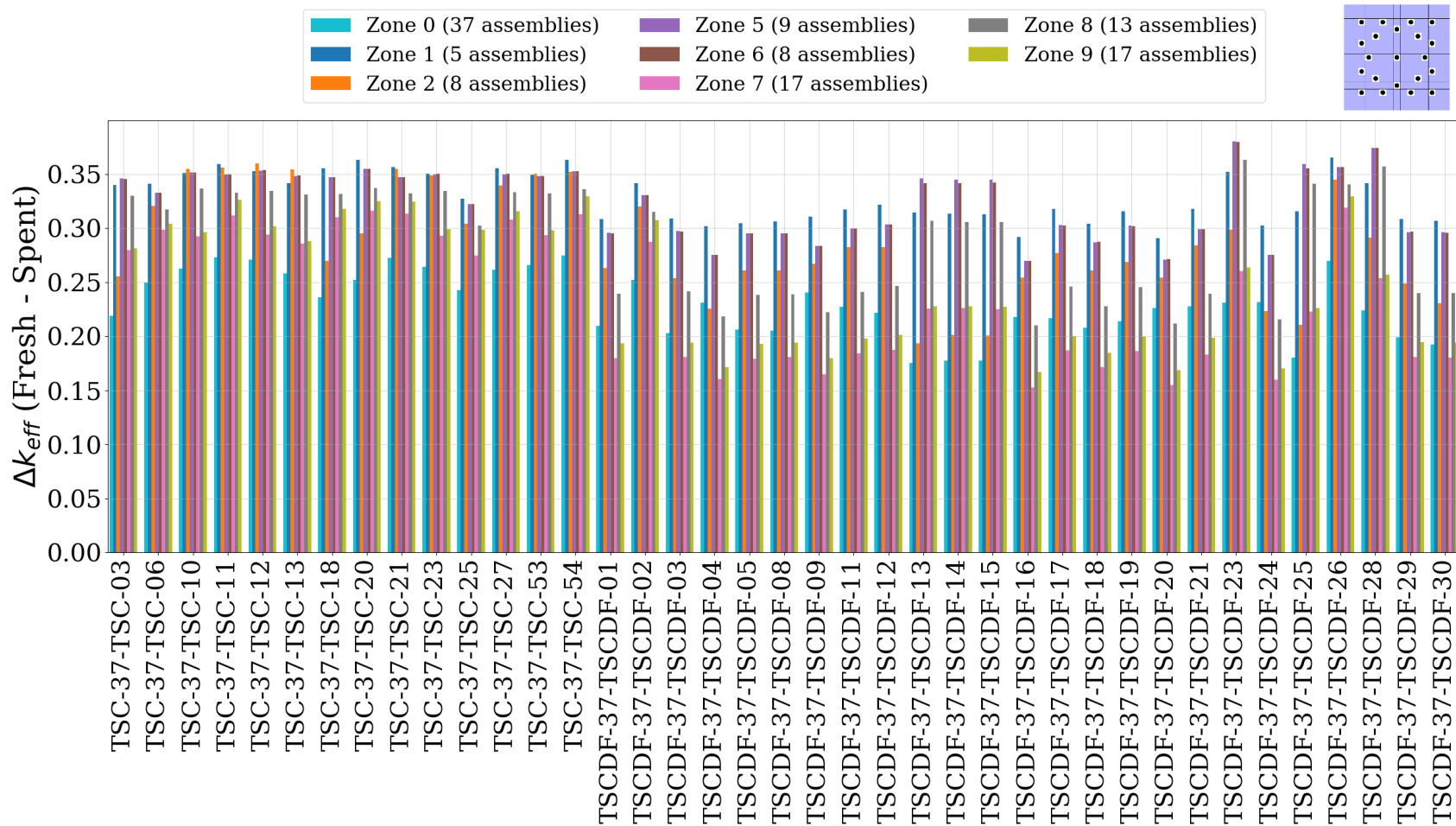


Figure 50. Delta-k of fresh-to-as-loaded spent fuel isotopic compositions for small diameter rods for all NA models with DCRA material  $WB_2$  for subzone all rods (21).



**Figure 51. Delta-k of fresh-to-as-loaded spent fuel isotopic compositions for large diameter rods for all NA models with DCRA material WB<sub>2</sub> for subzone all rods (21).**

### 3.1.3 Results for the DB Dataset

As discussed above, the calculations in this report consider both the NA models (see Section 3.1.2) and the DB models. The only difference between these two models is that in the DB model, in addition to the loss of the neutron absorber panel in the basket (replaced by water), the basket itself is considered lost and replaced by water. With the loss of the basket and subsequent introduction of more water into the system in the DB scenario, the system reactivity increases substantially, with a maximum  $k_{\text{eff}}$  of approximately 1.1 for the NA model to about 1.2 for the DB model (as seen when comparing Figure 3 and Figure 4). Although this UNF-ST&DARDS-based methodology to evaluate post-closure criticality using these very conservative assumptions is the current practice, other approaches or models and modifications will likely be developed and implemented in the future to meet regulatory requirements. However, it is expected that the NA, and especially the DB methodologies, are conservative relative to future methodologies for post-closure criticality in DPCs. Therefore, any DCRA method evaluated with the DB model is expected to be bounding.

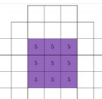
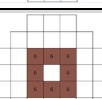
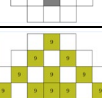
DB calculations are provided in this report to demonstrate the reactivity effect of the zone and subzones and to provide a reactivity comparison between the NA and DB models. The results of the DB calculations are provided in Table 10 and Table 11 and in Figure 52 through Figure 63. The reactivity trends seen in the results presented in the tables and figures below show the following:

- The results shown in Figure 52 provide a generic overview of the reactivity of the DPCs for the DB dataset by comparing the reactivity of each DPC for fresh fuel, as-loaded spent fuel isotopic compositions, no DCRA, DCRA in every location and every guide tube, and as compared with the base model (i.e., the unmodified inputs from Walker [2]).
  - The results in Figure 52 show that the DCRA has more than sufficient potential to preclude criticality in the DB models, even for fresh fuel. This conclusion provides a significant amount of leeway and margin for the analysis when providing technical justification for regulatory considerations.
  - Furthermore, the scenario in which all rods are inserted for the as-loaded spent fuel isotopic compositions is significantly subcritical at 0.8, which also provides a substantial amount of technical justification for regulatory considerations.
- Results for subzone 2, subzone 2 corners, inner 12, and all rods (21) are provided in Figure 53 through Figure 64. For each subzone, results are provided for small diameter rods, large diameter rods, and the delta-k between large-to-small. As expected, reactivity trends for DB models are similar to the NA models discussed in Section 3.1.2.
- The results provided in Table 10 and Table 11 show the effectiveness of each zone and subzone combination compared to three subcritical limits.

**Table 10. Summary of zone and subzone results for DB datasets with large diameter rod DCRA's with WB<sub>2</sub>**

Zone	Subcritical limit	Subzone 2 (8 rods)	Subzone 2 corners (4 rods)	Subzone 3 (12 rods)	Inner 12 (12 rods)	All rods (21 rods)	Zone layout
Zone 0 (37 assemblies)	0.95	41/61 (67.2%)	4/61 (6.6%)	61/61 (100.0%)	61/61 (100.0%)	61/61 (100.0%)	
Zone 0 (37 assemblies)	1	56/61 (91.8%)	37/61 (60.7%)	61/61 (100.0%)	61/61 (100.0%)	61/61 (100.0%)	
Zone 0 (37 assemblies)	1.03	61/61 (100.0%)	43/61 (70.5%)	61/61 (100.0%)	61/61 (100.0%)	61/61 (100.0%)	
Zone 1 (5 assemblies)	0.95	0/61 (0.0%)	0/61 (0.0%)	0/61 (0.0%)	0/61 (0.0%)	0/61 (0.0%)	
Zone 1 (5 assemblies)	1	1/61 (1.6%)	0/61 (0.0%)	2/61 (3.3%)	2/61 (3.3%)	2/61 (3.3%)	
Zone 1 (5 assemblies)	1.03	17/61 (27.9%)	4/61 (6.6%)	27/61 (44.3%)	27/61 (44.3%)	31/61 (50.8%)	
Zone 2 (8 assemblies)	0.95	0/61 (0.0%)	0/61 (0.0%)	2/61 (3.3%)	2/61 (3.3%)	2/61 (3.3%)	
Zone 2 (8 assemblies)	1	4/61 (6.6%)	2/61 (3.3%)	33/61 (54.1%)	33/61 (54.1%)	35/61 (57.4%)	
Zone 2 (8 assemblies)	1.03	37/61 (60.7%)	19/61 (31.1%)	37/61 (60.7%)	37/61 (60.7%)	44/61 (72.1%)	
Zone 5 (9 assemblies)	0.95	0/61 (0.0%)	0/61 (0.0%)	0/61 (0.0%)	0/61 (0.0%)	1/61 (1.6%)	
Zone 5 (9 assemblies)	1	3/61 (4.9%)	2/61 (3.3%)	21/61 (34.4%)	16/61 (26.2%)	33/61 (54.1%)	
Zone 5 (9 assemblies)	1.03	44/61 (72.1%)	25/61 (41.0%)	61/61 (100.0%)	61/61 (100.0%)	61/61 (100.0%)	
Zone 6 (8 assemblies)	0.95	0/61 (0.0%)	0/61 (0.0%)	0/61 (0.0%)	0/61 (0.0%)	1/61 (1.6%)	
Zone 6 (8 assemblies)	1	2/61 (3.3%)	2/61 (3.3%)	20/61 (32.8%)	16/61 (26.2%)	32/61 (52.5%)	
Zone 6 (8 assemblies)	1.03	40/61 (65.6%)	21/61 (34.4%)	58/61 (95.1%)	57/61 (93.4%)	61/61 (100.0%)	
Zone 7 (17 assemblies)	0.95	2/61 (3.3%)	0/61 (0.0%)	36/61 (59.0%)	35/61 (57.4%)	39/61 (63.9%)	
Zone 7 (17 assemblies)	1	37/61 (60.7%)	11/61 (18.0%)	48/61 (78.7%)	44/61 (72.1%)	59/61 (96.7%)	
Zone 7 (17 assemblies)	1.03	45/61 (73.8%)	38/61 (62.3%)	61/61 (100.0%)	57/61 (93.4%)	61/61 (100.0%)	
Zone 8 (13 assemblies)	0.95	0/61 (0.0%)	0/61 (0.0%)	5/61 (8.2%)	4/61 (6.6%)	19/61 (31.1%)	
Zone 8 (13 assemblies)	1	29/61 (47.5%)	3/61 (4.9%)	48/61 (78.7%)	48/61 (78.7%)	50/61 (82.0%)	
Zone 8 (13 assemblies)	1.03	56/61 (91.8%)	39/61 (63.9%)	61/61 (100.0%)	61/61 (100.0%)	61/61 (100.0%)	
Zone 9 (17 assemblies)	0.95	1/61 (1.6%)	0/61 (0.0%)	25/61 (41.0%)	19/61 (31.1%)	39/61 (63.9%)	
Zone 9 (17 assemblies)	1	35/61 (57.4%)	5/61 (8.2%)	46/61 (75.4%)	43/61 (70.5%)	59/61 (96.7%)	
Zone 9 (17 assemblies)	1.03	41/61 (67.2%)	36/61 (59.0%)	57/61 (93.4%)	56/61 (91.8%)	61/61 (100.0%)	

**Table 11. Summary of zone and subzone results for DB datasets with small diameter rod DCRA's with WB<sub>2</sub>**

Zone	Subcritical limit	Subzone 2 (8 rods)	Subzone 2 corners (4 rods)	Subzone 3 (12 rods)	Inner 12 (12 rods)	All rods (21 rods)	Zone layout
Zone 0 (37 assemblies)	0.95	9/61 (14.8%)	0/61 (0.0%)	39/61 (63.9%)	39/61 (63.9%)	61/61 (100.0%)	
Zone 0 (37 assemblies)	1	39/61 (63.9%)	10/61 (16.4%)	54/61 (88.5%)	54/61 (88.5%)	61/61 (100.0%)	
Zone 0 (37 assemblies)	1.03	46/61 (75.4%)	37/61 (60.7%)	57/61 (93.4%)	57/61 (93.4%)	61/61 (100.0%)	
Zone 1 (5 assemblies)	0.95	0/61 (0.0%)	0/61 (0.0%)	0/61 (0.0%)	0/61 (0.0%)	0/61 (0.0%)	
Zone 1 (5 assemblies)	1	0/61 (0.0%)	0/61 (0.0%)	1/61 (1.6%)	1/61 (1.6%)	2/61 (3.3%)	
Zone 1 (5 assemblies)	1.03	6/61 (9.8%)	4/61 (6.6%)	16/61 (26.2%)	15/61 (24.6%)	27/61 (44.3%)	
Zone 2 (8 assemblies)	0.95	0/61 (0.0%)	0/61 (0.0%)	0/61 (0.0%)	0/61 (0.0%)	2/61 (3.3%)	
Zone 2 (8 assemblies)	1	2/61 (3.3%)	2/61 (3.3%)	4/61 (6.6%)	4/61 (6.6%)	33/61 (54.1%)	
Zone 2 (8 assemblies)	1.03	25/61 (41.0%)	8/61 (13.1%)	37/61 (60.7%)	37/61 (60.7%)	37/61 (60.7%)	
Zone 5 (9 assemblies)	0.95	0/61 (0.0%)	0/61 (0.0%)	0/61 (0.0%)	0/61 (0.0%)	0/61 (0.0%)	
Zone 5 (9 assemblies)	1	2/61 (3.3%)	1/61 (1.6%)	4/61 (6.6%)	3/61 (4.9%)	17/61 (27.9%)	
Zone 5 (9 assemblies)	1.03	28/61 (45.9%)	8/61 (13.1%)	43/61 (70.5%)	40/61 (65.6%)	61/61 (100.0%)	
Zone 6 (8 assemblies)	0.95	0/61 (0.0%)	0/61 (0.0%)	0/61 (0.0%)	0/61 (0.0%)	0/61 (0.0%)	
Zone 6 (8 assemblies)	1	2/61 (3.3%)	1/61 (1.6%)	2/61 (3.3%)	2/61 (3.3%)	14/61 (23.0%)	
Zone 6 (8 assemblies)	1.03	26/61 (42.6%)	6/61 (9.8%)	39/61 (63.9%)	37/61 (60.7%)	58/61 (95.1%)	
Zone 7 (17 assemblies)	0.95	0/61 (0.0%)	0/61 (0.0%)	2/61 (3.3%)	2/61 (3.3%)	35/61 (57.4%)	
Zone 7 (17 assemblies)	1	19/61 (31.1%)	2/61 (3.3%)	37/61 (60.7%)	36/61 (59.0%)	44/61 (72.1%)	
Zone 7 (17 assemblies)	1.03	38/61 (62.3%)	26/61 (42.6%)	45/61 (73.8%)	43/61 (70.5%)	57/61 (93.4%)	
Zone 8 (13 assemblies)	0.95	0/61 (0.0%)	0/61 (0.0%)	0/61 (0.0%)	0/61 (0.0%)	5/61 (8.2%)	
Zone 8 (13 assemblies)	1	7/61 (11.5%)	2/61 (3.3%)	27/61 (44.3%)	26/61 (42.6%)	48/61 (78.7%)	
Zone 8 (13 assemblies)	1.03	40/61 (65.6%)	21/61 (34.4%)	54/61 (88.5%)	53/61 (86.9%)	61/61 (100.0%)	
Zone 9 (17 assemblies)	0.95	0/61 (0.0%)	0/61 (0.0%)	1/61 (1.6%)	1/61 (1.6%)	19/61 (31.1%)	
Zone 9 (17 assemblies)	1	8/61 (13.1%)	2/61 (3.3%)	35/61 (57.4%)	35/61 (57.4%)	43/61 (70.5%)	
Zone 9 (17 assemblies)	1.03	38/61 (62.3%)	15/61 (24.6%)	41/61 (67.2%)	41/61 (67.2%)	56/61 (91.8%)	



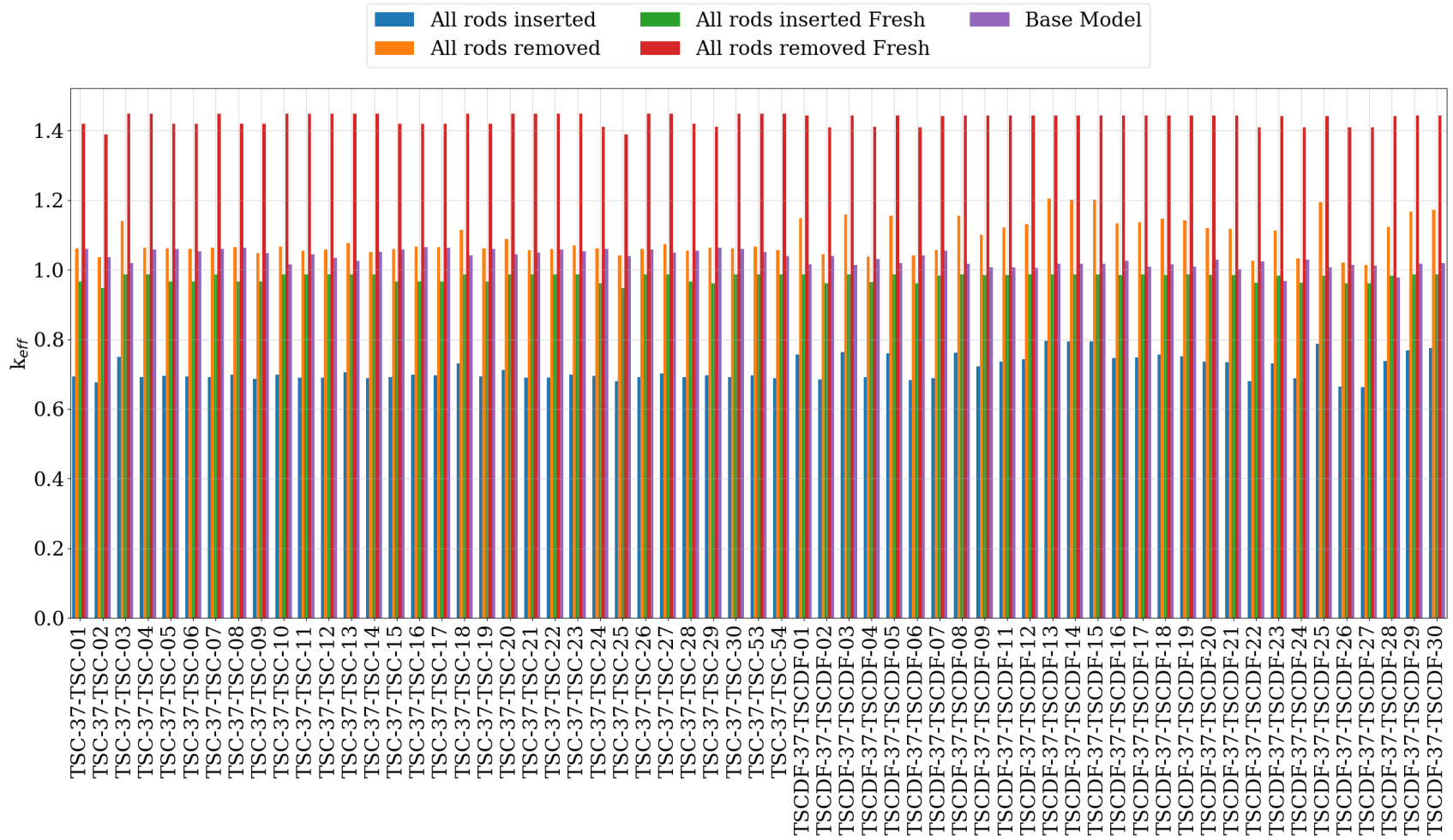


**Figure 52. Results of all DB models for various bounding combinations of fresh fuel, as-loaded spent fuel isotopic compositions, all DCRA with material large WB<sub>2</sub> rods in every location and with no rods compared to the Walker [2] DB results.**

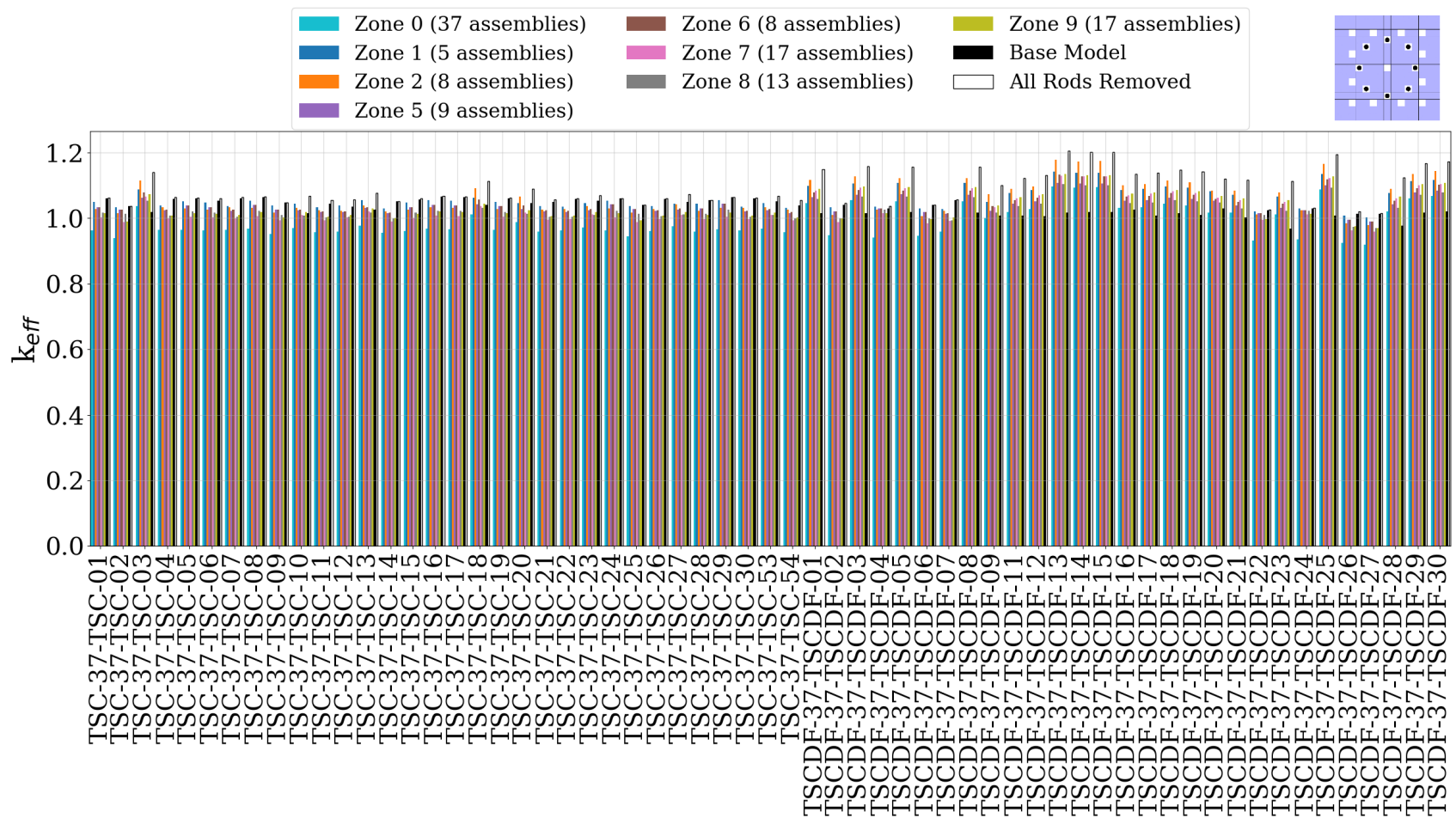


Figure 53. Results of all DB models with DCRA material  $WB_2$  and as-loaded fuel isotopic compositions; subzone 2 with small diameter rods.

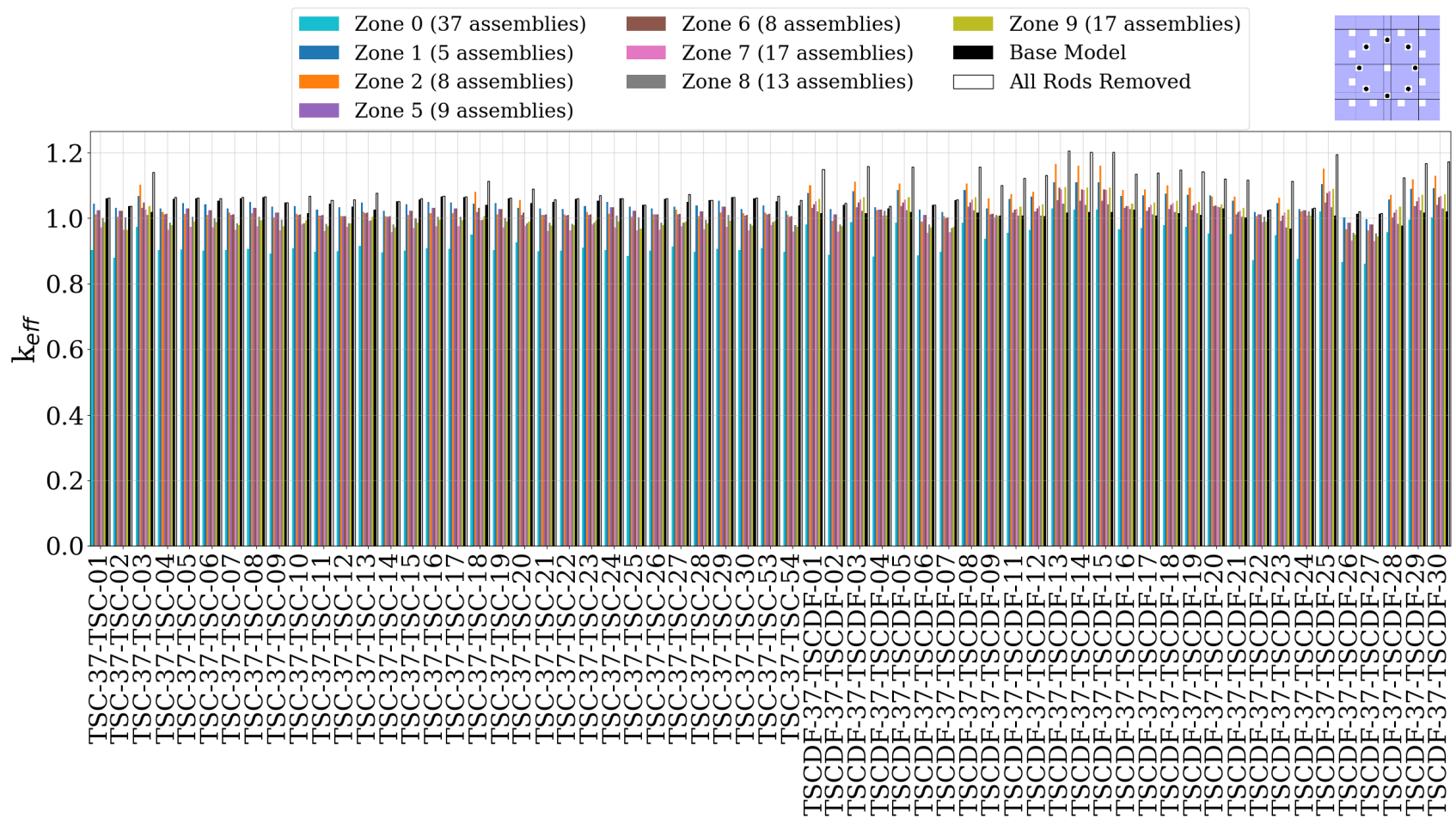
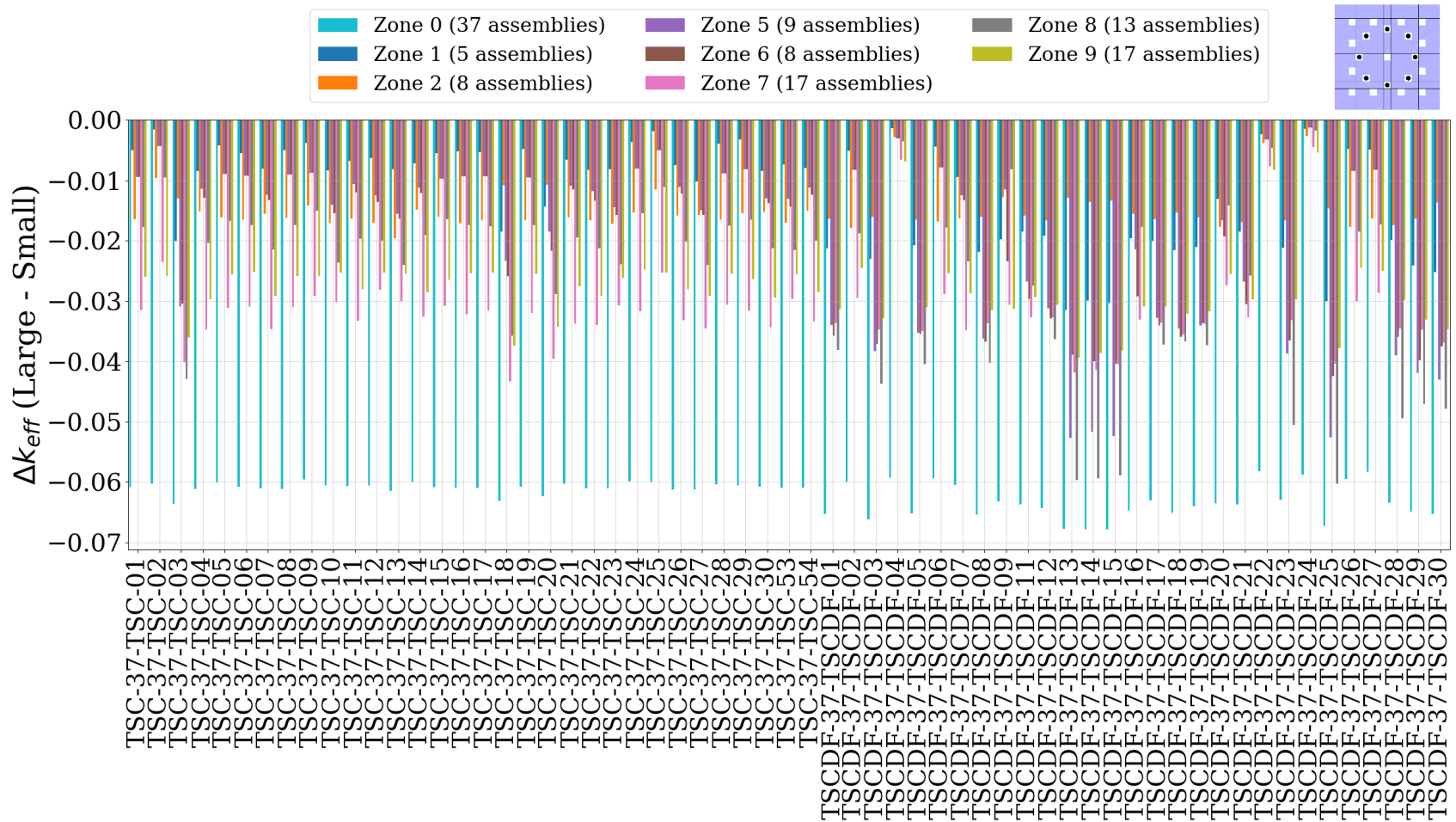


Figure 54. Results of all DB models with DCRA material  $WB_2$  and as-loaded fuel isotopic compositions; subzone 2 with large diameter rods.



**Figure 55. Delta-k of large-to-small diameter rods for all DB models with DCRA material  $WB_2$  and as-loaded fuel isotopic compositions for subzone 2.**

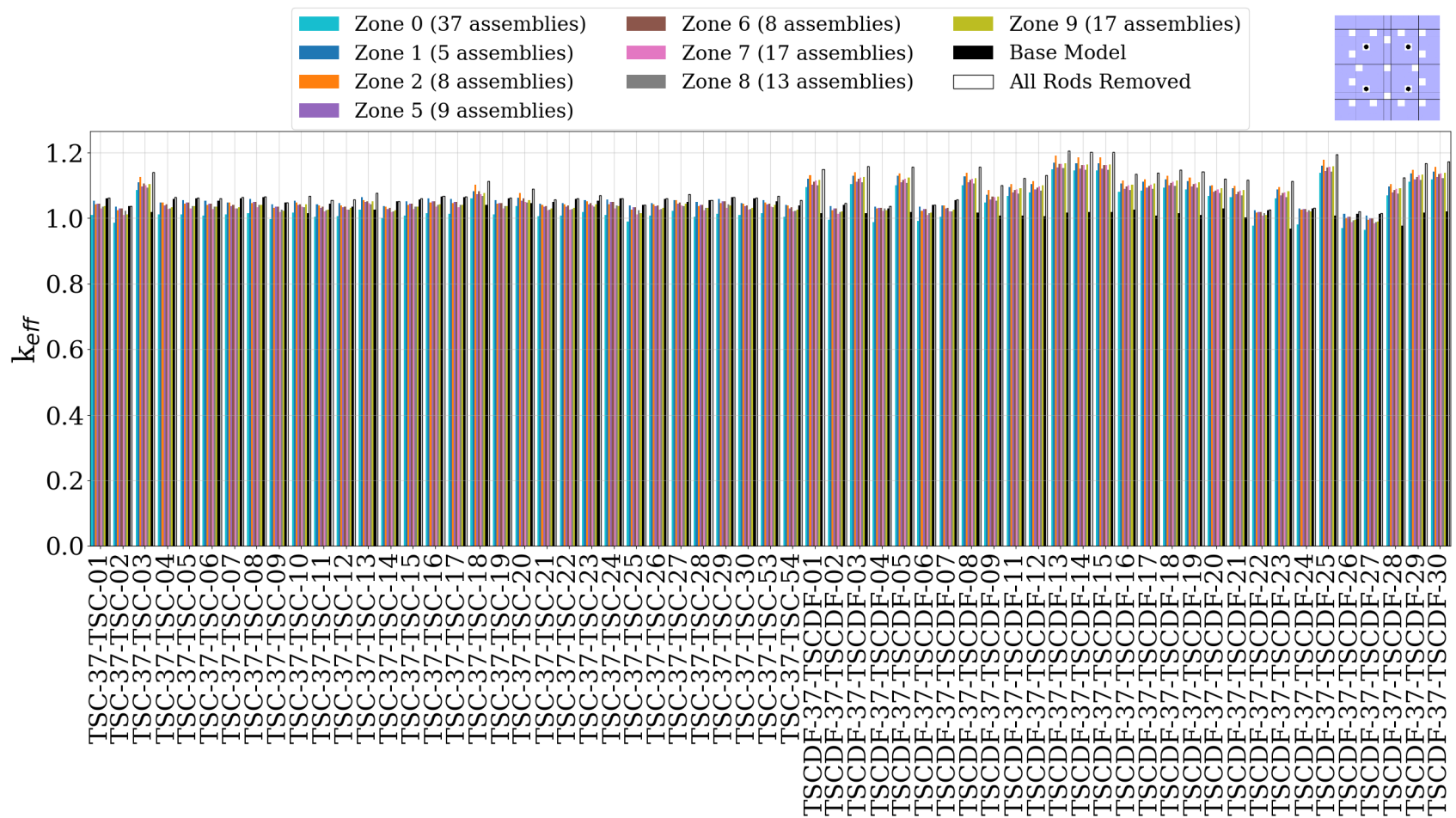


Figure 56. Results of all DB models with DCRA material  $WB_2$  and as-loaded fuel isotopic compositions; subzone 2 corners with small diameter rods.

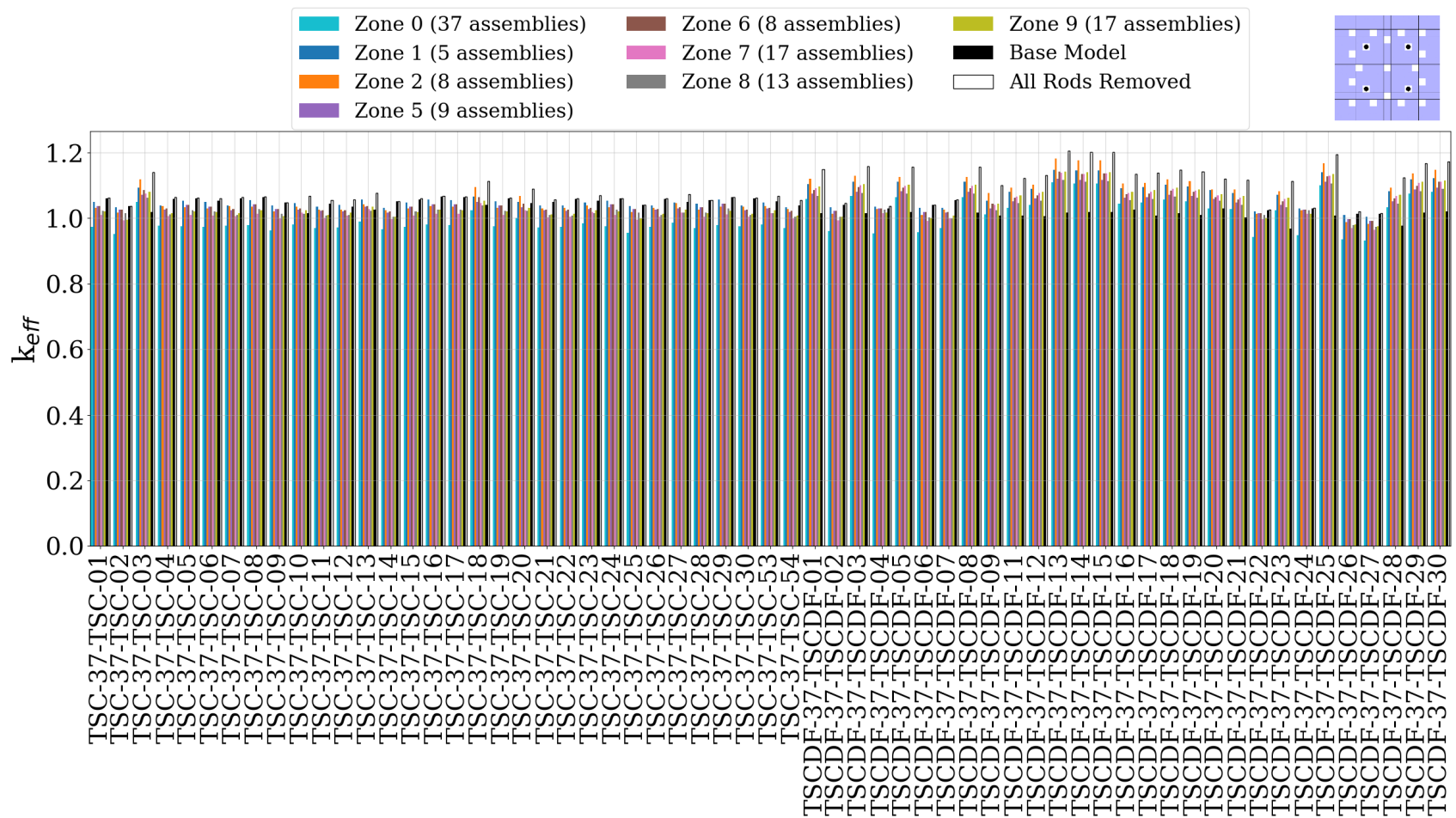
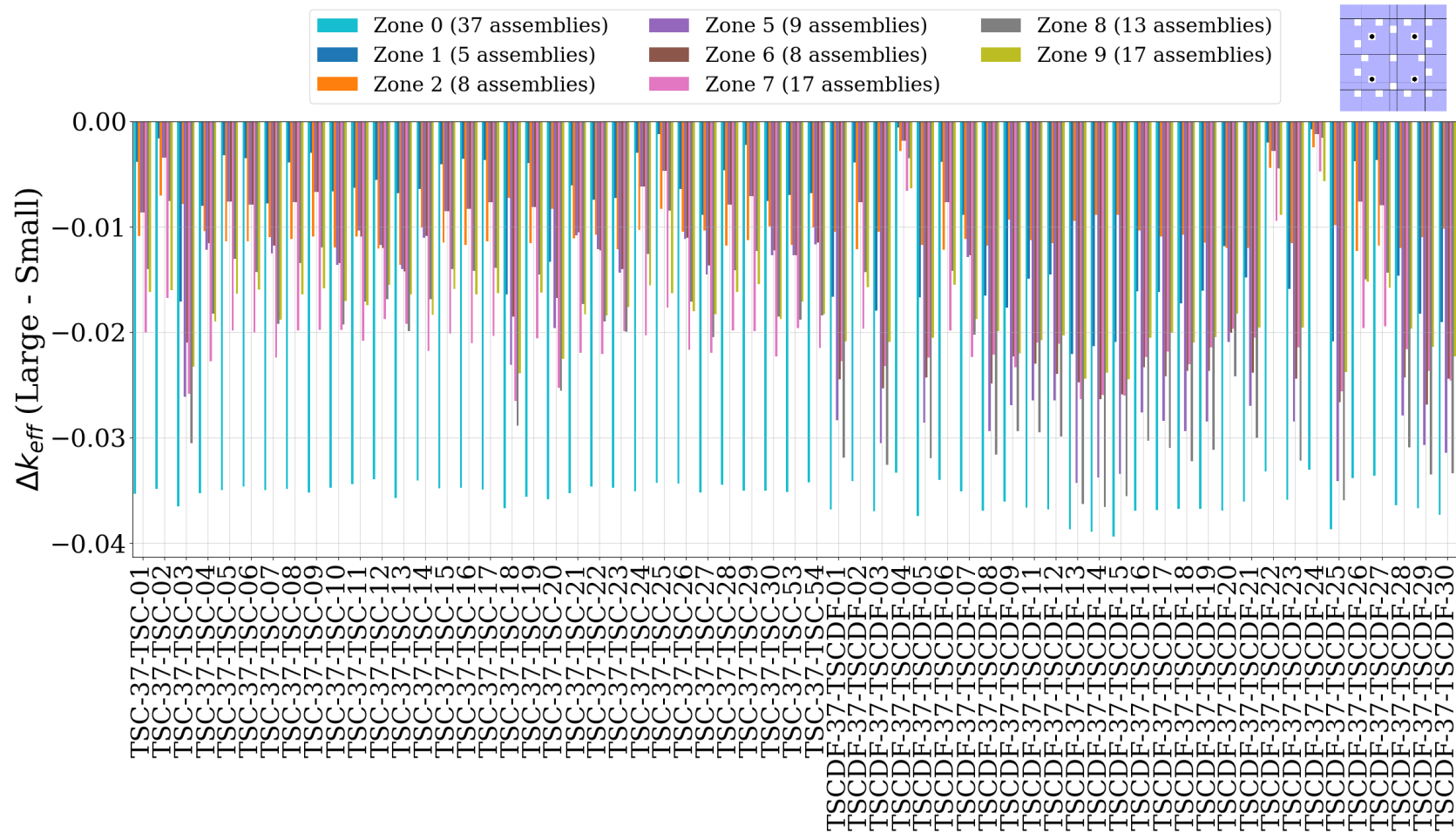


Figure 57. Results of all DB models with DCRA material  $WB_2$  and as-loaded fuel isotopic compositions; subzone 2 corners with large diameter rods.



**Figure 58. Delta-k of large-to-small diameter rods for all DB models with DCRA material WB<sub>2</sub> and as-loaded fuel isotopic compositions for subzone 2 corners.**

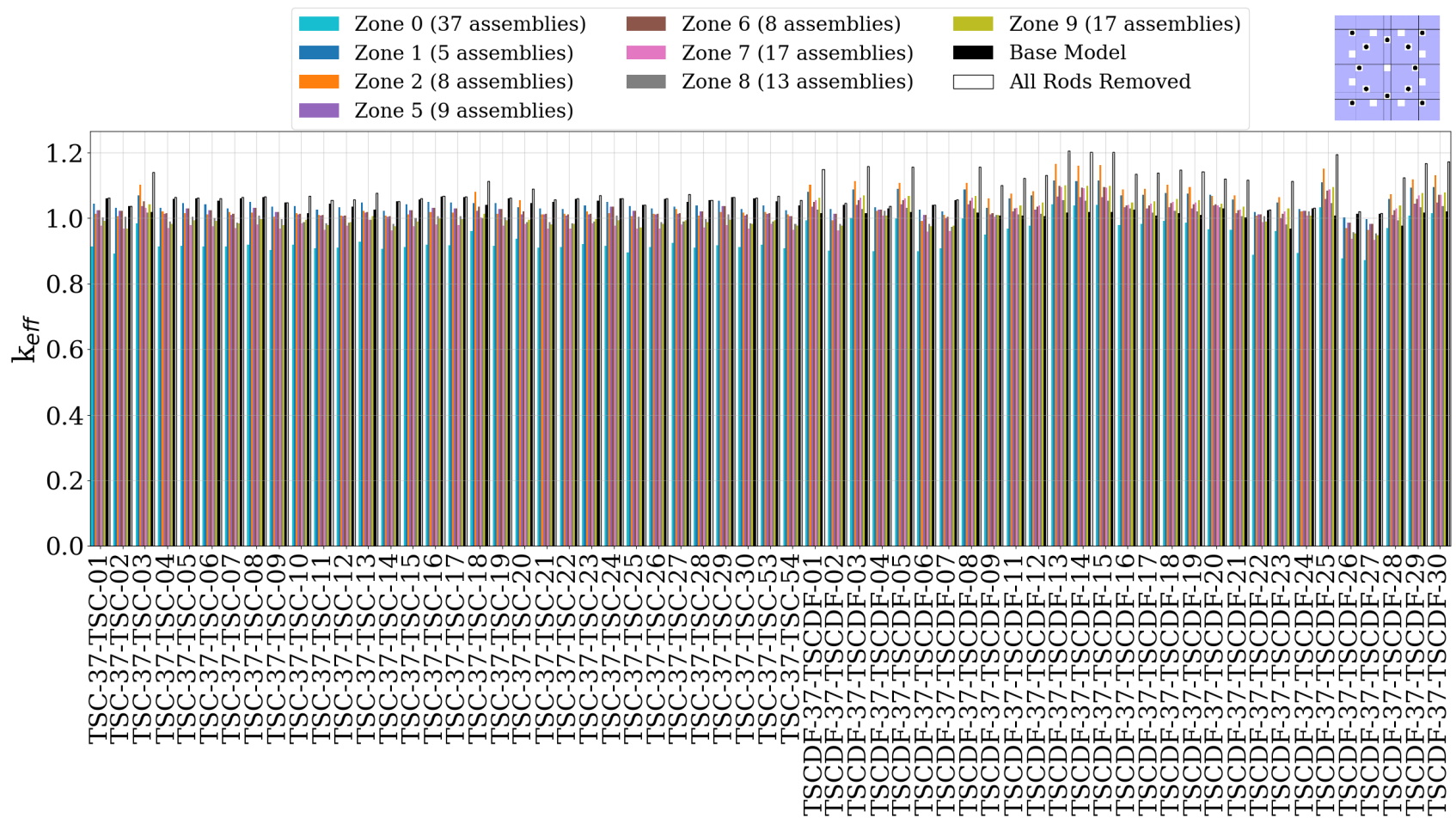


Figure 59. Results of all DB models with DCRA material  $WB_2$  and as-loaded fuel isotopic compositions; subzone inner 12 with small diameter rods.



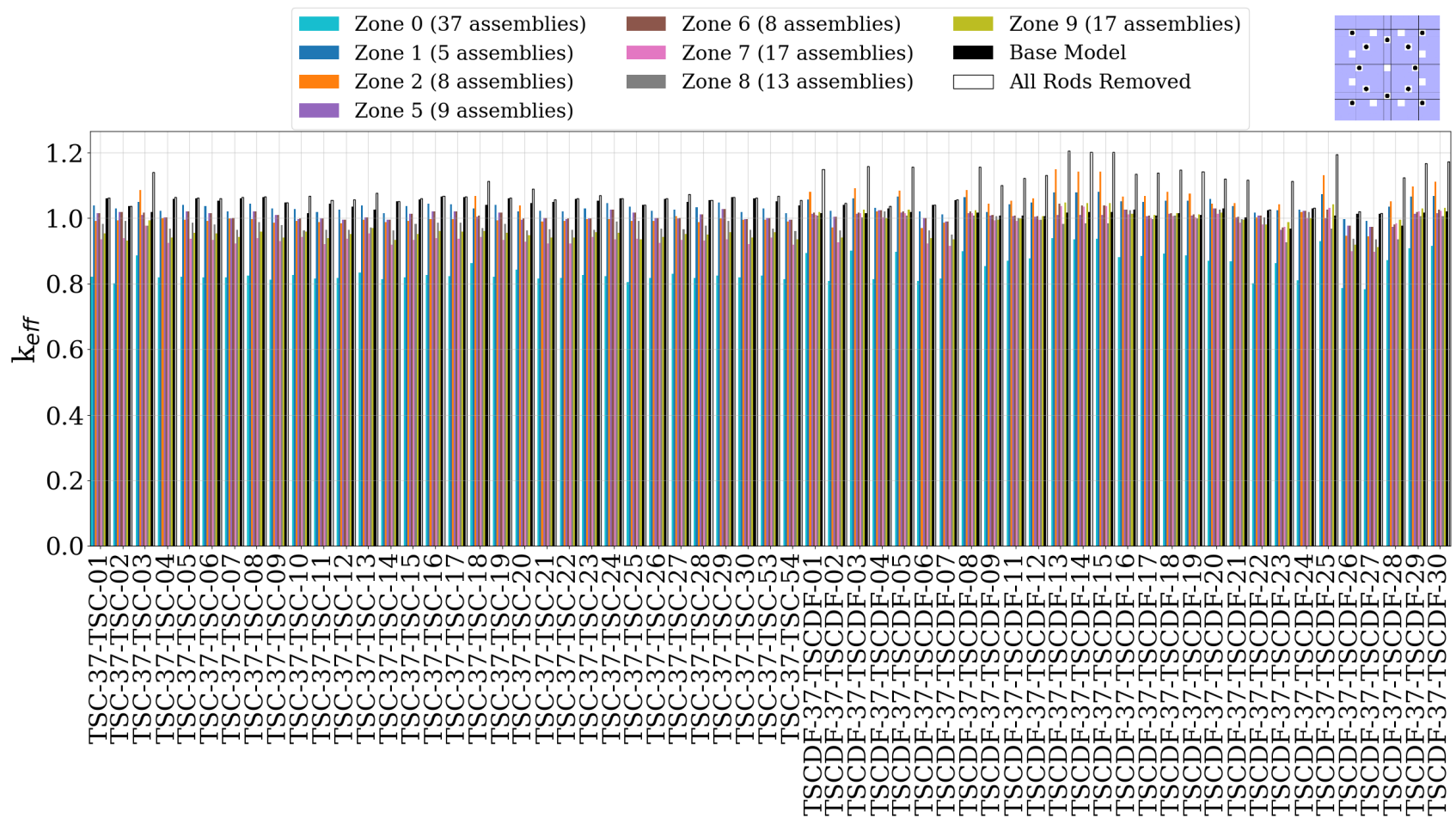
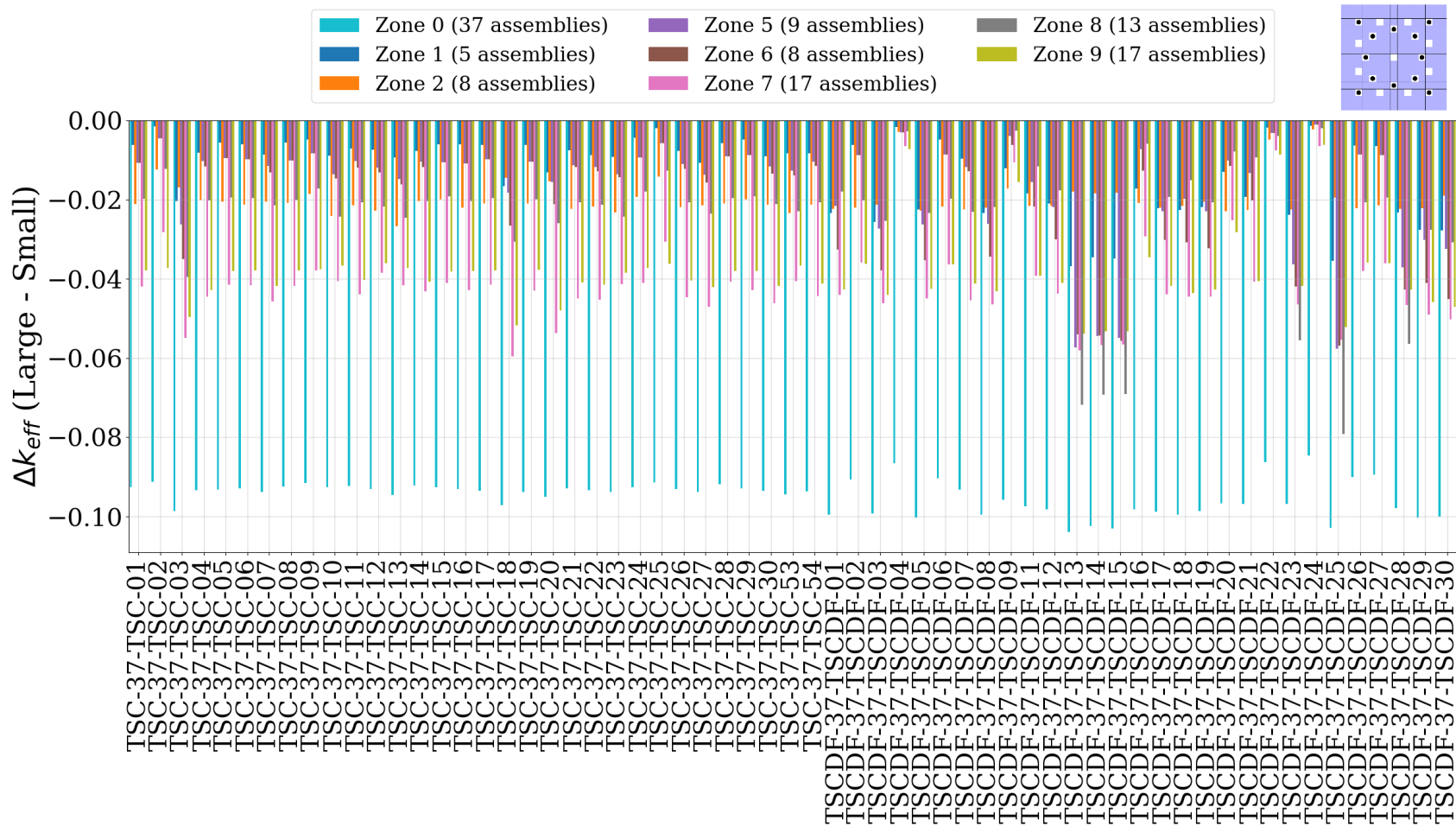


Figure 60. Results of all DB models with DCRA material  $WB_2$  and as-loaded fuel isotopic compositions; subzone inner 12 with large diameter rods.



**Figure 61. Delta-k of large-to-small diameter rods for all DB models with DCRA material WB<sub>2</sub> and as-loaded fuel isotopic compositions for subzone inner 12.**

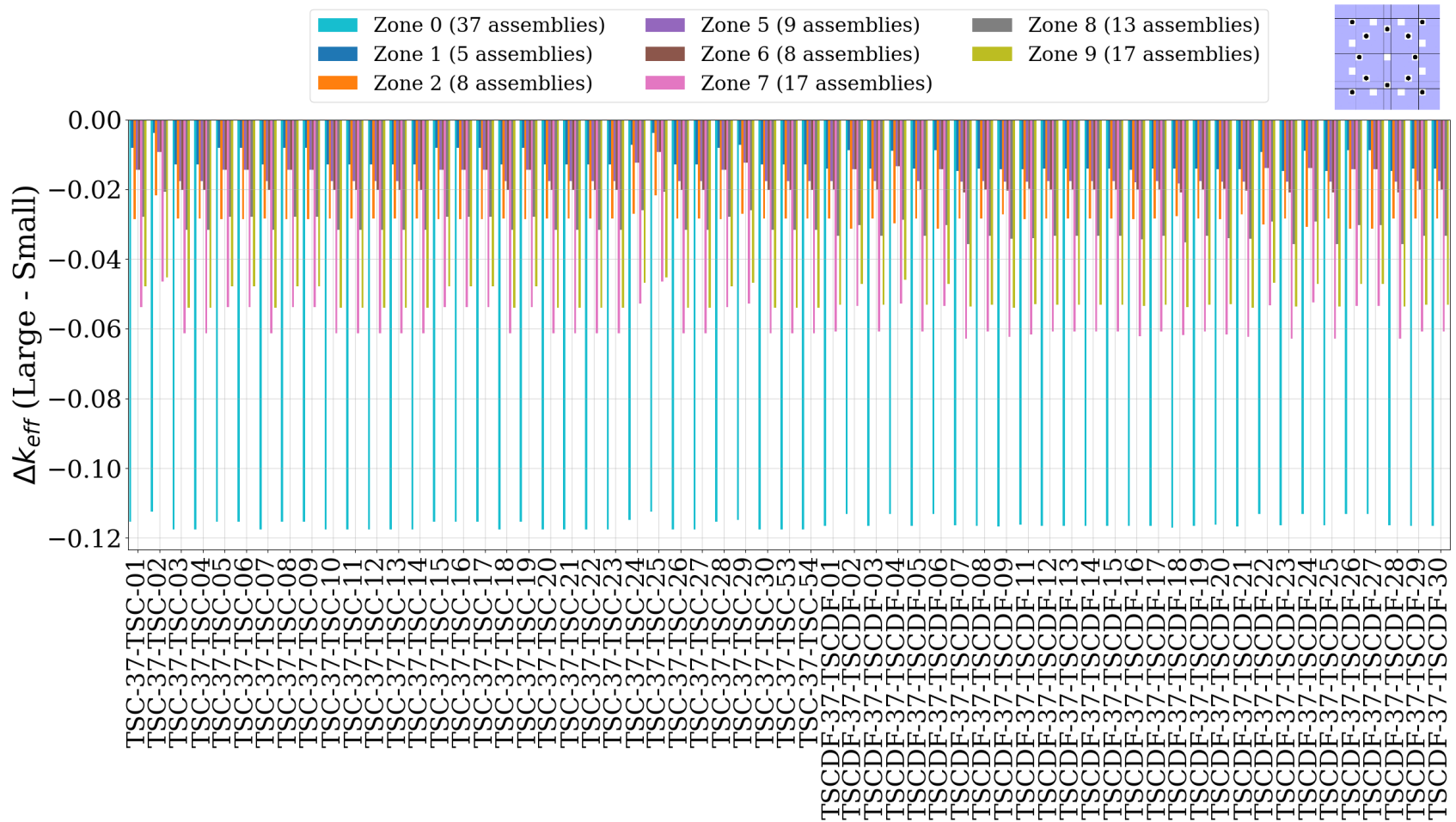


Figure 62. Results of all DB models with DCRA material  $WB_2$  and as-loaded fuel isotopic compositions; subzone all rods (21) with small diameter rods.

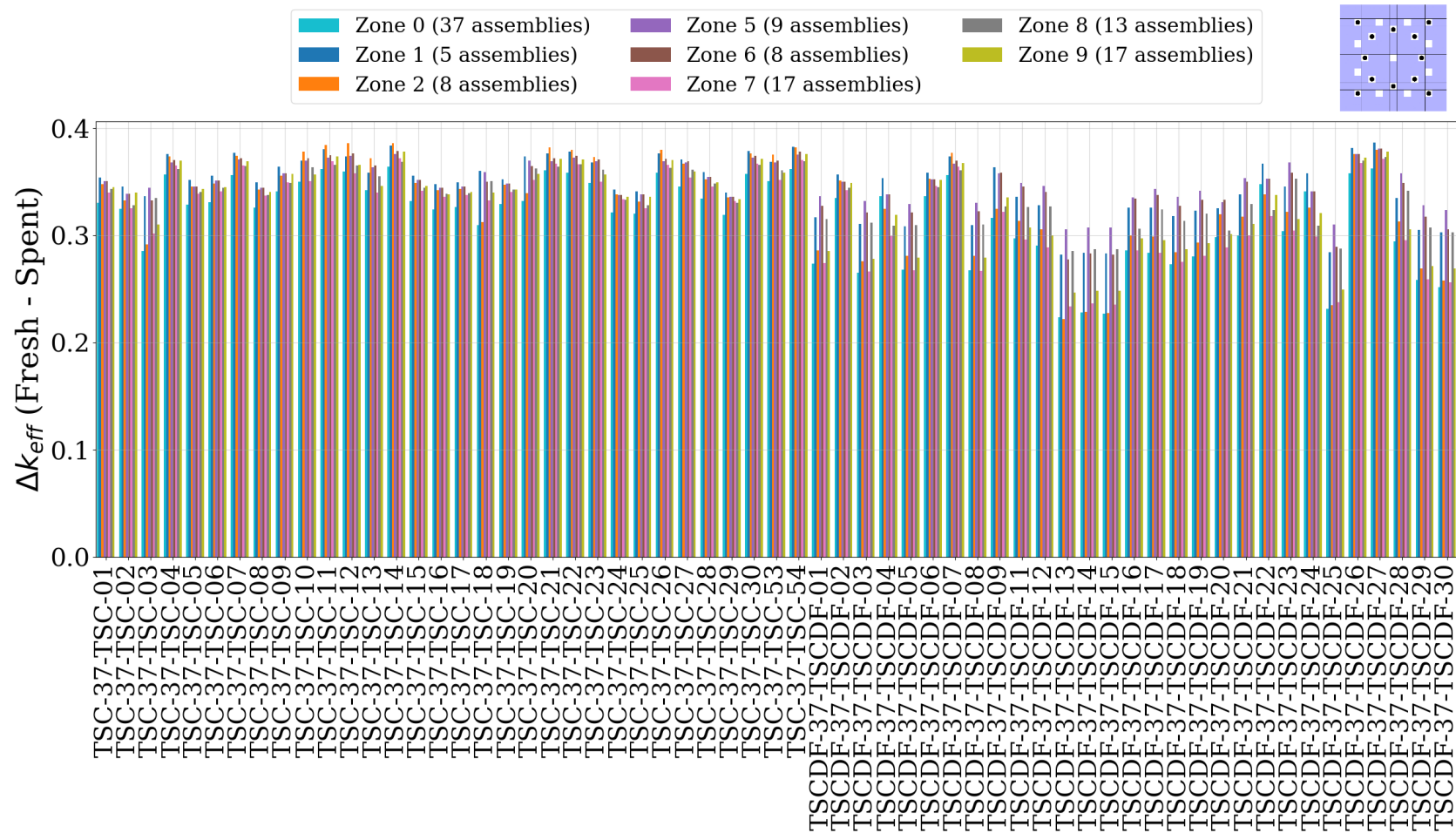
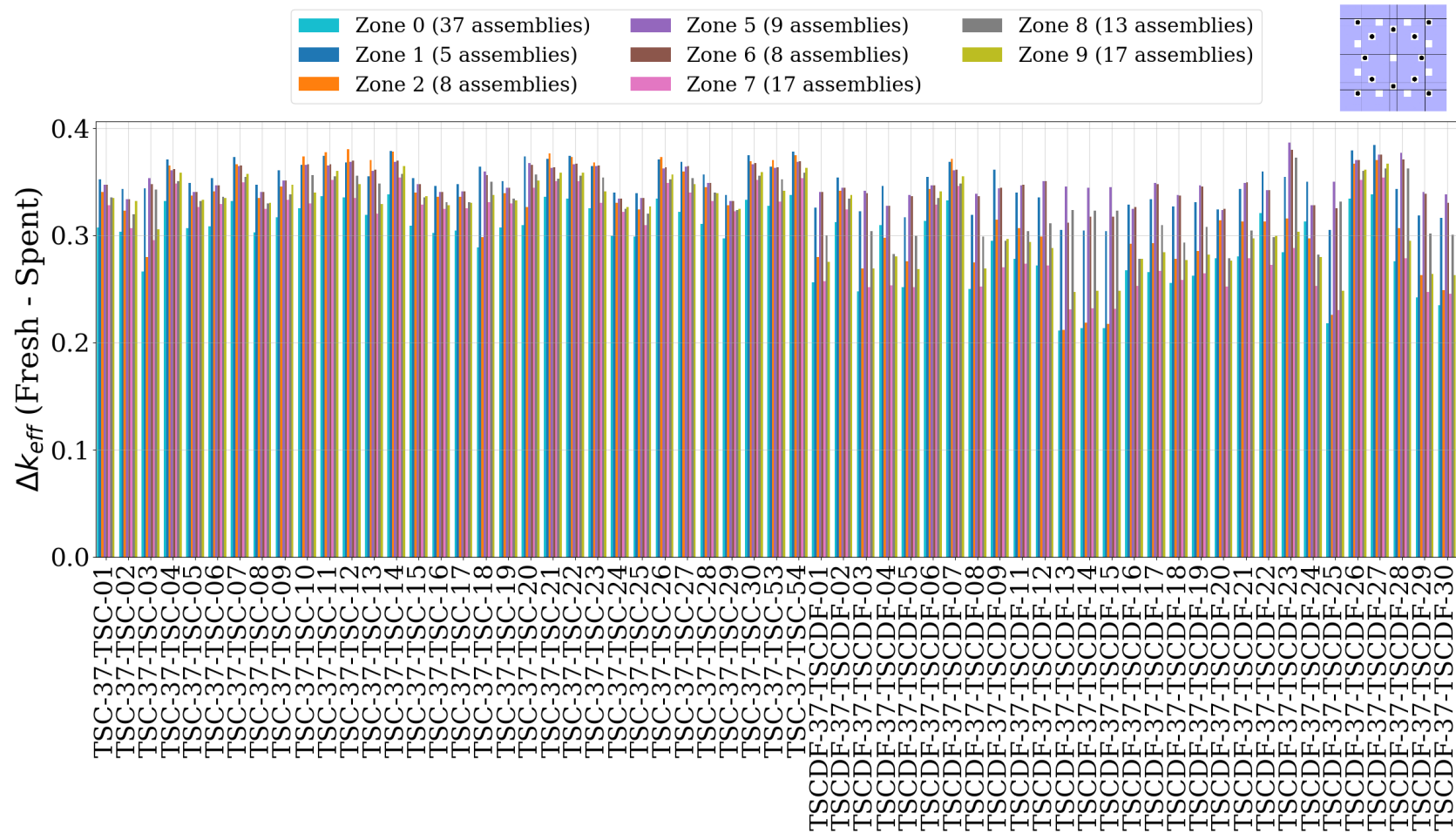


Figure 63. Results of all DB models with DCRA material  $WB_2$  and as-loaded fuel isotopic compositions; subzone all rods (21) with large diameter rods.



**Figure 64. Delta-k of large-to-small diameter rods for all DB models with DCRA material WB<sub>2</sub> and as-loaded fuel isotopic compositions for subzone all rods (21).**

#### 4. ASSUMPTIONS

- The DCRA is assumed to be the same length as the fuel.
- The RCCA material density is the same as the reduced density presented in Walker [2].
- The DPC model neglects all materials except the DPC wall and the basket walls. The neutron absorber material is neglected in the NA models, and the basket material is neglected in the DB models.
- All values provided for total number of rods and total mass of rods and rod materials are based on the assumption that every location in the basket has a fuel bundle capable of receiving DCRA's.

## 5. CONCLUSIONS

This report documents initial evaluations to support future work to use DCRA for post-closure criticality control in DPCs. The work performed is an extension of the work conducted by Walker [2] using UNF-ST&DARDS-generated inputs for the Zion site DPCs with as-loaded isotopic compositions. The results of this analysis demonstrate that there are multiple pathways to using DCRA for post-closure criticality control. Various combinations of DCRA material, diameter, number of rods per DCRA, and number and location of DCRA within a DPC were shown to be effective in various degrees for the set of DPCs utilized by Walker [2]. Because of the variations in DPC as-loaded isotopic compositions, it can be concluded that a DPC specific methodology is feasible, so a one-size-fits-all approach may not be needed. Rather, the utility program created for this work can be expanded to develop capabilities to provide DPC-specific DCRA arrangements which limit cost, weight, and operational considerations. Future work should consider the following focus areas, at a minimum:

- Expansion of capabilities to include all PWR DPCs in UNF-ST&DARDS
- Additional zone and subzone combinations
- Machine learning-generated DCRA loading optimization
- Expansion to BWR DPC and fuel designs
- Investigation of integration with UNF-ST&DARDS

## 6. REFERENCES

- [1] J. Kessler et al., *Analysis of Solutions for the Geologic Disposal of Dual-Purpose Canisters*, Revision 1, M2SF-19SN010305051, March 2020.
- [2] E. Walker, *Insert Modeling in UNF ST&DARDS*, ORNL/SPR-2022/2616, 2022.
- [3] S. Bhatt, K. Banerjee, and P. Miller, *UNF-ST&DARDS User Documentation*,” Oak Ridge National Laboratory, 2021.
- [4] A. M. Shaw et al., *Dual Purpose Canister Reactivity and Groundwater Absorption Analyses*, Revision 8, ORNL/SPR-2022/2609, September 2021.



